

Structural and Biochemical Analysis of GTPases of IMMUNITY-Associated Proteins (GIMAPs) and their Interaction Partners

Dissertation zur Erlangung des akademischen Grades des
Doktors der Naturwissenschaften (Dr. rer. nat.)

eingereicht im Fachbereich Biologie, Chemie, Pharmazie der
Freien Universität Berlin

vorgelegt von

Arasu Balasubramaniam Sivanandam

(Arasu B.S)

aus Puducherry, Indien

Berlin

2015

Die vorliegende Arbeit wurde im Zeitraum Mai 2011 bis November 2015 am Max-Delbrück-Centrum für Molekulare Medizin Berlin-Buch unter Anleitung von

PROF. DR. OLIVER DAUMKE

angefertigt.

1. Gutachter: Prof. Dr. Udo Heinemann
2. Gutachter: Prof. Dr. Oliver Daumke

Tag der Disputation:

30 März 2016

.....dedicated to my Ayya and Amma

Contents

List of Figures	xii
List of tables	xv
Abstract	xvii
1. Introduction	1
1.1 Immune system and its components.....	1
1.2 The adaptive immune system.....	3
1.3 Lymphocytes and development.....	4
1.3.1 T cell development	4
1.3.2 B cell development.....	6
1.4 Apoptosis and autophagy in lymphocytes.....	7
1.4.1 Autophagy	8
1.4.2 Apoptosis.....	10
1.5 GTPase	13
1.5.1 Ras GTPases	13
1.5.2 Septin.....	16
1.6 GTPases of IMMunity Associated protein – GIMAP	18
1.6.1 Discovery and domain architecture	19
1.6.2 Expression and subcellular localization of GIMAP	21
1.6.3 GIMAP1	22
1.6.4 GIMAP2	23
1.6.5 GIMAP3	23
1.6.6 GIMAP4	24
1.6.7 GIMAP5	25

1.6.8 GIMAP6	26
1.6.9 GIMAP7, GIMAP8 and GIMAP9	27
1.7 Structure and biochemical function of GIMAPs	27
1.7.1 GIMAP2	28
1.7.2 GIMAP7	30
Scope of this work	33
2. Materials and methods	35
2.1 Materials	35
2.1.1 Chemicals	35
2.1.2 Enzymes.....	35
2.1.3 Kits.....	35
2.1.4 Microorganisms	36
2.1.5 Vectors.....	36
2.1.6 cDNA clone	37
2.1.7 Cloning and mutagenesis primer	37
2.1.8 Media and Antibiotics	37
2.1.9 Buffers	37
2.1.10 Peptides.....	38
2.2 Molecular biology methods	38
2.2.1 Polymerase chain reaction	38
2.2.2 DNA digestion.....	38
2.2.3 Agarose gel electrophoresis.....	39
2.2.4 DNA extraction from Agarose gel.....	39
2.2.5 Ligation.....	39
2.2.6 Transformation of chemically competent <i>E.coli</i>	39

2.2.7 Isolation of plasmid DNA.....	39
2.2.8 DNA sequencing.....	39
2.2.9 Site directed mutagenesis	39
2.2.10 Bacterial storage	40
2.2.11 Co-transformation for co-expression.....	40
2.3 Biochemical methods.....	40
2.3.1 SDS PAGE	40
2.3.2Determination of protein concentration.....	40
2.3.3Protein storage	40
2.3.4Nucleotide hydrolysis assay	40
2.3.5Nucleotide detection using reversed-phase HPLC	41
2.3.6 Isothermal Titration Calorimetry (ITC).....	41
2.3.7 Protein over-expression and solubility test in <i>E.coli</i>	41
2.3.8Large scale protein over-expression in <i>E.coli</i>	42
2.3.9 GIMAP protein purification	42
2.3.10 Purification of GIMAP6-GABARAPL2 complex	43
2.3.11 Biolayer interferometry (BLI)	44
2.4 Cell biological methods	44
2.4.1 Jurkat cell culture and transfection.....	44
2.4.2 Stable Isotope Labelling by Amino acid in Cell culture (SILAC)	45
2.4.3 Apoptosis assays.....	46
2.4.4 Induction of autophagy.....	47
2.4.5 Microscopy.....	47
2.5 Crystallographic and computational methods	47
2.5.1 Crystallization screening	47
2.5.2 Cryo-protection of crystals.....	48
2.5.3 Data collection.....	48

2.5.4 Protein structure solution.....	48
2.5.5 Atomic Model building and refinement	51
2.5.6 Protein structure validation and deposition	52
3. Results	53
3.1 Development of SILAC assay to identify interaction partners of GIMAPs	53
3.1.1 Interaction partners of GIMAP7.....	53
3.1.2 Interaction partners of GIMAP2.....	55
3.2 Purification of GIMAP6 and GABARAPL2	57
3.3 Nucleotide binding properties of GIMAP6.....	59
3.4 GIMAP6 inhibits the GTPase activity of GIMAP7	60
3.5 Modelling the GIMAP6-GIMAP7 interaction	61
3.4.1 Homology model of GIMAP6.....	61
3.4.2 GIMAP6:GIMAP7 heterodimer	64
3.5 Biochemical characterization of inhibition mechanism of GIMAP6.....	67
3.6 Biochemical characterization of GIMAP6 and GABARAPL2 interaction	69
3.7 Structure of GABARAPL2	72
3.8 Purification and crystallization of GIMAP6- GABARAPL2 complex.....	75
3.9 GIMAP6:GABARAPL2 complex inhibits GIMAP7.....	78
3.10 Influence of GTPase activity within GIMAP family	79
3.11 Cellular localization and function of GIMAPs in Jurkat T cells.....	82
5. Discussion	87
5.1 GIMAP6 homology model and GIMAP6-GIMAP7 structural interface.....	87
5.2 GIMAP6-GABARAPL2 interaction	90
5.3 GIMAPs a master regulator of apoptosis, autophagy and lymphoid cell development.	94
5.4 GIMAPs-Current understanding and a working model	95
APPENDIX A- G motifs in GIMAPs	99
APPENDIX B – Instruments	100

APPENDIX C- Chemicals	102
APPENDIX D- List of Clones	105
APPENDIX E- List of Abbreviations	107
References	109
Zusammenfassung	121
Publication	123
Acknowledgements	125
Erklärung	127

List of Figures

Figure 1:	Hematopoiesis	2
Figure 2:	T cell maturation	5
Figure 3:	B cell development	7
Figure 4:	Autophagic pathway	8
Figure 5:	Apoptotic pathway	11
Figure 6:	The GDP/GTP switch and crystal structure of Ras bound to GppNHp•Mg ²⁺	15
Figure 7:	Domain architecture of septins	16
Figure 8:	Crystal structure of septin	17
Figure 9:	Classification of G protein superfamily	18
Figure 10:	Genomic organisation of human GIMAP genes on chromosome 7	19
Figure 11:	Domain architecture of human GIMAPs	20
Figure 12:	Crystal structure of GIMAP2	29
Figure 13:	Structure and GTPase activity of GIMAP7	31
Figure 14:	Experimental workflow for identification of interaction partners of GIMAP	53
Figure 15:	Interaction partners of GIMAP7	54
Figure 16:	Interaction partners of GIMAP2	55
Figure 17:	Interaction partners of GIMAP7 and GIMAP2	56
Figure 18:	Typical GIMAP6 and GABARAPL2 purification procedure	57
Figure 19:	ITC experiment for nucleotide binding of GIMAP6	59
Figure 20:	GIMAP6 inhibits GIMAP7	60
Figure 21:	GIMAP6 inhibits GIMAP7 (L100Q)	61
Figure 22:	Homology model of GIMAP6	63
Figure 23:	Model of GIMAP6-GIMAP7 heterodimer	65
Figure 24:	GIMAP6 residues involved in inhibition of GIMAP7	66
Figure 25:	GIMAP6 deletion constructs	67
Figure 26:	GIMAP6 (R134D) inhibits GIMAP7 (L100Q)	68
Figure 27:	Identification of GIMAP6 motif responsible for inhibition of GIMAP7	69
Figure 28:	Biochemical characterization of GIMAP6-GABARAPL2 interaction	70
Figure 29:	GIMAP6 interacts with GABARAPL2 in Bio-Layer Interferometry	71
Figure 30:	Crystals of GABARAPL2	72
Figure 31:	Crystal structure of GABARAPL2	73
Figure 32:	Analytical gel filtration of GABARAPL2-GIMAP6 (R134D) complex	76
Figure 33:	Typical GIMAP6wt-GABARAPL2 complex purification procedure	76
Figure 34:	Crystallization of GIMAP6wt-GABARAPL2 complex	77
Figure 35:	GIMAP6:GABARAPL2 complex inhibits GIMAP7	79
Figure 36:	Arginine fingers of GIMAP2 and GIMAP7 are required for the stimulated GTPase reaction	80
Figure 37:	GIMAP6 did not influence GIMAP5 in GTP hydrolysis assay	81
Figure 38:	GIMAP6 and GIMAP7 did not influence GIMAP2 and GIMAP5 respectively in GTP hydrolysis assays	81
Figure 39:	Localization screen of GIMAP1, GIMAP5 and GIMAP6 in Jurkat T cells	83
Figure 40:	Effect of apoptosis and autophagy on the localization of GIMAP7	85
Figure 41:	Modes of interaction in GIMAP6-GIMAP7 heterodimer	89
Figure 42:	Structural superimposition of GABARAPL2 and GABARAP	92
Figure 43:	Structure of Ras:RalGDS-RID complex	93
Figure 44:	Model of GIMAP function in Jurkat cell	97

List of Tables

Table 1:	Expression and localization of GIMAPs.....	21
Table 2:	Data collection statistics of GABARAPL2.....	74
Table 3:	Refinement statistics of GABARAPL2.....	75

Abstract

GTPases of IMMunity Associated Proteins (GIMAPs) comprise a family of septin-related GTPase associated with the adaptive immune system. They have been implicated in lymphocyte development, mitochondrial DNA segregation, apoptosis and autophagy. Structural studies revealed that some GIMAPs can form GTP-dependent protein scaffolds by oligomerizing via two interfaces on the surface of membranes. Biochemical studies indicated that other members may facilitate the disassembly of these scaffolds. The aim of this doctoral thesis was to characterize the cellular role of GIMAPs by identifying their interaction partners and to carry out an extensive structural and biochemical analysis on them.

Interaction partners of GIMAPs were identified by mass spectrometric analysis and were involved in functions like apoptosis, autophagy, protein folding and vesicular trafficking. In particular, GABARAPL2, an autophagy-associated protein, and GIMAP6 were identified as specific interaction partners of GIMAP7. Subsequently, the GIMAP6-GIMAP7 interaction was biochemically characterized, and it was established that GIMAP6 can down-regulate the GTPase function of GIMAP7 at equimolar concentrations. Based on homology models and biochemical analysis, it was shown that the G domain of GIMAP6 is the main determinant for GTPase inhibition, whereas the C-terminal helices contribute to some extent. Also the interaction between GABARAPL2 and GIMAP6 was biochemically and structurally characterized. GABARAPL2 interacted with GIMAP6 with nanomolar affinity, as measured in isothermal titration calorimetry (ITC) and bio-layer interferometry. Interestingly, a C-terminal 10 amino acid peptide of GIMAP6 previously implicated in the interaction did not bind to GABARAPL2 in the ITC measurement suggesting of a novel mode of interaction. The crystal structure of GABARAPL2 was solved to atomic resolution. GABARAPL2 exhibited a conserved ubiquitin superfamily fold and oligomerized in the crystal in a head to tail fashion leading to a speculation that it might form protein scaffold on the surface of autophagosomes upon induction of autophagy. Finally, a model for the function of GIMAP6, GIMAP7 and GABARAPL2 together with GIMAP2 is proposed. Obtained findings from this thesis will form a basis for many mutational and cell biological studies in order to understand the molecular function of GIMAPs.

1. Introduction

1.1 Immune system and its components

The immune system is a remarkably dynamic self defence mechanism that has evolved to fight against invading microorganisms and parasites in host. It is capable of producing varieties of cells and molecules in order to specifically identify and eliminate the invading threat. These cells and molecules works as a network in a sophisticated manner for the survival of the organism. The human body constitutes many organs in order to form, develop and maintain the immune system. This organ system is called the lymphoid system (1). It consists of primary and secondary lymphoid organs. Thymus and bone marrow constitute the primary lymphoid organs where the formation and maturation of the cells involved in the immune system takes place. The secondary lymphoid organs mainly include spleen and lymph nodes where the foreign pathogen is actively engaged and eliminated. Both primary and secondary organs are connected through a network of lymphatic and blood vessel through which the immune system is constantly active. Upon encountering the foreign material or antigen, the immune system reacts to eliminate it and the reaction is called immune response. All the cells involved in the immune response arise from a process called hemotopoiesis (Figure 1) (2). It is a process which takes place mainly in bone marrow in adults which leads to formation and development of both red and white blood cells.

During hemotopoiesis, the resident stem cells of bone marrow called as hemotopoietic stem cells (HSCs) with self-renewing capacity, differentiate into two different progeny called myeloid and lymphoid cells. Myeloid cells further develop and differentiate into red blood cells or erythrocytes, platelets, basophil, eosinophil, neutrophil, monocyte and macrophages. Lymphoid cells further develop into white blood cells which constitute natural killer (NK) cells, T cells and B cells. As an exception, dendritic cells can arise from both myeloid and lymphoid lineage (3). With such a complex interplay of organs and cells, the human immune system can be classified into innate and adaptive immune systems. Although both the systems work in concert for the protection of the human, each of them is significantly different in their mode and time of response. Innate immune system is the first line of defence and immediate responder towards the infection (4). Cells involved in innate immune response are neutrophils, eosinophils, basophils, monocyte, macrophages and dendritic cells. Their response is less

specific and does not confer long lasting immunity to the organism. Cells like macrophages and dendritic cells carry receptor called Toll-like receptors (TLRs) which recognize broad and general pattern of pathogen associated danger and neutralize it (5). Importantly, some innate immune cells also play an important role in activating adaptive immune system.

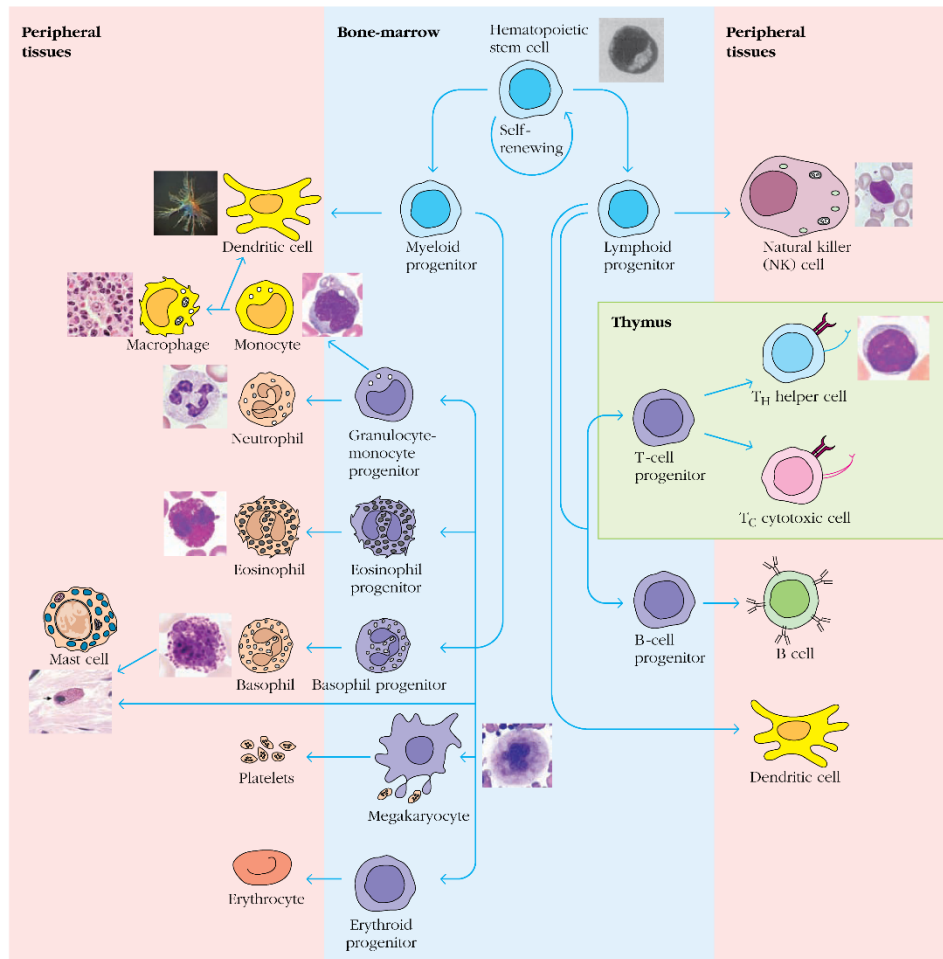


Figure 1: Hematopoiesis. Self-renewing HSC differentiate into lymphoid and myeloid progenitors. All red and white blood cells arise from myeloid and lymphoid progenitor cells respectively. Dendritic cell arise from both the lineage. Figure adapted from Kubly, Immunology, 2007, 7th edition.

In contrary to innate immune system, adaptive immune system does not come into play unless it is challenged with antigen (6). Once activated, the response is specific and can confer long lasting immunity. T and B lymphocytes are the major players of the adaptive immune system. Since the adaptive immune system and its components are the subject of this thesis, it will be introduced in detail in the sections below.

1.2 The adaptive immune system

The human Adaptive Immune System (AIS) is composed of highly specialized cellular machinery and molecules which fight infection and eliminate them. Characteristic features of AIS are antigenic specificity, diversity, immunologic memory and self/nonself-recognition (3). The antigen specificity allows it distinguish small molecular differences among antigens. At the same time, AIS generates a large repertoire of recognition molecules (antibody) which in turn specifically recognize the antigen. Recognition of antigen and the immunologic reaction towards it is called immune response. After the immune response, AIS retains the memory of first encounter with the antigen which is called immunologic memory (7). Immunologic memory helps to neutralize the same antigen on subsequent encounter in a swift manner. Vaccination works on the basis of immunologic memory and confers lifelong immunity against certain pathogens. Finally, AIS responds only to foreign antigens and has the ability to distinguish between the host and foreign antigen. Key players of the adaptive immune system are T and B lymphocytes which are specialized cells that mature in central or primary lymphoid organs.

The process of AIS can be broadly classified into five stages (8), a) formation, maturation and development of lymphocytes, b) diversification of antigen-binding receptors, c) recognition of a specific antigen, d) clonal selection of T and B cells, e) mechanisms to induce and control overall immune response. Among these five stages, clonal selection plays a crucial role in defending the host from the pathogens. The theory of clonal selection was proposed by Burnet in the late 1950s (9). It hypothesizes that each B cell can synthesize only one of the millions of possible antibodies which is displayed on its surface. When B cell encounter an antigen of the proper specificity, the surface antibody interact and form a complex with it. This recognition and antigen-antibody complex formation lead to the activation of the B cells. The B cells which do not undergo this activation do not develop further. The activated B cell begin to divide rapidly, produce a clone of B cell which differentiate into plasma cells and memory cells. Plasma cells produce the specific antibody against antigen that provoked its formation, whereas memory cells remain in circulation and do not produce antibodies unless become activated by a later challenge by the same antigen. The clones which carry an antibody against the self-molecules are eliminated at the early stages of development. Interestingly, at the time of formulation of this hypothesis, neither antigen receptors nor the function of lymphocytes themselves were known. The mechanisms of how adaptive immunity is achieved were confirmed in extensive studies which followed the initial postulates.

As on date, it is understood that the diverse repertoire of T and B receptors are generated by V (D) J recombination events in their respective gene during development (10, 11). The receptors which recognize and react towards the host itself are eliminated by apoptosis (12). This led to the evolution of the current advanced immune system which can generate infinitesimally divergent binding specificities. Apart from the defence provided by B cells, T cells also helps in the fighting the infection. The difference in this case is that the antigen has to be processed by the antigen presenting cells (APC), for instance by macrophages, in order to be recognized by the T cell receptor on the surface of the T cell. This recognition lead to the proliferation of the T cells with a specific T cell receptor. These cells further differentiate into effector cells called T helper, T memory and cytotoxic effector T cells. Cytotoxic effector cells fight and eliminate the infected cells, T helper works in concert with B cell and lead to increased antibody production against the antigen and T memory cells are retained in the circulation and kept in reserve to elicit an immune response on secondary encounter of the same antigen.

1.3 Lymphocytes and development

As explained in the sections earlier, the main cellular effectors of adaptive immune reactions are T and B cells. Even though both of them are derived from lymphoid cell lineage (13), they exhibit differences in various stages of their development and function. While the anatomical locations of their development are separated, the genetic network regulating their development (14) and the functioning of their antigen receptor are different (15). The development of both T and B cells will be elaborated below.

1.3.1 T cell development

A functional immune system requires the selection of T lymphocytes expressing receptors that are major histocompatibility complex restricted but also tolerant to self-antigens. This selection occur predominantly in the thymus. T cells originate from hematopoietic stem cells (HSC) in bone marrow and migrate to the thymus. The immature and undifferentiated lymphoid progenitors in the thymus are called thymocytes or generally termed as precursors. Their development requires signals from thymic epithelial cells (TECs) and mesenchymal fibroblasts. These cells reside in distinct anatomical locations in the thymus, and movement of thymocytes between these micro anatomical structures is necessary for acquiring signals leading to their differentiation (Figure 2) (16).

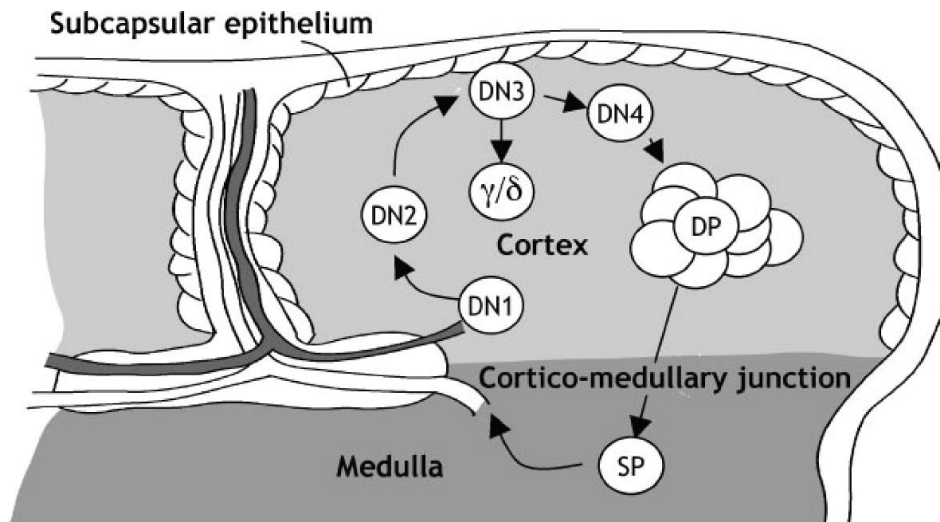


Figure 2: T cell maturation. Bone marrow progenitors enter the adult thymus near the cortico-medullary junction and migrate toward the subcapsular epithelium. They differentiate and mature passing through various checkpoint during this migration. Cells surviving these checkpoints migrate through the medulla before exiting the thymus as mature T cells. Figure adapted from (17)

Differentiation is marked by the temporally coordinated expression of cell surface proteins on the thymocytes including CD4, CD8, CD44, and CD25 (Figure 2). While entering the thymus, precursors lack expression of CD4 and CD8 and are called double negative (DN). It was demonstrated that precursor cells enter the thymus at the cortico-medullary junction (CMJ) and move through the cortex (18). During this migration, cells progress through DN1 ($CD44^+/CD25^-$) and DN2 ($CD44^+/CD25^+$) stages. Further on, the cells migrate towards the periphery of the thymus called subcapsular epithelium where they enter the DN3 ($CD44^-/CD25^+$) and DN4 ($CD44^-/CD25^-$) stage (Figure 2). As cells progress through the DN2 to DN4 stages, they express pre- T Cell Receptors (TCR) which are composed of the pre-T α chain and a TCR β -chain (17). Successful pre-TCR expression leads to cell proliferation during the transition from DN4 to double positive (DP) stages. Rearranged TCR α -chains together with β -chains form a complete $\alpha\beta$ TCR on the DP cells. The $\alpha\beta$ -TCR- $CD4^+CD8^+$ (DP) thymocytes interact with cortical epithelial cells that express a high density of MHC class I and class II molecules associated with self-peptides. The selection of the DP thymocytes depends on signalling that is mediated by interaction of the TCR with these self-peptide-MHC ligands (19, 20). Very strong affinity binding and signalling leads to apoptosis (negative selection) which is common in the medulla on encounter with strongly activating self-ligands on dendritic cells (21). The appropriate, intermediate level of TCR signalling initiates effective maturation

(positive selection). Thymocytes that express TCRs that bind self-peptide-MHC-class-I complexes become CD8⁺ T cells, whereas those that express TCRs that bind self-peptide-MHC-class-II ligands become CD4⁺ T cells. Subsequently, these cells are ready for export from medulla to peripheral lymphoid sites.

1.3.2 B cell development

B cells undergo several maturation stages in the bone marrow (22). The B cell precursors are regulated by reticular and stromal cell secreting chemokine CXCL12 and interleukin- 7 (IL-7), respectively in a spatiotemporal manner. The transcription factors E2A, early B cell factor (EBF) and Pax5 are crucial to the early development stage, where the decision to differentiate from HSC to pre-pro- B cell occur (Figure 3) (23). Based on overexpression of proteins like RAG-1, RAG-2, IL-7 and Pax5, B cell receptor gene in the pro- B cell undergo somatic recombination (24). This process is popularly called VDJ recombination. Certain gene segments called variable (V), diversity (D) and joining (J) segments which are found within the immunoglobulin heavy chain (IgH) locus undergo rearrangement in order to generate variation in the receptor structure (24). In case of productive rearrangement, the pro- B cells mature to pre- B cells which carry pre-B Cell Receptors (pre-BCR) on their surface. The pre-BCR is comprised of a rearranged heavy chain and a surrogate light chain (shown as split bar in Figure 3) which in turn is composed of two different protein called $\lambda 5$ and V_{preB} . Before developing further, pre-B cells are subjected to surveillance. As a first surveillance measure, the functionality of the pre-BCR is checked. Upon crosslinking of pre-BCRs to the surface of stromal cells, pre-BCR signalling is initiated which results in cell proliferation and subsequent down-regulation of the surrogate light chain and *rag1/2* genes (25). Also pre-B cells migrate away from IL- 7 expressing stromal cells and stop responding to IL-7 and hence stop dividing (24). Subsequently, somatic recombination of the Ig light (IgL) chain is initiated and only V and J segments are rearranged, therefore the process is called VJ-recombination. Productive rearrangement of these segments gives rise to a functional BCR complex which is necessary for cell survival and further development of the immature B cell.

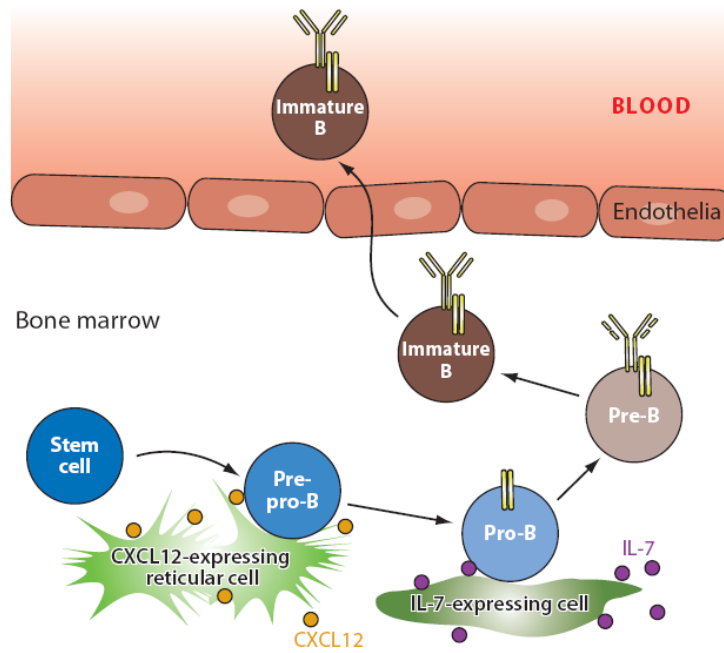


Figure 3: B cell development. A model of the movement of early B cells as they develop in the bone marrow. Figure adapted from (24).

As a second surveillance measure, the BCR is probed for recognition by self-antigens (23). Upon recognition of self-antigens, the cell ceases to develop and undergoes apoptosis. In order to circumvent this, a process called receptor editing comes into action. This changes the specificity of the BCR from self to non-self through somatic gene rearrangement in the IgL chain (26). Subsequently, the immature B cells leave the bone marrow and reach the spleen through the blood stream. Further differentiation and homeostasis of B cells is dependent on BCR signalling and B cell activating factor belonging to the TNF family mediated environmental survival signals (24).

1.4 Apoptosis and autophagy in lymphocytes

Lymphocytes are subjected to a variety of stress and stimulation throughout their life span from development to death. Upon receiving a signal at the early stages of their development, lymphocytes are subjected to decisions which will decide about their survival or death. Apoptosis and autophagy are two major processes which mediate these decisions. Since the proteins of study in this thesis are associated to both apoptosis and autophagy in lymphocytes, an overview of these processes in lymphocytes is discussed below.

1.4.1 Autophagy

At first, autophagy is a major intracellular degradation process through which cytoplasmic materials are delivered to and degraded in lysosome. It involves the generation of a double-membraned structure, sequestration of various cytoplasmic components and delivery of bound cellular matter to lysosome (27, 28). However, the purpose of autophagy is not only elimination of materials, but it also serve as a dynamic recycling system that produce new building blocks and energy for cellular renovation and homeostasis. In yeast, at least 35 Atg (autophagy) proteins are identified (28). The main components of this machinery are Atg1–10, 12–14, 16, 18; these are called the ‘core Atg proteins’ (29). These proteins are required for autophagosome formation, in addition to Atg17, 29, and 31. The core Atg proteins act in a similar hierarchical manner in both yeast and mammals as they are highly conserved among eukaryotes (30, 31). The Atg proteins are grouped into several functional units, including the Atg1/ULK (unc-51- like kinase) complex, the class III phosphatidylinositol 3-kinase (PI3K) complex, and the Atg12 and Atg8/LC3 conjugation systems. (Figure 4)

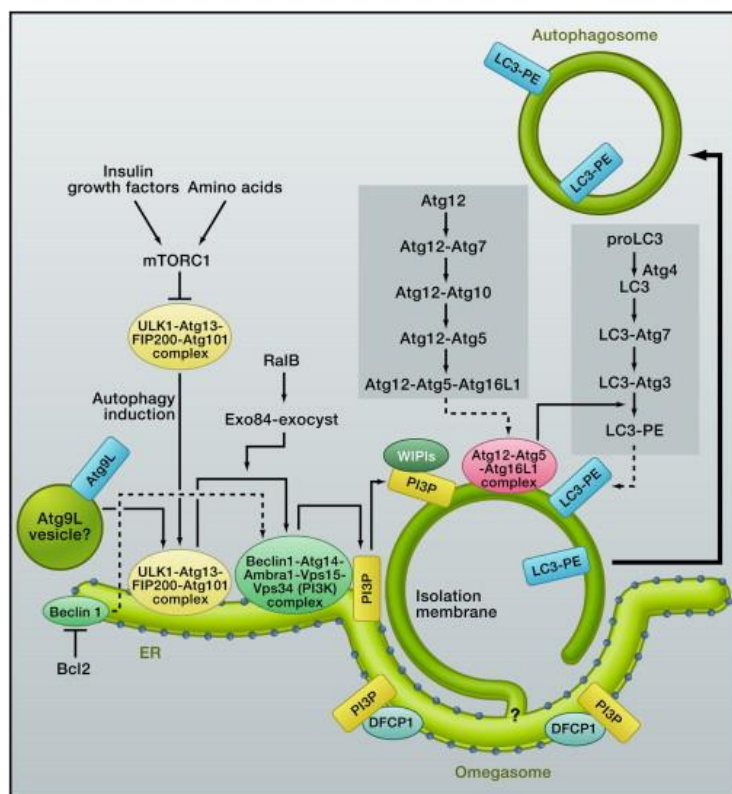


Figure 4: Autophagic pathway. Model for autophagosome formation and maturation in mammalian cells (32).

Starvation or induction of autophagy lead to the inhibition of protein kinase target of rapamycin (TOR) which in turn result in activation of the Atg1/ULK complex and class III PI3K complex. The class III PI3K complex generate phosphatidylinositol 3-phosphate (PI3P) at the site of autophagosome formation, which is termed the pre-autophagosomal structure (PAS) in yeast and probably corresponds to the ER-associated omegasome in mammals. An ubiquitin-like conjugation system act downstream on the Atg members to execute autophagy. Further downstream, Atg12 is activated by the E1-like enzyme Atg7 and subsequently transferred to its target Atg5 via the E2-like enzyme Atg10. Atg12 finally interact with Atg16 and form a complex which is a marker of the PAS and the expanding phagophore. This Atg12 conjugation system is coupled to the Atg8/LC3 system. Atg8 and its mammalian orthologues are synthesised as precursor proteins with additional amino acids at their C-termini. Atg4 proteolytically cleaves the additional amino acids yielding truncated products (form I) with a conserved terminal glycine residue. Upon further activation by E1-like Atg7 and E2-like Atg3 downstream, Atg8/LC3 gets covalently linked to phosphatidylethanolamine (PE) resulting in the membrane associated protein-phospholipid conjugate (form II) which is a potential marker of autophagy. Figure 4 summarizes their functional steps in mammalian cells. The detailed description of the whole mechanism of autophagy can be found in (32).

1.4.1.1 Autophagy in lymphocyte development

In this paragraph, the role of autophagy in lymphocytes will be discussed. Despite limited by cytosolic volume and rather small size (10-20 μM), lymphocytes form the core component and mediators of the adaptive immune system. They also express autophagy genes, including Vps34, Atg3, Atg5, Atg7, Beclin-1, LC3, and p62 (33, 34). Generally, all eukaryotic cells studied so far exhibited autophagy but the signal of induction and the levels of autophagic flux vary widely in different cell types. For instance, thymic epithelial cells have high basal level of constitutive autophagy (35) whereas mature naive T lymphocytes display very low level of constitutive autophagy. In general, starvation of either serum or nutrients induce moderate level of autophagy in most cell types, whereas stimulation of several immunity-related receptors, such as the TCR or Toll-like receptors (TLRs), convey potent autophagy induction signals. Autophagy also provide an alternative source of nutrients scavenged from the cytoplasm, and a major pathway for intracellular remodelling to reflect changes in the developmental or metabolic requirements of the cell (27). For instance, T cells utilize autophagy in order to meet the high energy demands during activation and proliferation (36).

Constitutive high levels of autophagy in thymic epithelial cells are necessary for optimal processing and presentation of endogenous antigens, and required for proper positive (17) and negative selection (37) of developing thymocytes. Autophagy also promote survival of B lymphocytes as well as the development of early B-cell progenitors. It was shown that Atg5 is required for efficient B cell development and for the maintenance of B-1 B cell numbers. Deletion of ATG5 in B lymphocytes lead to dramatic reduction in B-1 B cells in the peritoneum. ATG5^{-/-} progenitors exhibited significant defect in B cell development at the pro-to pre-B cell transition. Inefficient B cell development in the bone marrow was associated with increased cell death, indicating that ATG5 is important for B cell survival during development. To conclude, autophagy play a complex role in lymphocytes development and homeostasis during their lifespan to ensure a healthy immune system.

1.4.2 Apoptosis

Apoptosis is an indispensable cellular pathway necessary for proper development and homeostasis of cells. Apoptosis is induced by both normal and pathologic stimuli and any imbalance in this pathway has been associated with human diseases, including autoimmunity, cancer, and immune deficiency. Apoptosis result in activation of a protease family known as caspases that exist as zymogens (38). Activated caspases may activate other caspases as well as other enzymes that cleave a variety of intracellular proteins to promote apoptosis (39). Many of these proteases are present under normal physiological condition as proenzymes that are only activated in appropriate cellular context during development or upon cellular stress. In humans, cell death downstream of death signals is regulated by two molecular pathways, both of which leads to caspase activation.

The extrinsic pathway is triggered by oligomerization of death receptors upon binding of death ligands such as Fas. This oligomerization leads to the recruitment of Death Inducing Signaling Complex (DISC) (Figure 5A) (40, 41). The DISC further recruit and activate Caspase-8 to act downstream. In the absence of death ligand, cellular FLICE (FADD-like IL-1 β -converting enzyme)-inhibitory protein (c-FLIP) bind to DISC and inhibit the activation of caspase-8. Upon its activation, downstream effector caspases, such as Caspase-3, gets activated and mediate proteolysis of variety of other substrates including other caspases and cytoskeletal proteins like actin and nuclear lamins. Inhibitor of Caspase Activated DNase (ICAD) is one of the primary target of the effector caspases. Cleaved by caspase-3, ICAD release CAD to initiate DNA degradation in the nucleus, ultimately leading to cell death (42). The intrinsic

pathway of apoptosis is executed with the involvement of mitochondria and Bcl-2 (B cell lymphoma) family of protein (43) (Figure 5B). BCL-2 family members comprise major regulators of intrinsic pathway. They consist of pro- and anti-apoptotic members and carry conserved domain denoted as BCL-2 homology (BH) domains numbered BH1–4. Anti-apoptotic family members (Bcl-2, Bcl-XL, A1 and Mcl-1) are highly conserved and contain four BH domains. The pro-apoptotic members (BAX, BAK, and BOK) possess the BH1–3 domains. In contrast, the ‘BH3-only’ subset of pro-apoptotic members (BID, BAD, BIM, BIK, BMF, NOXA, and PUMA) carry only the minimal BH3 domain. BH3-only proteins are attractive candidates in controlling apoptosis as they are dynamically regulated by several mechanisms including transcriptional and post-translational control (44)

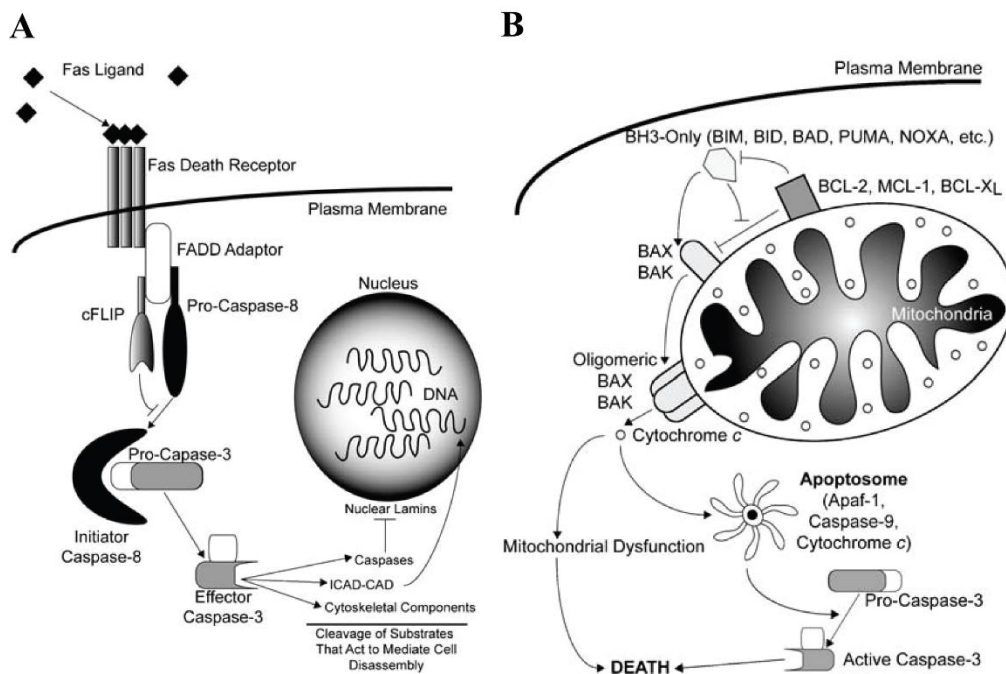


Figure 5: Apoptotic pathway. A) Death receptor mediated extrinsic apoptotic pathway. B) Bcl-2 family mediated intrinsic apoptotic pathway. Figure adapted from (45).

Upon activation by death signals, activated BAX and BAK oligomerize at the mitochondrial surface which results in permeabilization of the outer membrane and release of cytochrome c (Figure 5B) (46). Upon release from the mitochondria, cytochrome c associate with APAF-1 and Caspase- 9 to form the ‘apoptosome’, which trigger activation of downstream cascade of effector caspases (47). These caspases coordinate proteolytic cleavage of key cellular proteins leading to controlled cell death. BH3-only molecules require BAX and BAK to mediate death and operate upstream of mitochondria connecting proximal death and survival signals to core intrinsic pathway. Anti-apoptotic family members function by

sequestering BH3-only molecules in stable complexes, preventing the activation of BAX and/or BAK or by directly antagonizing BAX and BAK (48-50).

1.4.2.1 Apoptosis in lymphocyte development

Apoptosis play an active role in lymphocyte development starting at very early stages of differentiation till the development of mature and functional lymphocytes. During maturation, lymphocyte undergo several process which are highly selective and specific which result in elimination of majority of developing lymphocytes (51). Developing lymphocytes exhibit extensive rearrangement at genetic locus of antigen receptors to generate highly diverse antigen repertoire. Despite tight regulation of this process, majority of lymphocytes fail to generate functional antigen receptors and are thus eliminated by apoptosis (52, 53).

With regards to T cell, apoptosis act at every stages of its development. As explained earlier, Common lymphoid progenitor (CLP) cells migrate from bone marrow to thymus to undergo maturation. This process is tightly regulated through apoptosis to maintain homeostasis and prevent generation of autoreactive T-lymphocytes. Transition during DN1 and DN2 stages are regulated by Interleukine-7 signalling (cytokines signalling) to mediate survival and differentiation. For instance, downstream signal from IL-7 pathway induce anti-apoptotic member Mcl-1 promoting further development of the cells. In addition to that, absence of IL-7 signal and presence of a pro-apoptotic BIM lead cells towards apoptosis (54). Further on, pre-TCR signalling promote survival and differentiation from DN3 to DN4 stage. Induction of anti-apoptotic Bcl-2 member through NF- κ B signalling cascade lead to survival of developing lymphocyte which acquire a completely functional TCR on its surface and enter double positive (DP) stage (55). The DP cells are then subjected to positive and negative selection. During negative selection, signals through TCR may induce pro-apoptotic BIM via the action of serine-threonine kinase misshapen-Nck-interacting kinase (MINK) (56). Those cells that react optimally with self-MHC molecule are positively selected and downregulate either CD4 or CD8 and become mature single positive (SP) T cells.

With respect to B cell development, common lymphoid progenitors (CLP) undergo development within bone marrow into B-cell progenitors. As in case of T cell development, early pro-B-cells are dependent on IL-7 cytokine signalling for their survival. Successful rearrangement of the pre-BCR complex is tested in pre-B-cells. Those cells which do not acquire productive BCR rearrangement are eliminated through apoptosis. pre-BCR expressing cells undergo rearrangement of Ig light chain and express surface-bound BCR and are now

called immature B cells. Immature B cells expressing autoreactive BCR are directed to undergo apoptosis with help of pro-apoptotic BIM. Members of TNF family play critical roles in regulating maturation of B cells. Additionally, B-cell activating factor BAFF (also widely known as BLyS) is a TNF-related ligand that are implicated in B-cell development (52). It was shown that transgenic BAFF expression caused accumulation of immature and mature B cells (57). BAFF signalling induced NF- κ B signalling cascade and in turn upregulate the anti-apoptotic Bcl-2, Bcl-X and Mcl-1 (58, 59) leading to maturation of competent B cells.

1.5 GTPase

GTPases, also referred to as G proteins, are a family of hydrolase enzymes that can bind and hydrolyse guanosine triphosphate (GTP) (60). Members of G protein family are crucial players in cellular functions like protein synthesis, hormone signalling, vision, cell proliferation and intracellular trafficking (61). G proteins bind GTP in its characteristic G-domain and hydrolyse it to GDP. As of 2011, a total of 37,767 proteins containing GTP binding domain (<http://supfam.org>) have been identified in 1,383 genomes and they are found in all three major kingdoms of life with a strong bias toward eukaryotes (62). According to Leipe *et al.* (63), superclass of G protein is broadly divided into the TRAFAC (Translation Factors) and SIMBI (signal recognition, MinD, and BioD) class. Translation factors, heterotrimeric G proteins, the Ras superfamily, septins, and dynamin superfamily are some of the notable members of TRAFAC class whereas SIMIBI class include signal recognition particle (SRP), its receptor SR, and a few other families. G-proteins are also extensively studied using structural biology techniques. There are more than 500 structures solved and deposited in the Protein Data Bank (PDB) (62). The main focus of this thesis is a family of G-proteins which belong to TRAFAC class and is named GTPases of IMMunity Associated Proteins (GIMAPs). They will be introduced in detail in forthcoming sections. As representative examples of this very large superfamily, one family acting as molecular switch (Ras GTPase) and one acting as membrane modulators (septins) will be described in the following sections.

1.5.1 Ras GTPases

The Ras superfamily consist of over 150 members. It is classified into subfamilies such as Ras, Rab, Rho, Rap, Arf, Ran, Rheb, RGK, Rit and Miro (64). Ras subfamily proteins are activated in response to many extracellular stimuli. Activated Ras interact with effector

proteins that regulate cytoplasmic signalling networks controlling gene expression leading to cellular proliferation, differentiation and survival (64)

The founding member of Ras subfamily, Ras (**Rat Sarcoma**) is used here as a representative example for the whole superfamily. Ras superfamily members are also called small GTPases. These small GTPases have molecular weight of about 21 kDa and carry typical G-domain which act as molecular switch (Figure 6A). The GDP-bound form is generally considered inactive while the GTP-bound form to be active since it activates downstream pathways by binding to effector proteins which in turn regulates cellular functions. In general, GTP hydrolysis is a slow process which requires GTPase activating proteins (GAPs). It results in tightly bound GDP which is turn interact with guanine nucleotide exchange factors (GEFs) facilitating GDP dissociation (65).

The structure of Ras protein gave fundamental insights into 3D structure of G proteins. The G domain (for Guanine nucleotide binding) of Ras consist of 166 amino acid residues and fold into a central curved six-stranded sheet, surrounded on either sides by five -helices (Figure 6C). The G domain provides an efficient platform for nucleotide binding by appropriate spatial arrangement of five loops which contain highly conserved sequence motifs, G1-G5 (Figure 6B). The G1 motif is also called the P loop (for phosphate binding) which is recognized by the sequence GxxxxGKS/T (66), originally termed the Walker A motif (67). G2 (xTx) has only a Thr which is highly conserved, and G3 has the sequence DxxG. G4, the N/TKxD motif is the major determinant of guanine base-binding specificity. G5 is also involved in binding guanine base and has the sequence motif SAK which is weakly conserved (62).The loop regions between helix 1 and strand 2 and between strand 3 and helix 2 are called switch I and II, respectively and are crucial for conformational switch mechanism

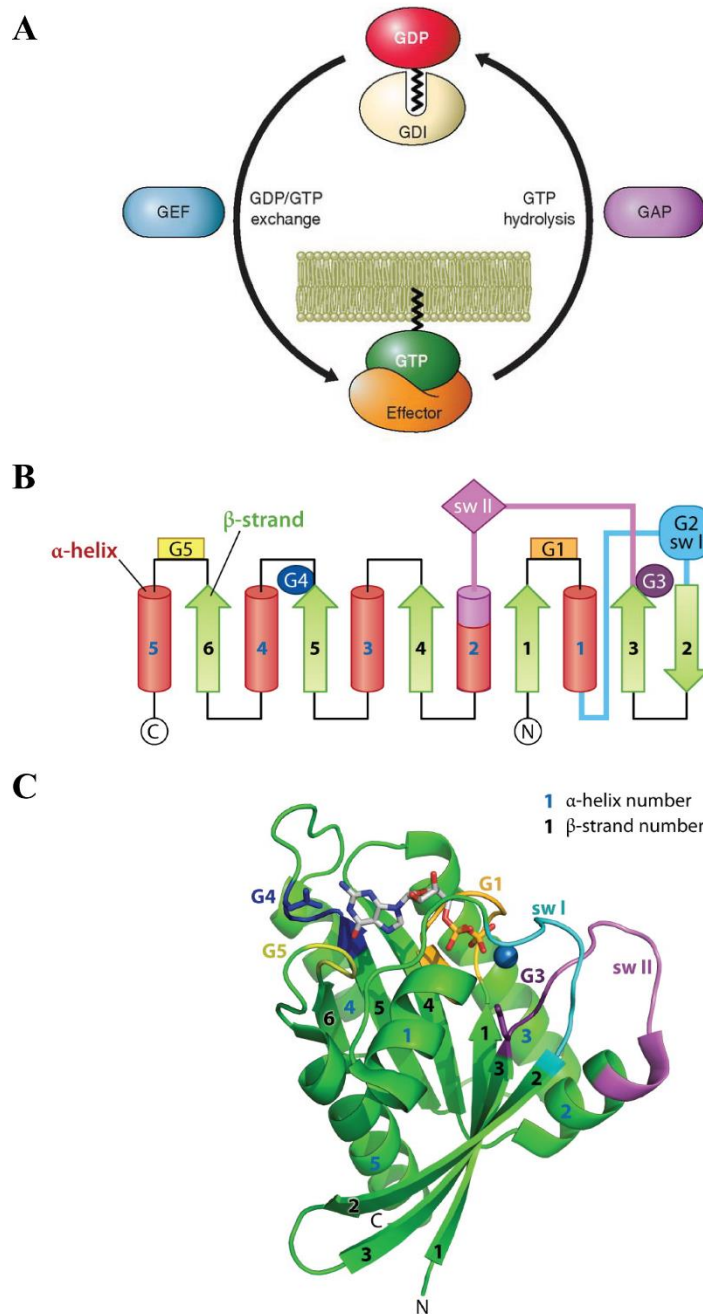


Figure 6: The GDP/GTP switch and crystal structure of Ras bound to GppNHp•Mg²⁺A) GEFs, GAPs regulate GDP/GTP switch. Small GTPases are activated by GDP/GTP exchange stimulated by GEFs (blue) and inactivated by GTP hydrolysis stimulated by GAPs (violet). Figure adapted from (68). B) Topology diagram of G domain with β -strands in green, α -helices in red, N- and C- termini as indicated. C) Cartoon representation of structure of Ras G domain in nucleotide bound state. The G domain is shown in green with G1 motif in yellow, switch I in cyan, switch II and G3 motif in shades of magenta, G4 in blue and G5 in gold yellow. The nucleotide is represented as sticks. α helices are numbered in blue and β strands in black. Figure B and C adapted from (62).

1.5.2 Septin

Septins comprise a family of GTP binding proteins classified under the TRAFAC subfamily (63). They were identified in budding yeast, *Saccharomyces cerevisiae* and found to be involved in cell division (69). They form ring-like structures around the neck between mother and bud in the dividing yeast (70). Septins are also implicated at sites where cilia and flagella attach to the cell body (71). Recently, it was shown that septins form a cage around bacterium in cells restricting their migration to other cells (72). Because of their filamentous appearance and its association with membranes, microtubules and microfilaments, septins are also ascribed as a cytoskeletal component (73). Septins form higher order oligomers and assemble into filaments and rings (74). It was proposed that such assembled filaments of septins act as a scaffold for localization of effector proteins. Sequence analysis revealed the presence of homologous proteins in all nearly all eukaryotes, but not in plants. In humans, the septin family consist of 13 members namely, SEPT1-SEPT12, and SEPT14, whereas SEPT13 is a pseudogene (75). Septins in general consist of three conserved domains, a phosphoinositide-binding polybasic region, G domain and a unique septin element flanked by N-terminal proline rich domain and C-terminal coiled coil domain (Figure 7). The length and sequence of the N- and C- terminal vary among septins.

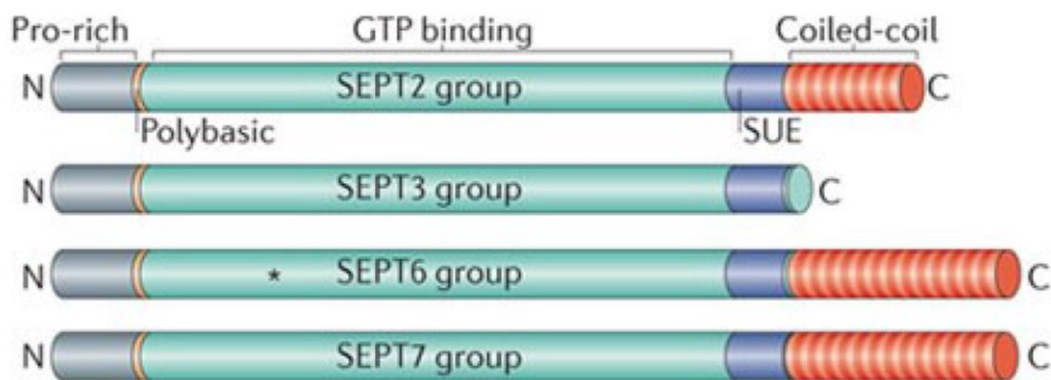


Figure 7: Domain architecture of septins. Human septins are categorized into four groups namely SEPT2, SEPT3, SEPT6 and SEPT7 based on their sequence similarity and named after their founding members. Figure modified from (73).

Structural studies performed on septins provided insights on mechanism of their oligomer formation. GDP-bound septin2 resembled canonical Ras G domain, with a central β sheet flanked by α helices. However, it also possessed additional structural elements like N-terminal helices α_0 , $\alpha_{5'}$ between α_4 and β_6 , the two anti-parallel strands β_7 and β_8 , and C-terminal helix α_6 (Figure 8) (74). Septin2 formed homo-dimers in the GDP bound form via the

'G' and 'NC' interface. The G interface is formed via nucleotide binding interface of opposing monomers whereas the NC interface is mediated by both N- and C-terminal helices. Mutational analysis revealed that septin-2 most likely associated with the G interface in solution. Additionally, septin formed heteromeric complexes with each other. To characterize this assembly mode, the crystal structure of a heteromeric human septin complex consisting of septin2-septin6-septin7 was solved, which resulted in molecular insights into the oligomerization mode of septins via the conserved G and NC interfaces (74)

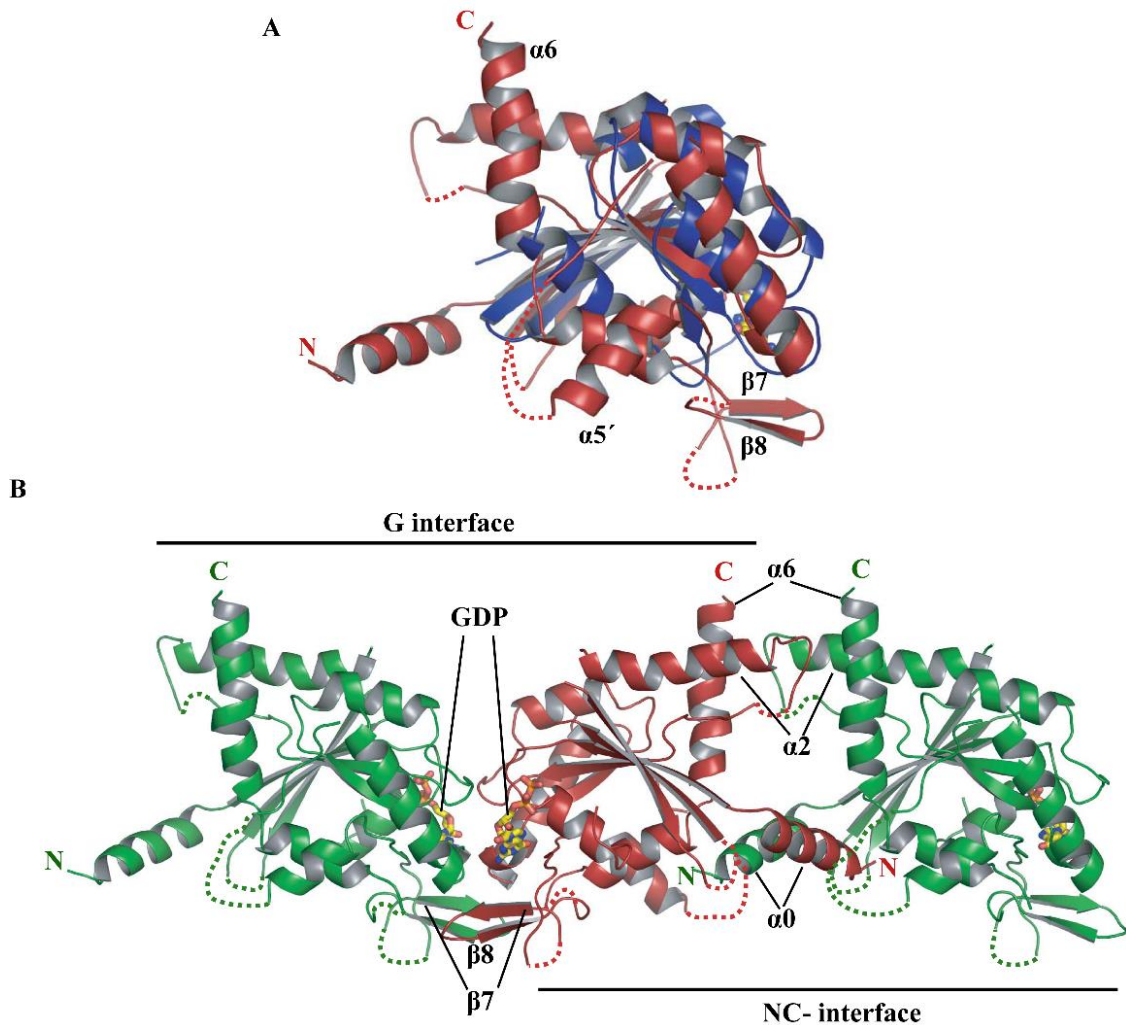


Figure 8: Crystal structure of septin A) Superimposition of septin2 (red) and Ras in GppNHp bound form (blue) (PDB: 121P). Additional septin specific secondary structural elements are numbered. B) Homodimer of septin (shown in green and red). Septin dimerized via two interfaces, which were named the G- and NC-interface. The secondary structural elements involved in the interfaces are marked. Figure modified from (74).

1.6 GTPases of IMMunity-Associated protein – GIMAP

GIMAPs, GTPases of IMmunity-Associated Proteins are a family of poorly understood GTPase which are sporadically found in plants (76), animals (77), and organism like molluscs and protists (78). As introduced in section 1.5, G proteins are broadly classified into TRAFAC and SIMBI classes. GIMAPs belong to TRAFAC class of G proteins. Among TRAFAC class, GIMAPs and Toc family form a distinct clade and are assigned to paraseptin subfamily (63) (Figure 9).

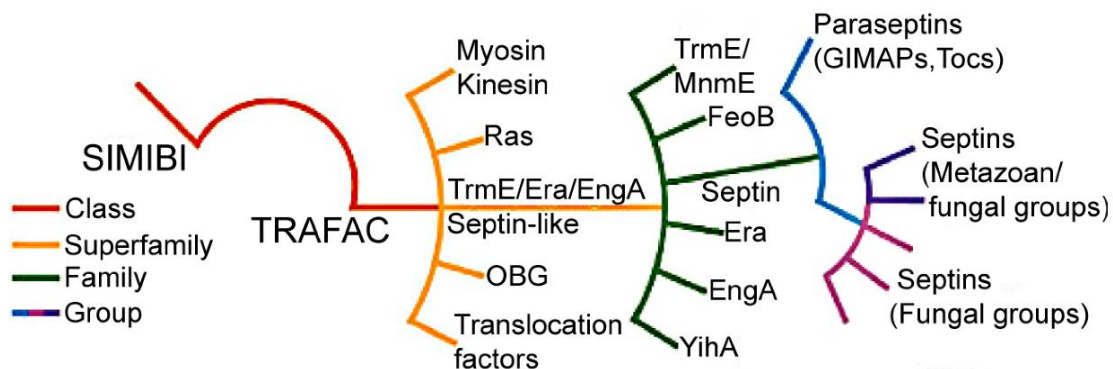


Figure 9: Classification of G protein superfamily. GIMAPS and Tocs are classified under paraseptins. Figure adapted from (75).

Toc (translocon on the outer chloroplast membrane) proteins are also a class of GTPases constituting the TOC complex which is located on outer membrane of chloroplast and are responsible for import of proteins across chloroplast membrane. (79). Septins are a group of G-proteins found primarily in fungi, animals and in some green algae (75, 80). Septins form complexes and assemble into filaments, rings and scaffolds. Such assembled septins act as a molecular platform for assembly of other interacting protein in order to carry out cell division, cytoskeletal dynamics and secretion (75). For instance, it was shown in budding yeast that septins assembled along the bud neck in a ring conformation and in turn served as a scaffold for the interaction partners. The GIMAP family of proteins were formerly known as IANs for Immunity Associated Nucleotide binding proteins. Lately, the GIMAP nomenclature has been widely accepted (81) and therefore will be adopted in this study.

1.6.1 Discovery and domain architecture

The GIMAP gene was discovered in *Arabidopsis thaliana* (76). Upon infection of plant with a virulent strain of *Pseudomonas syringae*, *avrRpt2* induced gene (*AIG*) was found to be overexpressed. The expressed protein contained a domain which exhibited high similarity towards G domain of guanine nucleotide binding proteins (82) and was subsequently named as AIG1 domain. An avirulent infection model revealed rapid and transient expression of AIG1 as part of hypersensitive reaction (analogous to immune response in mammals) and lead to onset of apoptosis at the site of infection. This suggested that AIG1 domain containing proteins are involved in defence mechanism or immunity in plants when challenged with bacterial infection. The prototype gene discovered in mice was *Gimap1* which was found to be induced upon infection with experimental malaria causing *Plasmodium chabaudi* strain and its expression is associated with development of immunologic memory against homologous secondary challenges (83). In humans, the prototype gene described was also *GIMAP1* and was found to be expressed in resting T and B lymphocytes (84, 85).

In humans, GIMAP family genes are organised in chromosomal clusters and are encoded by a single locus on chromosome 7 (86) whereas in mouse, they reside on chromosome 6 (78). The human chromosomal region 7q36.1, within about 300 kb, display 10 distinct sequences encoding the AIG1 GTP binding domains 11, 10, 9, 7, 1, 6, 12, 2, 5, and 4 from proximal to distal direction (87). It was therefore suggested that about 10 human *GIMAP* genes existed (Figure 10).

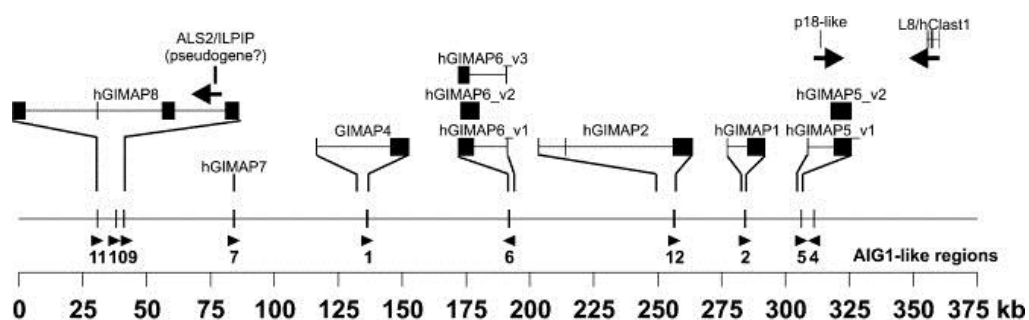


Figure 10: Genomic organisation of human *GIMAPs* on chromosome 7. Exon/intron structure of the coding region on the chromosome are shown along with distribution and designation of regions with similarity towards AIG1. Figure modified from (86).

It was later revealed that there are only seven distinct human *GIMAP* genes namely *GIMAP1*, *GIMAP2*, *GIMAP4*, *GIMAP5*, *GIMAP6*, *GIMAP7* and *GIMAP8*. Human *GIMAP3* is a pseudo gene and *GIMAP8* carries three consecutive AIG1 domain (encoded by sequence

numbered as 11, 10 and 9). The genomic organisation of mouse *Gimap* is similar to the human. However, mouse has a functional *Gimap3* which is ortholog to the human pseudogene *GIMAP3*. Additionally it lacks an ortholog to human *GIMAP2*.

Since this thesis deals with only human GIMAPs, the domain architecture of the human GIMAPs will be elaborated here in detail. The encoded proteins have molecular mass varying from 33 to 75 kDa and are comprised of an N-terminal G domain containing a GIMAP-specific signature motifs, the conserved box (CB), followed by distinct C-terminal extensions (Extn.) of 60-130 amino acids length. The 75 kDa GIMAP8 differ in carrying three consecutive GIMAP-specific G domains. GIMAP1, GIMAP2 and GIMAP5 have one or two additional hydrophobic amino acid sequences (HS) at their C-terminal helix that are responsible for membrane association (Figure 11).

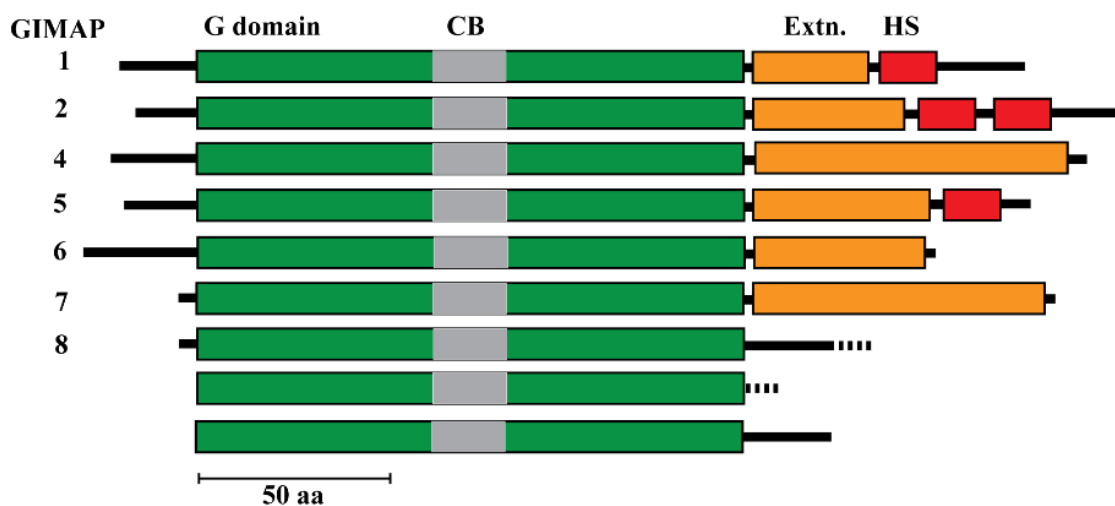


Figure 11: Domain architecture of human GIMAPs. G domain is interspersed by conserved box (CB) followed by C terminal extension (Extn.) and some GIMAPs terminate with hydrophobic sequences (HS). The bar corresponds to the length of 50 amino acids (aa).

Based on the presence of hydrophobic sequences, GIMAPs can be classified into membrane-associated (GIMAP1, GIMAP2 and GIMAP5) and cytosolic GIMAPs (GIMAP4, GIMAP6, GIMAP7 and GIMAP8). Even though human GIMAPs share similar domain architecture, slight variations exist. For instance, GIMAP6 has the longest disordered N terminal region whereas GIMAP4 and GIMAP7 have the longest C terminal extensions. GIMAP2 has two distinct hydrophobic sequences for membrane association. Sequence analysis of GIMAPs exhibited all conserved motifs found in typical G domain. All G motifs, namely the G1-G5 motifs were identified and in addition to it some GIMAP specific sequence elements were found. The conserved sequences of these motifs and their role in nucleotide binding could be

recollected from section 1.5.1. The G motif sequences from all GIMAPs are as listed in Appendix A.

1.6.2 Expression and subcellular localization of GIMAP

Northern blot analysis probing for presence of GIMAP specific mRNA were performed in several human tissues in order to decipher expression pattern of human GIMAPs (86). This comprehensive expression study unequivocally proved that human GIMAPs are predominantly expressed in tissues of immune system such as spleen, lymph nodes and to a lesser extent also in thymus, heart and lung (Table 1). GIMAPs also showed differential subcellular localization which is summarized in Table 1.

Human GIMAP	Molecular weight (KDa)	Organ of expression	Subcellular localization
GIMAP1	34.4	↑ Spleen, and lymphocytes and lymph node	ER (Over expression in CHO-K1 cells) (85)
GIMAP2	45.4	↑ Spleen, lymph node, peripheral leukocytes and thymus	Lipid droplets (Antibody against endogenous protein in Jurkat cells) (88)
GIMAP4	37.5	↑ T cell, B cell, thymus, lymph nodes, placenta, prostate and testis	ER and Golgi (Over expression in CHO-K1 cells) (86)
GIMAP5	34.8	↑↑ spleen, lymph node, lung, placenta, liver, muscle and heart	Lysosome (Antibody against endogenous protein in Jurkat cells) (89)
GIMAP6	32.9	↑↑ Spleen, lymph node, lung and placenta. ↑ thymus, kidney, heart and digestive tract	Cytosol (Over expression in Jurkat cells) (90)
GIMAP7	34.5	↑↑ Spleen, lymph nodes, thymus, foetal kidney, heart and small intestine. ↑ lung, kidney, liver, thyroid, salivary and mammary glands	Diffused localization with lipid droplets (Over expression in Jurkat cells) (90)
GIMAP8	74.9	↑ Brain, thymus, bone marrow and leukocytes	Cytosol (Over expression in Jurkat cells) (90)

Table 1: Expression and localization of GIMAPs. GIMAPs showed differential expression with varying levels in specific tissues. ↑↑ represents a predominant expression in the tissue

whereas ↑ depicts a weaker expression (86). Localization of GIMAPs were confirmed by fluorescent confocal microscopy.

Recently, expression of all the GIMAPs at mRNA level was investigated by semi quantitative reverse transcriptase PCR in a panel of both T cell leukemia (Jurkat, KE-37, Molit-14 and H9) and Anaplastic Large Cell Lymphoma (ALCL) derived cell lines (K299, SU-DHL1, DEL, JB6, FE-PD, Mac-1, Mac-2A, DL-40). Purified CD³⁺ and CD⁴⁺ T cells from healthy donors were used as control. mRNA expression of all seven GIMAP family members were detectable in the control. Except GIMAP8 and GIMAP4 in KE-37 and Molt-14 respectively, all other GIMAPs were found to be expressed in all T cell lines. Strikingly, mRNA expression of most of the GIMAPs were disturbed, notably, expression of GIMAP7 and GIMAP4 was completely lost. Only expression of GIMAP2 was not altered, suggesting differing requirements of GIMAPs during oncogenic transformation (90).

Even though cellular functions of GIMAPs are not deciphered, several interesting facts have been established in the last decade relating to cellular role of GIMAPs. Most importantly, GIMAPs are implicated in development and maintenance of both T and B cells in mice and rat models (78). Several *Gimap* knockout mice and rat strains were generated in order to understand the phenotype it conferred on the host. It was also shown to interact with both anti-apoptotic and pro-apoptotic members of Bcl-2 family members, thereby regulating the survival and death of the cells in which they are expressed (91). The function of individual GIMAPs will be discussed in the following sections.

1.6.3 GIMAP1

Contradicting the previous report (83), it was shown that GIMAP1 was constitutively expressed in all lymphocyte lineages (92) and not expressed as a result of *Plasmodium chabaudi* challenge, thus revealing a definitive role in lymphocyte development. The up-regulation of GIMAP1 at mRNA level was demonstrated when T lymphocyte mature from DN to DP stage in mice and rat (91, 93) thereby establishing its role in thymocytes maturation. Quantitative proteomics revealed that GIMAP1 was downregulated when activated T cells differentiate into Type 2 T helper cells (94) by IL-4/STAT6 signalling pathway thus suggesting that expression of GIMAP1 is suppressed during the process.

A biochemical study on GTP binding ability of GIMAP1 suggested that it does not bind GTP by blotting GST-fused GIMAP1 on radio-labelled GTP (85). The same study,

however, revealed that mouse homolog (IMAP38) does bind to GTP. A conditional knock out model for GIMAP1 led to an unexpected discovery. It revealed that loss of GIMAP1 in mice lead to severe deficiency of both mature T and mature B cells. Loss of GIMAP1 affects both B and T lineages suggesting that it could be involved in the regulation of common survival pathways like the NF κ -B pathway rather than lineage specific pathways mediated by BAFF-R and IL-7R in B and T cells respectively.

1.6.4 GIMAP2

Apart from its localization to lipid droplets (LDs), it was shown that overexpression of GIMAP2 doubled LD numbers per cell in Jurkat T cells in a poorly understood mechanism (88). Lipid droplets are fat storage organelle which regulate storage and hydrolysis of neutral lipids in adipose tissue (95). The relationship between GIMAP2 and lipid metabolism is yet to be established. Being absent in mice and rat, the function of human GIMAP2 is poorly understood and requires further research.

1.6.5 GIMAP3

GIMAP3 is a pseudogene in humans and is absent in rat. In mice, *Gimap3* was discovered in murine 32D hematopoietic precursor cells and found to be induced in cells expressing BCR/ABL oncoproteins which are responsible for development of chronic myeloid leukemia (CML) (96). Apart from GTP binding motifs, GIMAP3 possessed C- terminal hydrophobic sequence stretches responsible for the localization to the outer mitochondrial membrane (96). Quantitative real time PCR analysis revealed that the expression of GIMAP3 was highly elevated during differentiation of double-positive (DP) into single-positive (SP) thymocytes (91). Additionally, co-immunoprecipitation assays showed association of GIMAP3 to both anti-apoptotic and pro-apoptotic Bcl-2 family of proteins suggesting that GIMAP3 might relay TCR signals for apoptosis regulation by the Bcl-2 family members (91). GIMAP3 is implicated in segregation of mitochondrial DNA in ALB/c and CAST/Ei mouse strains (97). More recently, *Gimap3* knockout mice revealed that the number of T cells were not disturbed even though a double knockout of *Gimap5* and *Gimap3* showed reduced cellularity compared to the single knockouts (98). This indicated that GIMAP3 complements the function of GIMAP5 in maintaining T cell numbers. Also, bone marrow cells from *Gimap3*-deficient mice showed reduced T-cell production in competitive hematopoietic environment. Furthermore,

retroviral overexpression of GIMAP3 in bone marrow elevated the number of T cells whereas shRNA mediated silencing reduced T cell numbers (98) suggesting that GIMAP3 is a critical regulator of T cell number in mice.

1.6.6 GIMAP4

An mRNA differential display technique led to identification of *Gimap4* gene, the first gene to be described in GIMAP family in mice. *Gimap4* is induced upon positive selection and predominantly expressed in lymphoid system. Protein expression analysis revealed that GIMAP4 play a crucial role in thymocytes development (77). Biochemical studies showed that GIMAP4 bound GDP and GTP with a K_d of 0.47 μ M and 6 μ M, respectively (84), and also hydrolysed GTP. Mice model suggested that expression of GIMAP4 is induced in DN stage (99). It was found to be expressed during DN, not in DP, but again in the SP stages of lymphocyte development (100). Additionally, overexpressed GIMAP4 in DN stage thymocytes increased apoptotic rate in DP cells. The same study also revealed that GIMAP4 co-immunoprecipitated with pro-apoptotic Bax and was implicated in negative selection (91). Lymphocytes isolated from *Gimap4* knockout mice show increased resistance to apoptotic stimuli, suggesting a pro-apoptotic function of GIMAP4 (99).

A severe *Gimap4* deficiency was discovered in inbred Brown Norway (BN) rat. Genetic analysis linked this trait to *Gimap* gene cluster in rat chromosome 4 (100). The likely cause for this is an AT dinucleotide insertion in the BN *Gimap4* allele (AT (+)). This allele encode a truncated *Gimap4* which lack 21 C-terminal residues when compared to wild type. In a yet to be identified mechanism, 95% reduction in GIMAP4 expression at the protein level was observed, whereas the mRNA levels remained undisturbed. T cells from BN rats showed delayed apoptosis phenotype but milder compared to that of GIMAP4 knock out mice. This phenomenon could be attributed to the fact that the BN rat is a hypomorph for GIMAP4 and not a total knockout (100). In addition to that, GIMAP4 is also implicated in activation of both B and T cells, since down regulation of GIMAP4 at protein level was found upon *in vitro* stimulation of isolated human lymphocytes (84). A quantitative proteomics analysis revealed that GIMAP4 is down-regulated during differentiation of activated T cells to T helper 2 cells (101) there by linking IL4/STAT6 signalling cascade. Additionally, it was also revealed that GIMAP4 could be induced by IL-7 (102). Finally, it was shown that the expression of GIMAP4 is under the control of PHF11 (PHD (plant homeodomain) finger like 11) which is a transcriptional co-activator of the NF κ B pathway (103).

1.6.7 GIMAP5

GIMAP5 is probably the best studied GIMAP member and is known to be involved in the maintenance of T cells (91). Functional studies of GIMAP5 in both animal models and cell lines have established a definitive role in maintenance of the T lymphocyte lineage. A prominent animal model of GIMAP5 is the BioBreeding (BB) rat model. BB rat spontaneously develop insulin-dependent diabetes similar to human type I diabetes (104). They exhibit T cell lymphopenia where peripheral single positive T lymphocytes are reduced. A frameshift mutation in *Gimap5* was identified in BB rat which resulted in truncated protein and was found to be responsible for the observed T lymphopenia (87, 105-107). The BB rat also showed premature death of peripheral T cells and reduced numbers of SP thymocytes (104, 108-110). SP thymocytes and peripheral T cells from BB rat showed accelerated apoptosis in cell culture suggesting that GIMAP5 deficiency led to increased vulnerability towards apoptosis (111-113). In positive selector DP thymocytes, GIMAP5 was found to be elevated during positive selection (91). Interestingly, *Gimap5* knock out mice imitated the lymphopenic phenotype of BB rat but did not develop type I diabetes and died after 15 weeks probably due to liver failure (114). Contrary to this findings, transplantation of *Gimap5*^{-/-} bone marrow in a healthy wild type animal did not recapitulate the BB rat phenotype suggesting the lymphocyte environment also contribute to the lymphopenic and diabetic phenotype (115). Furthermore, knockdown of *Gimap5* in developing thymocytes disturbed the generation of DP thymocytes. GIMAP5 showed specific interactions with pro- and anti-apoptotic proteins like Bax, Bcl-2 and Bcl-xL in immunoprecipitation (IP) assay (91). Furthermore, co-IP of endogenous Bcl-2 and Bcl-xL with GIMAP5 established a genuine role of this interaction. Recently, mice models lacking *Gimap3*, *Gimap5* or both were generated. The T cell number of *Gimap3* deficient mice was not affected but when both *Gimap5* and *Gimap3* were disrupted, there was a severe loss in T cell numbers which was higher than that in *Gimap5* single knockout mice. This showed that GIMAP5 together with GIMAP3 participated in the regulation of T cell number (98).

Another GIMAP5 deficient mouse model called *sphinx* carries G38C mutation in the P-loop which leads to an unstable protein and result in a phenotype resembling that of GIMAP5 knock out mice (116). *Sphinx* mice showed defects in both T and B cell lineages. B cells generated from *sphinx* mice were incapable of generating antigen-specific antibody responses despite an intact B cell receptor signalling. Also cell cycle was arrested in S phase in B cells suggesting a novel mechanism connecting B cell responses and cell cycle progression (116). Additionally, GIMAP5-deficient rat exhibited spontaneous intestinal inflammation associated

with elevated T cell activation (117). Interestingly, the intestinal inflammation in rat resembled that of the symptoms associated with human eosinophilic gastroenteritis. Furthermore a single nucleotide polymorphism (SNP) in *Gimap5* is associated with IA2-autoantibodies in the type I diabetes and systemic lupus erythematosus (118-120). However a genetic survey on patients from UK and USA did not establish any association between SNP found in GIMAP5 and the susceptibility to type I diabetes (121).

1.6.8 GIMAP6

GIMAP6 is a poorly characterized GIMAP, with no animal models existing to understand its biological function. A microarray study revealed that GIMAP6 is strongly downregulated in non-small cell lung cancer tissue samples from 6 patients, when compared to the surrounding non-tumour tissue (122). Also a recent microarray study implicated GIMAP6 in Johne's diseases in ruminants. The disease is caused by a bovine pathogenic strain of *Mycobacterium avium* subsp. *paratuberculosis* (MAP) and GIMAP6 was found to be downregulated when calves were challenged with MAP (123). Furthermore, a cell biological study confirmed the independent discovery of the interaction between GIMAP6 and an autophagy protein, GABARAPL2 during this doctoral work (124). Since the GIMAP6-GABARAPL2 interaction is extensively studied in this thesis, more information of GABARAPL2 is provided in the following paragraph.

GABARAPL2 is one of the mammalian homologues of yeast autophagy protein Atg8. The prototype Atg8 to be identified was the mammalian LC3B (formerly LC3). It associates with microtubule-associated proteins (MAPs) 1A and 1B (125) and is implicated in regulation of MAP1 binding to microtubule (126). LC3B in humans can be divided into two subgroups, namely LC3 and GABARAP family. The LC3 subfamily consists of LC3A, LC3B, LC3B2 and LC3C, whereas the GABARAP subfamily consists of GABARAP, GABARAPL1/GEC1, GABARAPL2/GATE-16 and GABARAPL3. All the members are ubiquitously expressed with moderate variations between different tissues (127). It could be recollected from section 1.4.1 that Atg8/LC3 is indispensable during the induction of autophagy and often has been exploited as the *bona fide* evidence of autophagy. It was reported that both endogenous GIMAP6 and GABARAPL2 readily associate under physiological conditions (124). Further on, it was revealed that the last 10 C-terminal amino acid residues in GIMAP6 are necessary but not sufficient for the interaction. Mutations in the G-domain (G50D, S54N, T76A, D95A and N98A) prevent the interaction whereas a mutation in the G4 motif (D167A) does not affect the

interaction. It was also confirmed that a putative LIR motif (for LC3 interacting region) or Atg-8 interacting motif (AIM) present at the N terminal end of GIMAP6 was not required for the interaction. Investigation of GABARAPL2 revealed that the first 10 N-terminal amino acids were sufficient for the interaction. Over-expression of GIMAP6 resulted in the elevation of endogenous GABARAPL2 expression in HEK293 cells suggesting that GIMAP6 regulates the cellular level of GABARAPL2. Interestingly, upon induction of autophagy either by starvation or mTOR kinase inhibition in Jurkat T cells, GIMAP6 was found to co-localize with GABARAPL2 suggesting that GIMAP6 is recruited to autophagosome upon induction of autophagy (124). Supporting this recruitment, GIMAP6 was found to be degraded over time along with the degradation of GABARAPL2. Thus, it was speculated that GABARAPL2 recruits GIMAP6 to autophagosome for its degradation in Jurkat cells. A detailed study of GIMAP6 in lymphocytes and its role in autophagy is required to understand its biological function completely.

1.6.9 GIMAP7, GIMAP8 and GIMAP9

Functional studies relating to GIMAP7, GIMAP8 and GIMAP9 are limited so far giving scope for further studies in identifying their roles in immune system maintenance. Nevertheless, a report revealed that the expression of GIMAP7 is reduced in thymocytes of both rat and mice (91, 93). Overexpression of GIMAP7 did not affect the LD number in Jurkat cells (90). Expression of GIMAP8 was found to be elevated in DP stage but lowered in mature SP rat thymocytes (93). Contrary to this, the level of GIMAP8 in mice was low in thymocytes but was elevated in splenic SP T cells (91). Also, the GIMAP8 mRNA levels in spleen were found to be 80% lower in mice infected with malaria parasite *Plasmodium chabaudi*. In addition to that, overexpression of GIMAP8 in fibroblasts seemed to exert an anti-apoptotic effect (128) suggesting a possible role in T cell maintenance. *Gimap9* gene is present only in mice and rats and its expression increased in positively selected thymocytes subsets (91).

1.7 Structure and biochemical function of GIMAPs

Detailed structural and biochemical studies have been carried out in our lab for human GIMAP2 (88) and GIMAP7 (90). These structures and the subsequent biochemical studies

revealed several interesting mechanisms related to nucleotide binding, dimerization modes and GIMAP scaffold formation on membranous structures.

1.7.1 GIMAP2

Construct of GIMAP2 (1-260) lacking the two C-terminal hydrophobic sequences (HS) was crystallized in both nucleotide-free and GDP-bound forms (88). The nucleotide-free structure revealed a typical G-domain with a central β -sheet sandwiched by 2 layers of α -helices. The domain also carried some GIMAP specific structural elements like helix $\alpha 3^*$ which is inserted between $\beta 5$ and the $\alpha 4$ helix, conserved box (CB) and a C-terminal extension comprising helices $\alpha 6$ and $\alpha 7$. Structural analysis revealed that helix $\alpha 6$ and $\alpha 7$ are unique to GIMAPs. They are located on the opposite face of nucleotide binding site. It is to be noted that $\alpha 7$ is linked to $\alpha 6$ via a highly disordered 16 amino acid linker and is in direct contact with switch II of G-domain (Figure 12) (88).

A construct of GIMAP2 (21-234) lacking helix $\alpha 7$ was crystallized in GTP bound state. Interestingly, it oligomerized via two interfaces, e.g. the G and C interface, in the crystals (Figure 12B). The G interface is formed between opposing G domains, with GTP bound at the interface whereas the C interface is formed by interaction of C terminals of the opposing monomers pointing pairwise in opposite direction (Figure 12B). The G interface is constituted by CB, switch I, G4 motif and $\alpha 3^*$ helix. A closer look into the G interface revealed that the conserved arginine finger and the exocyclic amino group from nucleotide base are involved in dimerization. The C interface is comprised of helices $\alpha 2$, $\alpha 3$ and $\alpha 6$ and upon deletion of $\alpha 6$, GIMAP2 was predominantly in the monomeric state reiterating the importance of $\alpha 6$ in the oligomerization process.

Removal of $\alpha 7$ resulted in stable dimerization. GDP bound GIMAP2 (21-260) (with $\alpha 7$ present) and GTP bound ($\alpha 7$ absent) GIMAP2 (1-234) structures were compared to observe the structural changes occurring during GTP binding (Figure 13). Switch II is not involved in G interface but interacted with $\alpha 7$ in the GDP bound form. In the GDP bound form, His 87 together with Glu89 (both in switch II) are involved in contacting Lys240 of $\alpha 7$ and kept it connected to G domain. Asp80 points towards the nucleotide binding pocket in the GDP bound form but is flipped out in the GTP bound form, due to the negative charge of the γ - phosphate. This leads to rearrangement disturbing the interaction of switch II with helix $\alpha 7$. This suggested that upon GTP binding, $\alpha 7$ is released from G domain to associate with binding partners or membranes thereby making GIMAP2 oligomer as molecular scaffold on the surface of LDs.

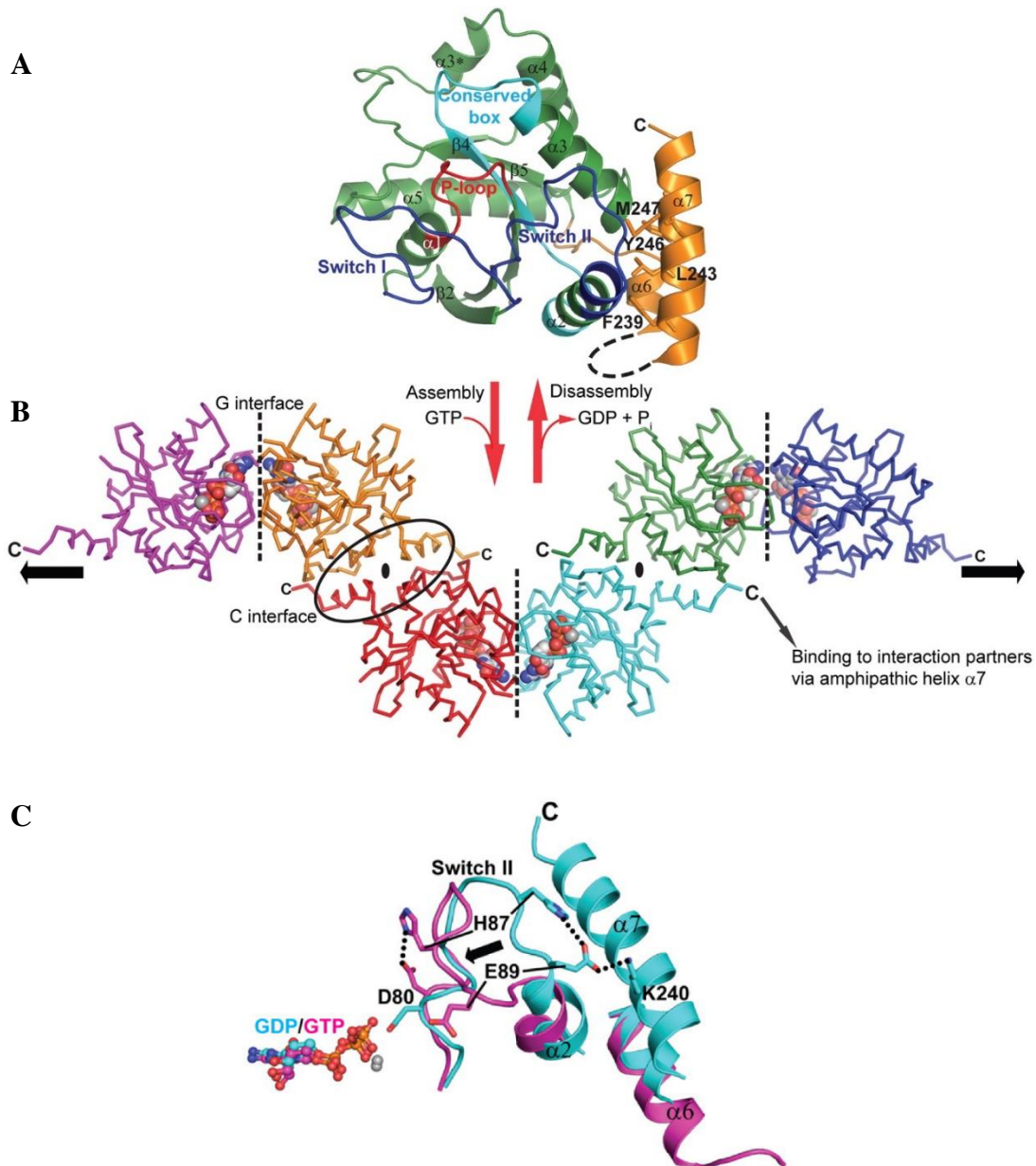


Figure 12: Crystal structure of GIMAP2. A) GIMAP2 featured a typical G domain with characteristic G motifs. P-loop (red), switch I and II (blue), conserved box (cyan) and $\alpha 6$ and $\alpha 7$ (orange). B) Oligomerization mode of GIMAP2. GTP binding promotes assembly of GIMAP2 and release of $\alpha 7$ from G-domain to bind putative interaction partners. GTP hydrolysis promoted disassembly of complex (88) C) An overlay of GDP bound GIMAP2 (21-260) (cyan) with the GTP bound GIMAP2 (1-234) (magenta) shows rearrangement of switch II upon GTP binding. Selected residues undergoing rearrangements are depicted as sticks. Figure modified from (88).

1.7.2 GIMAP7

GIMAP7 was found to co-localize with GIMAP2 on LDs (Table 1). Based on this observation, biochemical and structural studies were conducted on GIMAP7 which showed that GIMAP7 can stimulate the GTPase activity of GIMAP2 (90). It was also shown that GIMAP7 showed protein-concentration and dimerization-dependent GTPase activity. The structure of GIMAP7 bound to non-hydrolysable GTP analogue (5'-Guanylyl imidodiphosphate, GMPPNP) suggested the mechanistic basis for it

The crystal structure of GIMAP7 revealed a typical Ras like G-domain along with GIMAP specific helix $\alpha 3^*$ and a conserved box (Figure 13). The overall structure of GIMAP7 was very similar to that of GIMAP2, with significant differences observed in switch II region and in the length of the C-terminal extension. Nearly half of the amino acids in the extension were charged and projected towards the solvent. It is to be noted that helix $\alpha 7$ folds against the hydrophobic path on the G-domain created by switch II and $\alpha 3$. The structure of the catalytically active dimer revealed the mechanism by which it carried out the GTP hydrolysis (Figure 13). The dimer interface known as G interface is composed of conserved box, switch I, G4 loop and $\alpha 3^*$. Most importantly, Arg103 in GIMAP7 formed water-mediated hydrogen bonds to the nitrogen between the β -phosphate and γ -phosphate of GMP-PNP in the opposing monomer. This orientation suggested that Arg103 could be the catalytic residue for the opposing monomer. Indeed, R103D mutation completely blocked the GTPase activity despite retaining its capacity to bind to GTP. By mutagenesis it was shown that dimerization via the G-interface is essential for GTPase activity.

Based on dimerization-dependent GTP hydrolysis, it was explored if GIMAP7 influenced the GTPase activity of GIMAP2. Surprisingly, addition of GIMAP7 to catalytically silent GIMAP2 increased the amount of GTP hydrolysed higher than that of GIMAP7 alone (Figure 13B). Control experiments with GST and Alkaline Phosphatase (AP) were performed to support this finding. This proved conclusively that GIMAP7 indeed stimulated the GTPase activity of GIMAP2 (90). This suggested that GIMAP7 act as a stimulator of GTPase activity of GIMAP2 thereby leading to disassembly of the scaffold formed on LDs.

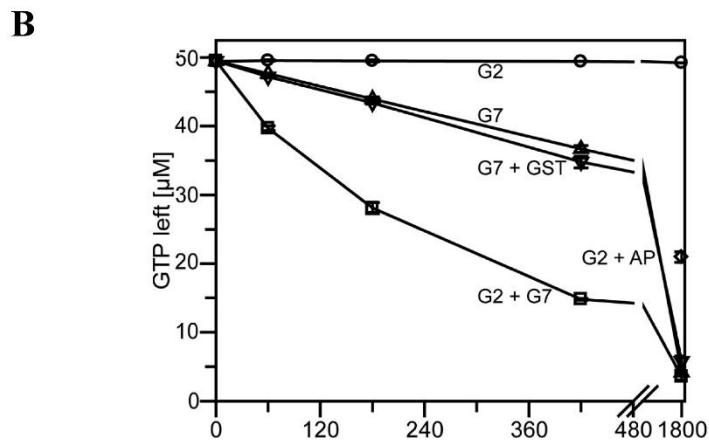
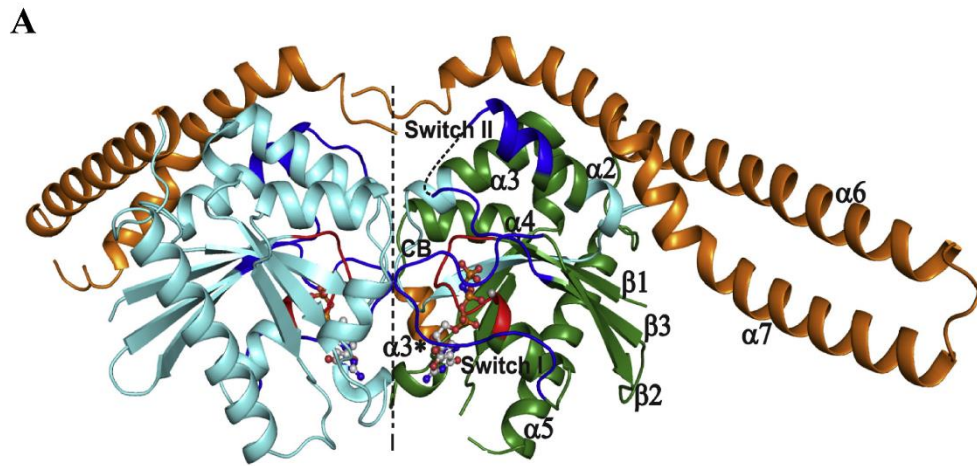


Figure 13: Structure and GTPase activity of GIMAP7. A) Structure of dimeric GIMAP7 featuring the typical G domain (green) with P-loop (red), switch I and II (blue), the conserved box (cyan) and C-terminal extensions, $\alpha 6$ and $\alpha 7$ (orange). The G-interface is marked by the dashed vertical line. B) Enhanced GTPase activity in the GIMAP2-GIMAP7 mix reaction. GIMAP2 (O) with no GTPase activity. GIMAP7 (Δ) showed GTP hydrolysis over time. 10-fold molar excess of GST and GIMAP7. Protection of GTP by GIMAP2 in the presence of AP (\diamond) for a period of 30 min. Increased GTPase activity of GIMAP7-GIMAP2 mixture (\square). Figure modified from (90).

Scope of this work

GTPases of IMMunity-Associated proteins (GIMAPs) are family of GTPases involved in adaptive immunity. Animal models established the role of GIMAPs in lymphocyte development and was showed to possess both anti-apoptotic and pro-apoptotic function. Biochemical and structural studies on selected human GIMAPs gave insights about the assembly and disassembly of GIMAP scaffold on membranous structures. Despite the wealth of this knowledge, biological function of GIMAPs are still poorly understood and the molecular pathways through which they execute their function are not known.

Identification of GIMAP function would help understand the biological function mediated by them. Hence, the aim of the thesis is to understand the biology of GIMAPs and to decipher molecular interactions mediating its functions. Additionally, identification of protein(s) which interact with GIMAP would provide insights about the biological process mediated by them as a complex. Furthermore, structural and biochemical characterization of the GIMAPs together with their interaction partners would help understand molecular mechanism through which they execute their function. Additionally, structure based mutagenesis experiments would aid in identification and understanding of the importance of protein domains involved in interaction between GIMAP and its interaction partner. Such understanding could be exploited in designing cell biological and animal model based experiments to understand the function of GIMAPs in cellular context.

2. Materials and methods

2.1 Materials

A detailed list of all materials including instruments, chemicals, enzymes and kits can be found in the appendices B and C.

2.1.1 Chemicals

The chemicals and consumables which are not mentioned in the following sections were procured from Roth, Jena Bioscience, Sigma-Aldrich and Merck.

2.1.2 Enzymes

DNaseI	Roche
<i>DpnI</i>	New England Biolabs
<i>Pfu</i> DNA polymerase	Stratagene
KOD polymerase	Novogene
BamHI	New England Biolabs
EcoRI	New England Biolabs
XhoI	New England Biolabs
T4 DNA ligase	New England Biolabs

2.1.3 Kits

NuPAGE [®] MES SDS buffer kit	Life Technologies
NuPAGE [®] MOPS SDS buffer kit	Life Technologies
NuPAGE [®] Novex 4-12% Bis-Tris	Life Technologies
Unstained protein marker	Thermo Scientific
Mark12 [™] unstained ps	Life Technologies
2-log DNA ladder	New England Biolabs

QIAprep™ spin mini prep kit	Qiagen
QIAquick gel extraction kit	Qiagen
Innuprep plasmid mini prep kit	AnalytikJena
GeneAmp® dNTPS	Life Technologies
JBS Classics I + II suite	Jena Bioscience
JBS JCSG suite	Jena Bioscience
MPD suite	Jena Bioscience
pHclear I + II suites	Jena Bioscience
PACT suite	Jena Bioscience
ComPAS suite	Jena Bioscience
Classic Lite suite	Jena Bioscience
PEGs I + II suites	Jena Bioscience
Additive Screen™	Hampton Research

2.1.4 Microorganisms

- *E.coli* TG1 *K12, supE, hsdΔ5, thi, Δ(lac-proAB), F[traD36, proAB⁺, lac^q, lacZΔM15]* promega
- *E.coli* BL21(DE3) Rosetta genotype *F ompT hsdS^B(rB⁻ mB⁻) gal dcm (DE3) pRARE(CmR) pRARE* containing the tRNA genes *argU, argW, leX, glyT, leuW, proL, metT, thrT, tyrU and thrU* (Novagen)
- Jurkat cells (Human T cell leukemia cell line) were a generous gift from the group of Stephan Mathas, MDC Berlin

2.1.5 Vectors

pGex6P1	AmpR, GE healthcare, Piscataway, USA
pSKB2-LNB	KanR, O. Daumke, MDC Berlin
pEGFP-C3-MCS	KanR, based on pEGFP-C3, Clontech, Mountain View, USA; MCS exchanged against MCS from pGex-6P-1, O. Daumke, MDC Berlin

pmCherry-C	KanR, based on pEGFP-C1, Clontech, Mountain View, USA; EGFP gene exchanged against mCherry gene, AG Lewin, MDC Berlin
pMAL-C2X	AmpR, New England Biolabs

2.1.6 cDNA clone

The cDNA clone for human GIMAPs and GABARAPL2 were procured from Source Bioscience

2.1.7 Cloning and mutagenesis primer

The primers used to introduce point mutations and truncations were procured from Eurofins MWG and can be seen in appendix D.

2.1.8 Media and Antibiotics

Luria-Bertani (LB)	10 g/L tryptone/peptone, 10g/L NaCl, 5g/L yeast extract
Terrific-Broth (TB)	powder, 50 g/L, 4 ml glycerol/L
SILAC heavy and light isotope	Sigma-Aldrich
Medium	
RPMI 1640	Sigma-Aldrich
Ampicillin sodium salt	50mg/ml in H ₂ O (1000x)
Chloramphenicol	34mg/ml in H ₂ O (1000x)
Kanamycinsulphate	10mg/ml in H ₂ O (1000x)
Penicillin/streptomycin	ready to use stock (100x) contained 10 U/ml Penicillin and 10 µg/ml streptomycin.

2.1.9 Buffers

Lysis buffer	50 mM HEPES pH 7.5, 800 mM NaCl, 2.5mM DTT, 2 mM MgCl ₂ , 10 mM KCl, 0.1 mM GDP, 1 mM ATP, 0.1 mM Pefabloc protease inhibitor and 1 µM DNaseI
Buffer 1	50 mM HEPES pH 7.5, 800 mM NaCl, 2.5 mM DTT, 2 mM MgCl ₂ , 10 mM KCl, 0.1 mM GDP and 1 mM ATP

Buffer 2	50 mM HEPES, pH 7.5, 800 mM NaCl, 2.5 mM DTT, 2 mM MgCl ₂ , 10 mM KCl, 0.1 mM GDP, 1 mM ATP and 1% CHAPS
Buffer 3	50 mM HEPES pH 7.5, 500 mM NaCl, 2.5 mM DTT and 20 mM Glutathione (pH readjusted to 7.5)
Buffer 4	20 mM HEPES pH 7.5, 150 mM NaCl, 2.5 mM DTT, 2 mM MgCl ₂
Buffer 5	10 mM HEPES pH7.5, 300 mM NaCl, 2.5 mM DTT
Buffer 6	20 mM HEPES pH 7.5, 150 mM NaCl, 5 mM MgCl ₂ , 5 mM KCL
Dulbecco's PBS 1	Sterile premix, without Ca ²⁺ and Mg ²⁺
Dulbecco's PBS 2	Sterile premix, with 2mM MgCl ₂
10x TBE buffer (1L)	108g Tris-Base, 55g Boric Acid, 9.3g Na ₂ EDTA pH 8.0
4x SDS buffer stock	0.2 M Tris-HCl pH 6.8, 40% (v/v) glycerol, 0.5 M 2-Mercaptoethanol, 0.3 M SDS, 1.2 mM bromophenol blue, 50mM EDTA for 10ml
HPLC buffer	100 mM potassium phosphate (pH 6.5) [K ₂ HPO ₄ 1M 65.9ml + KH ₂ PO ₄ 1M, 134.1ml] 10 mM TBAB, 7.5 % Acetonitrile.

2.1.10 Peptides

Required peptides were procured from Proteogenix, France

2.2 Molecular biology methods

2.2.1 Polymerase chain reaction

cDNAs of GIMAP6, GIMAP5, GIMAP4, GIMAP1 and GABARAPL2 were amplified with gene specific primer using *Pfu* DNA polymerase and subsequently cloned into desired vectors using standard protocol.

2.2.2 DNA digestion

DNA restriction digestion and digestion of methylated DNA template were performed using enzymes from New England Biolabs according to manufacturer's protocol.

2.2.3 Agarose gel electrophoresis

Agarose gels were prepared and ran according to standard protocols using 1x TBE buffer with 0.3 µg/ml ethidium bromide.

2.2.4 DNA extraction from Agarose gel

Desired DNA bands were excised from the gel and subsequently purified using the QIAquick gel extraction kit according to the manufacturer's protocol.

2.2.5 Ligation

Plasmids and DNA inserts were quantified by means of spectrometry at a wavelength of 260 nm in Nanodrop 2000 spectrophotometer (Thermoscientific). 10 ng of plasmid was ligated with 6-fold molar excess of insert using T4 DNA ligase. Ligation was carried at 4 °C overnight.

2.2.6 Transformation of chemically competent *E.coli*

After insertion of the desired cDNA into the vector, *E.coli* TG1 was transformed with ligation mixture according to standard protocol. The colonies appeared after overnight incubation of the plates at 37 °C. Isolated clones were picked and confirmed by sequencing. The expression bacteria *E.coli* BL21 (DE3) Rosetta was transformed with the vector carrying the correct insert of interest.

2.2.7 Isolation of plasmid DNA

Plasmids were isolated using the Analytica mini kit or the QIAprep Spin miniprep kit according to the manufacturer's protocol. The isolated plamid DNA was eluted with 70 µl ddH₂O.

2.2.8 DNA sequencing

The plasmids carrying the gene of interest were sequenced at Eurofins MWG operon and Source Bioscience using Sanger sequencing method.

2.2.9 Site directed mutagenesis

Site-directed mutagenesis was performed using KOD DNA polymerase according to the protocol described in Sambrook *et al* 2001.

2.2.10 Bacterial storage

Bacterial stock were made with cultures frozen with 33.3% (v/v) glycerol for long term storage at -80°C.

2.2.11 Co-transformation for co-expression

Equal amount of pGEX6P-1 and pSKB-LNB carrying insert of GABARAPL2 and GIMAP6 respectively, were co-transformed as explained in 2.2.6. Clones expressing both the vectors were confirmed by restriction digestion with appropriate restriction enzymes and also by plasmid DNA sequencing.

2.3 Biochemical methods

2.3.1 SDS PAGE

Separation of proteins of different molecular weight was performed according to Laemmli, 1970 using a denaturing, discontinuous SDS-polyacrylamide gel electrophoresis (SDS-PAGE) kit (Invitrogen, Karlsruhe) at a neutral pH (Moos et al., 1988) according to manufacturer's protocol.

2.3.2 Determination of protein concentration

The extinction coefficient (E) of different protein construct was determined online according to (129) and protein concentration was subsequently determined using the Nanodrop 2000 at wavelength, $\lambda = 280$ nm.

2.3.3 Protein storage

Purified and concentrated protein were aliquoted in desired volume and flash frozen in liquid nitrogen and stored at -80°C.

2.3.4 Nucleotide hydrolysis assay

GTPase activity of a given concentration of GIMAP construct were determined at 20 °C in 20 mM HEPES pH7.5, 150 mM NaCl, 5 mM MgCl₂, 5 mM KCl in the presence of 0.5 mM GTP. Reactions were initiated by adding the protein to the reaction tube. Reaction aliquots were taken at a 5 min, 10 min, 20 min, 45 min and 60 min interval, diluted 10-fold in water

and frozen in liquid nitrogen. The hydrolysed and non-hydrolysed nucleotide was measured as mentioned in 2.3.5. Rates were derived from the linear fit to the initial reaction (< 40% GTP hydrolysis).

2.3.5 Nucleotide detection using reversed-phase HPLC

Nucleotide detection using reversed-phase HPLC was performed as described in (130). Principle of this separation is based on the interaction between hydrophobic static phase and ion pairs of nucleotides and TBA in the mobile phase. Depending on the number of phosphates, a variable number of TBA ions are bound by nucleotide which increase the retention time on column. The samples were diluted 10 fold (50 μ M in 20 μ l volume) and injected to the ODS-2 C18 HPLC column (250 x 4 mm). Flow rate was maintained at 1.3 ml/min. Nucleosil 100 C18 pre-column was used as guard column to adsorb denatured protein. The running buffer contained 10 mM TBAB, 100 mM potassium phosphate (pH 6.5) with 7.5% acetonitrile. The eluting nucleotides were detected at the wavelength of 254 nm. 50 μ M of pure nucleotides were used as standards.

2.3.6 Isothermal Titration Calorimetry (ITC)

ITC experiments were carried out at 8 °C in VP-ITC in buffer 6 at a GIMAP6 concentration of 50 μ M. GDP and GTP- γ -S at concentration of 1mM were used to detect binding towards GIAMP6. 320 μ M GABARAPL2 was titrated against 40 μ M of GIMAP6 or GIMAP6 (1-282) to determine the interaction between GIMAP6 and GABARAPL2 using microCal iTC200. Similarly, 300 μ M GIMAP7 was titrated against 30 μ M of GIMAP6 to investigate the interaction between GIMAP6 and GIMAP7. For GIMAP6 peptide binding to GABARAPL2 measurements, concentration of GIMAP6 peptide at 1.5mM in syringe was titrated against 100 μ M GABARAPL2. The volume required was 70 μ l and 300 μ L in the syringe and cell respectively in microCal iTC200. Binding isotherms were fitted and equilibrium dissociation constants were calculated using the Microcal ORIGIN software.

2.3.7 Protein over-expression and solubility test in *E.coli*

In order to test the over-expression and solubility of a given construct, cryostocks of *E.coli* BL21 (DE3) carrying the same was inoculated in LB medium supplemented with appropriate antibiotic. Primary culture was grown overnight at 37°C. The primary culture was inoculated in 1:100 dilution to the 1lit TB medium with appropriate antibiotics. The culture

was grown at 37 °C till the OD reached 0.5-0.6 whilst shaking. The cells were induced with 40 µM IPTG and the temperature changed to 18°C for over expression of protein for 18-20 hrs. The cells were pelleted at 5,000 rpm for 15 min at 4 °C and were re-suspended in 30ml lysis buffer. The bacterial cells were lysed by passing thrice through the Fluidizer at 8000 psi. The lysate was cleared at 35,000 rpm at 4°C for 45 min in an Optima-L100K ultracentrifuge using Ti45 rotor. The supernatant was filtered using 0.2 µm filter and applied on GSH sepharose column pre-equilibrated with buffer 1. The column was washed with 20 CV buffer 1 followed by 10 CV of buffer 2 and 5 CV of buffer 1. Overexpressed and soluble protein was eluted with buffer 3 and analysed using SDS-PAGE

2.3.8 Large scale protein over-expression in *E.coli*

Large scale protein over-expressions were typically carried out in culture volumes varying between 10 to 20L of TB medium. The over-expression strategy is as explained in 2.3.7. The re-suspended bacterial cells were stored at -20°C or lysed for purification.

2.3.9 GIMAP protein purification

All chromatographic procedures were carried out at 4 °C. The filtered supernatant from the cleared lysate was applied on chromatography column packed with 20 ml GSH sepharose beads pre-equilibrated with 5 CV buffer 1. The column was extensively washed with 20 CV of buffer 1 until E₂₈₀ signal reached basal level. Subsequently, the column was washed with 10 CV buffer 2 followed by 5 CV buffer 1 to remove non-specifically bound impurities and detergent. In case of purification of GST fusion protein, the fusion protein was eluted with 50ml buffer 3. And in case of GST tag free protein purification, the column was unpacked and the protein-bound GSH sepharose was re-suspended in 40 ml of buffer 1 and 0.5 mg preScission protease was added and incubated overnight at 4 °C. After the incubation, GSH sepharose was packed again into chromatography column and the cleaved protein was eluted. 2 CV of buffer 1 was passed through the column again to elute non-specifically bound cleaved protein. The eluate was concentrated in desired molecular weight cutoff Amicon centrifugal filters up to a volume varying from 1-5 ml and injected into Superdex 200 column pre equilibrated with buffer 5. Fractions were analysed on SDS-PAGE and the fractions containing the protein of right molecular mass were pooled and concentrated. Final concentration of protein was estimated and flash frozen aliquots were stored at -80°C.

2.3.10 Purification of GIMAP6-GABARAPL2 complex

In order to obtain the pure GIMAP6-GABARAPL2 complex, various purification techniques were tested. Firstly, both GIMAP6 and GABARAPL2 were individually purified, mixed and subsequently subjected to gel filtration to isolate the active complex. The yield from this method was not high enough to carry out further studies. Secondly, purified GIMAP6 was added to the GST-GABARAPL2 bound to the glutathione sepharose beads to capture the active GIMAP6-GABARAPL2 complex. The mixture containing Glutathione sepharose bound GST-GABARAPL2 and GIMAP6 were treated with PreScission protease to cleave GST tag from GABARAPL2. After overnight cleavage, the mixture was packed again into column and the buffer was eluted. The eluted buffer contained the GIMAP6-GABARAPL2 complex and free GABARAPL2. This method was adapted since the amount of GABARAPL2 was in excess and all of the added GIMAP6 would ideally bind to GABARAPL2 and elute as a complex. Also this method did not yield high amount of the complex as availability of purified GIMAP6 was limited for the reasons explained in section 3.2.

Finally, method of co-transformation of plasmids containing the gene of interest with different antibiotic selection markers was adopted. pGEX-6P-1 contained GABARAPL2 with ampicillin resistance whereas pSKB-LNB contained GIMAP6 with kanamycin resistance. It is to be noted that both pGEX-6p-1 and pSKB-LNB vectors carried pBR322 origin of replication which is conventionally believed to be incompatible for stable co-existence in cell. The common notion is that incompatible plasmids compete during replication and subsequent partition to daughter cells lead to difference in copy numbers of plasmid. Over the course of multiple cell divisions, these small difference lead to severe imbalance of copy number and ultimately result in loss of one of the plasmid. But this notion does not take in account of selection pressure contributed by antibiotics. It was shown previously in 2001 by Yang et al that the antibiotic selection pressure could stably maintain incompatible plasmids for about 14 hrs for protein expression and purification (131). Based on this finding, the feature of antibiotic selection pressure was implemented to co-transform plasmids (see section 2.2.11) containing GABARAPL2 and GIMAP6. The clone containing both the plasmids was sequence-verified and used for expression and purification of GABARAPL2-GIMAP6wt complex from *E.coli* cells. The method for purification is as described in 2.3.9

2.3.11 Bio-layer interferometry (BLI)

BLI is an emerging biochemical method for measuring molecular interactions. The method is based on the principle that it analyses interference pattern of white light reflected from two surfaces, a layer of immobilized protein (ligand) on the biosensor tip, and an internal reference layer. Any change in the number of molecules (analyte) bound to the biosensor tip causes a shift in the interference pattern that can be measured in real-time. The interaction between ligand on the biosensor surface and analyte leads to an increase in optical thickness at the biosensor tip which leads to wavelength shift, $\Delta\lambda$. Only association or dissociation of proteins on the biosensor can lead to a shift in the interference pattern and can generate a response on the BLItz system. Interactions are measured in real time, providing ability to monitor binding specificity, rates of association and dissociation, or concentration, with precision and accuracy. Sample concentration requirements are in the range of 1-80 $\mu\text{g/ml}$ in volumes ranging between 4-200 μL .

The advanced kinetic assays conducted for the interaction analysis used five distinct steps: baseline for equilibration with the buffer; the loading step where the ligand, GST-GABARAPL2 was immobilized on the biosensor; a second baseline for stabilizing the signal; in the association step the analyte, GIMAP6 interacts with the immobilized protein; dissociation where the analyte dissociates from the immobilized ligand. In order to obtain kinetic parameters, the assay is conducted ideally with at least six different concentrations of analyte ranging from 10-20X above to 0.1X below the expected K_D . 2.5, 1.75, 1, 0.5 and 0.25 μM of GIMAP6 was used for association on 0.1 μM of immobilized GST-GABARAPL2 in 5 different runs for the kinetic analysis. BLI was measured at room temperature with BLItz system (ForteBio). A single biosensor was used to measure binding at each concentration. BLI responses to only buffer on immobilized GABARAPL2 were subtracted from each binding curve using the ForteBio analysis suite. The association and dissociation part of the run were used for analysis and was globally fitted. 1:1 binding reactions were fitted with the BLItz Pro 1.2 software.

2.4 Cell biological methods

2.4.1 Jurkat cell culture and transfection

Jurkat T cells were routinely maintained at 37 °C with 5% CO_2 in RPMI 1640 medium with 10% fetal bovine serum, 100 U/ml penicillin, 0.1 mg/ml streptomycin and 2 mM

glutamine. The cells were split every 2 or 3 days. 30 µg of plasmid DNA coding for appropriate GIMAP in either mCherry or EGFP were electroporated using BioRad Gene Pulser (exponential protocol, V=300 V, C=500 µF). Live cells were analyzed for localization using Olympus FV1000 confocal microscope

2.4.2 Stable Isotope Labelling by Amino acid in Cell culture (SILAC)

2.4.2.1 Cell culture in SILAC medium

Jurkat T cells were cultured as mentioned in 2.4.1 but with SILAC media. SILAC media was prepared from SILAC RPMI 1640 lacking L-arginine, L-lysine and L-glutamine supplemented with 10% (v/v) dialyzed FCS (Sigma-Aldrich), 4 mM L-glutamine, penicillin (100 U/ml), streptomycin (100 µg/ml). ‘Heavy’ SILAC medium was prepared by addition of 28 mg/ml ¹³C₆¹⁵N₄ L-arginine and 49 mg/l ¹³C₆¹⁵N₂ L-lysine (Sigma Isotec). ‘Light’ SILAC medium was prepared by addition of corresponding amino acids with standard isotope distribution. Cells grown in normal RPMI 1640 was completely exchanged to SILAC medium. The cells were split for at least 6 times for maximal incorporation of isotopes.

2.4.2.2 Jurkat cell lysis for SILAC pull down

10 X 10⁶ cells were cultured per pull down. Cells in the SILAC medium were centrifuged at 1,500 rpm at 20 °C for 5 min. The pellet was washed twice with PBS and lysed using Jurkat lysis buffer containing PBS, 2.5 mM DTT, 1 protease inhibitor cocktail tablet (Roche) per 10 ml buffer, 1 µM DNase mix, 1% NP-40 detergent and 100 µM GTPγS. The lysate was gently pipetted up and down 15 times avoiding air bubbles. The lysate was centrifuged at 13,200 rpm for 15 min. The supernatant was separated without disturbing the pellet and used for pull down assay.

2.4.2.3 SILAC Pull down assay

For pull down assays, cell lysates were freshly prepared from Jurkat T cells as described in 2.4.2.2. SILAC experiments were conducted as label swap experiments. In a forward experiment, GST-GIMAP7 (L100Q) was incubated with heavy labelled cell lysate and GST was incubated with light labelled cell lysate. The reverse experiment was performed with swapped labels. A SILAC experiment included four pull downs, two pull downs of the forward experiment (GST-GIMAP7(L100Q) + heavy lysate and GST + light lysate) and two pull downs

of the reverse experiment (GST-GIMAP7(L100Q) + light lysate and GST + heavy lysate). The same method was also followed for GIMAP2 with GST as control.

Active NHS (N-Hydroxy-Succinimide) sepharose beads were used for covalent coupling of recombinant proteins. The storage solution was removed from bead slurry by centrifugation (1,000 g, 2 min). Beads were washed in 500 μ L ice-cold equilibration buffer (1 mM HCl) and the supernatant removed by centrifugation. The beads were re-suspended in 1 ml of Washing buffer (PBS, 5 mM MgCl₂) and incubated with 2 mg of respective recombinant protein for at least two hours at RT. The beads were washed with 1000 μ L of buffer A (0.5 M ethanolamine, 0.5 M NaCl, pH 8.3) and centrifuged, and the supernatant was removed. Subsequently, the beads were treated with 1000 μ L buffer B (0.1 M Na-acetate, 0.5 M NaCl, pH 4.0) and the supernatant removed by centrifugation. As the next step, the beads were incubated in buffer A for 30 min. After wash steps with buffer B, A and again B the beads were washed twice with washing buffer. The beads of respective recombinant proteins were equally divided and the heavy and light cell lysates were added to beads separately and incubated for 60 min at 4 °C. Post incubation, the supernatant was removed. The heavy and light beads were mixed (1:1) to obtain the desired combination of pull down pair. The mixed beads were washed in Jurkat lysis buffer twice and bound proteins were eluted with 200 μ l denaturation buffer (6 M urea and 2M thio-urea in 10 mM HEPES, pH 8) by shaking at 1,400 rpm on an Thermo shaker (Eppendorf) for 15 min.

2.4.2.4 Liquid Chromatography mass spectrometry and data analysis

The eluted protein complex was processed in the lab of Prof. Dr. Matthias Selbach to identify specific interaction partners of GIMAPs using mass spectrometry.

2.4.3 Apoptosis assays.

5 x 10⁶ Jurkat cells were washed with phosphate buffered saline (PBS), centrifuged at 1,500 g for 5 min and re-suspended in 0.5 ml OPTIMEM medium (Invitrogen). 30 μ g of plasmid DNA coding for mCherry-GIMAP7 was electroporated using the BioRad Gene Pulser (exponential protocol, V=300 V, C=500 μ F). 24 h after transfection, cells were sorted (BD FACSAria III) for mCherry positive cells and then cultured in the presence of 40 ng/ml agonistic anti-CD95 antibody CH-11 (Coulter-Immunotech, Hamburg, Germany) or the respective IgM isotype control (Qbiogene, Heidelberg, Germany) for additional 6 h. Subsequently, cells were stained for lipid droplets by BODIPY (493/503) and washed twice

before staining the nucleus with 0.05 ug/ml DAPI. After a washing step with PBS, cells were re-suspended in 20 µl RPMI medium. Live cells were analyzed for mCherry-GIMAP7 localization using an Olympus FV1000 confocal microscope.

2.4.4 Induction of autophagy.

5 x 10⁶ Jurkat cells were washed with phosphate buffered saline (PBS), centrifuged at 1,500 g for 5 min and re-suspended in 0.5 ml OPTIMEM medium (Invitrogen). In co-expression experiment, cells were electroporated with 15 µg and 30 µg of plasmid DNA coding for EGFP-LC3B and mCherry-GIMAP7 respectively, in a BioRad Gene Pulser (exponential protocol, V=300 V, C=500 µF). 5 µM Suberoylanilide Hydroxamic Acid (SAHA) (Cayman Chemicals) was added to induce autophagy (Li et al., 2010) in the electroporated cells which were grown in RPMI 1640 medium (Invitrogen). 48 h later, cells were washed twice with PBS and re-suspended in 25 µl RPMI medium. Live cells were imaged using an Olympus FV1000 confocal microscope.

2.4.5 Microscopy.

For live cell microscopy, 5 x 10⁶ cells were washed with phosphate buffered saline (PBS), centrifuged at 1,500 g for 5 min and resuspended in 0.5 ml OPTIMEM medium (Invitrogen). Cells were electroporated with 30 µg of plasmid DNA coding for mCherry or EGFP fused N-terminally to the indicated construct in a BioRad Gene Pulser (exponential protocol, V=300 V, C=500 µF). 48hrs later, cells were washed with PBS and stained with BODIPY 493/503 according to(Gocze et al., 1994). After two more washing steps with PBS, cells were resuspended in 25µl RPMI medium, and live cells were imaged using Zeiss LSM 510 or Olympus FV1000 confocal microscopes (BODIPY: λ_{exc} =488 nm, λ_{em} =BP505-530nm).

2.5 Crystallographic and computational methods

2.5.1 Crystallization screening

GABARAPL2 was screened for crystallization at concentration of 15 mg/ml in buffer containing 10 mM HEPES, pH7.5, 150 mM NaCl and 2.5 mM DTT. Sitting drop vapour diffusion method was adopted for screening in 96 well crystallization plates. Pipetting in 96 well plates were carried out using fully automated Gryphon with 96 channel dispenser. 75 µL of the precipitant solution was used in the reservoir. The sitting drop contained 300 nl of protein

and 300 nl of precipitant solution. GABARAPL2 formed crystals in many conditions after two days at both 4 °C and 20 °C

Crystallization trials were carried out with GIMAP6 and GIMAP6-GABARAPL2 complex. The frozen protein was thawed on ice and diluted to 10 mg/ml. All crystallization experiments were carried out at 4 °C. Crystallisation conditions were screened in both sitting drop (96 well plates) and hanging drop (24 well plates) vapour diffusion method. In case of 96 well plate, 75µL of precipitant was used in reservoir well whereas in 24 well plates, 1000µL of screen was used. The sitting drop contained 300nl of protein and 300nl of precipitant solution. The hanging drop contained 1 µl protein and 1 µl reservoir solution and also in varying ratio (1:2, 2:1) with respect to the precipitant solution.

2.5.2 Cryo-protection of crystals.

All crystals were cryo-protected to minimize radiation damage occurring during the diffraction. 20% PEG400, 20% Ethylene glycol and 20-50% of glycerol were used as cryo-protectant. The cryo-protectant was diluted using the reservoir solution from the respective condition containing crystals to obtain cryo-solution. Crystals were fished from drop and soaked in 5-6 µl of cryo-solution and flash frozen in liquid nitrogen. Crystals were tested for diffraction at Beamline (BL) 14.1 and BL 14.3 at BESSY II, Berlin.

2.5.3 Data collection

All data were obtained at BL 14.1 in BESSY II, Berlin using a Pilatus detector. For structure determination of GABARAPL2, a native data set was collected from a single crystal using the rotation method with an ϕ increment of 0.3° at a temperature of 100K. The incident X-ray beam had a wavelength of 0.918 Å and the distance between crystal and detector was 180 nm. 950 images were recorded with 2 sec exposure time. Initial indexing and determination of an optimal data collection strategy was done using Mosfilm (132).

2.5.4 Protein structure solution

A short overview of principles of macromolecular X-ray crystallography is given here even though the complete background and derivation of all equations is beyond the scope of this thesis. The building block of protein crystals are the asymmetric units. By the application of crystallographic symmetry operations such as reflections, inversions or rotations to the asymmetric unit, a unit cell of the crystal is determined. Regular and highly ordered packing

of unit cell in three dimension leads to the formation of macroscopic crystals. The dimension of the unit cell along with the symmetric operation applied to the asymmetric unit defines the space group of the crystal. In total, there are 230 possible space groups and since inversion or reflections cannot be applied to chiral molecules, only 65 of them are found in protein crystals (133).

The electrons present in crystal diffract X-rays incident on them in a process called elastic or Thomson scattering. The information about the dimension of unit cell and crystallographic symmetry of the crystal are revealed by direction of diffraction of the incident X-ray beam. The intensities of diffracted beam carry information regarding electron density distribution in the unit cell. The total scattering from a unit cell can be described as sum of the scattering by the individual atoms of the unit cell and is given by structure factor $\vec{F}(S)$,

$$\vec{F}(S) = \sum_{j=1}^n f_j \cdot e^{(2\pi\vec{r}_j\vec{S})}$$

Equation 1: Structure factor $\vec{F}(S)$ of an unit cell

where j is the number of atoms in the unit cell, \vec{r}_j is the position of the atom j with respect to the origin, f_j is the atomic scattering factor, which can be looked up in tables, and $\vec{S} = \vec{s} - \vec{s}_0$ with \vec{s} as the scattered wave vector and \vec{s}_0 as incident wave vector. Therefore $\vec{F}(S)$ depends on the structure of the unit cell.

A crystal consists of a large number of unit cells: n_1 in direction \vec{a} , n_2 in direction \vec{b} and n_3 in direction \vec{c} . The position of each unit cell with respect to origin can be described as $\vec{a} + u \cdot \vec{b} + v \cdot \vec{c}$. The total wave $\vec{K}(S)$ scattered by the summation of all unit cells in a crystal can be shown as,

$$\vec{K}(S) = \vec{F}(S) \cdot \sum_{t=1}^{n_1} e^{(2\pi it\vec{a}\vec{S})} \cdot \sum_{u=0}^{n_2} e^{(2\pi iu\vec{b}\vec{S})} \cdot \sum_{v=0}^{n_3} e^{(2\pi iv\vec{c}\vec{S})}$$

Equation 2: Total scattering of a wave $\vec{K}(S)$

$\vec{K}(S)$ is almost always equals to zero, unless $\vec{a} \cdot \vec{S}$, $\vec{b} \cdot \vec{S}$, $\vec{c} \cdot \vec{S}$ are integers of h , k and l respectively. These conditions are also known as Laue conditions with h , k and l being the Miller indices which describes the equivalent set of planes in the reciprocal crystal lattice.

The equivalent of the Laue condition in real space is known as the Bragg's law,

$$n\lambda = 2d\sin\theta$$

Equation 3: Bragg's law

Where λ is the wavelength of incident X ray beam, d is the spacing between the planes in the crystal lattice and θ being the angle between the incident ray and the scattering plane. The discrete intensity maxima of diffracted X-rays form the reflections on the detector. $\vec{F}(S)$ could also be represented as the integral sum of all the electrons in the unit cell,

$$\vec{F}(S) = \int_{cell} \rho(\vec{r}) e^{(2\pi i \vec{r} \cdot \vec{S})} dv$$

Equation 4: Structure factor of unit cell as an integration over all electrons.

where $\rho(\vec{r})$ is the electron density at position \vec{r} . Given that x, y and z are fractional coordinates and V as unit cell volume, it could be derived that dv equals $V \cdot dx dy dz$ and $\vec{r} \cdot \vec{S} = (\vec{a} \cdot x + \vec{b} \cdot y + \vec{c} \cdot z) \cdot \vec{S} = hx + ky + lz$. Now the $\vec{F}(S)$ can be represented in terms of h, k and l ,

$$\vec{F}(h, k, l) = V \int_{x=0}^1 \int_{y=0}^1 \int_{z=0}^1 \rho(x y z) \times e^{(-2\pi i(hx+ky+lz))} dx dy dz$$

Equation 5: $\vec{F}(S)$ as a function of $h k l$

$\vec{F}(h, k, l)$ is the Fourier transform of $\rho(h, k, l)$ and the reverse is also true. In accordance with Laue condition, scattering occurs only in discrete directions therefore the integration can be substituted with a simple summation. Substituting $\vec{F} = |F|e^{i\alpha}$ will derive to,

$$\rho(x y z) = \frac{1}{V} \sum_h \sum_k \sum_l |F(h k l)| \cdot e^{-2\pi i(hx+ky+lz)+i\alpha(h k l)}$$

Equation 6: Electron density in a crystal based on Laue condition

As observed in Equation 6, two terms are required to calculate the electron density for every position in the unit cell. $|F(h k l)|$ is obtained experimentally as they are proportional to the measured intensities on the detector. The $(h k l)$, phase angles cannot be obtained directly from the diffraction pattern since they are lost during the measurement. This phenomena is

called crystallographic phase problem and can be addressed by several methods for structure solution (134). One of the methods to solve the phase problem is by usage of anomalous scattering (single or multiple wavelength anomalous dispersion, SAD or MAD respectively). The anomalous difference is the difference in the reflection pairs $\vec{F}(h, k, l)$ and $\vec{F}(-h, -k, -l)$ which occurs if the energy of the incident X-ray is close to the absorption edge of the given element. Selenium is used to obtain selenomethionine derivatized protein which in turn can be recombinantly expressed and purified. The resulting anomalous difference can be used to determine the location of anomalous scatterers (selenium positions) in crystal and to approximate the phase angles.

Another method to obtain phases is Multiple Isomorphous Replacement (MIR). This method requires incorporation of heavy atoms into the protein. If the crystals obtained from derivatized protein are isomorphous to the crystals of the native protein, the difference of the reflection amplitude can be used to approximate the heavy atom structure factor amplitudes. Both the positions and phases of the heavy atoms can then be obtained using the Patterson or direct methods. The phase angle of the protein of interest can be determined by using the heavy atom phase angles. Since the emergence of protein structure data base like Protein Data Bank (PDB) gave access to the thousands of protein structure solved till date, the structure of the protein of interest can be easily solved by the help of a readily available structure of a homologues protein. This method is hence called Molecular Replacement (MR). The structural information of the homologues protein can be used to approximate the phase angle of the crystallized protein of interest and to solve its structure. An important obligation of this method is that the sequence identity and a r.m.s.d of both the proteins should be >25% and <2 Å of the C_α position respectively.

2.5.5 Atomic Model building and refinement

Molecular replacement was applied to solve the structure of GABARAPL2 using the structure of GABARAP1 (PDB: 2R2Q) as search model. The atomic model was built and fitted into the electron density using the program COOT (135) and repeatedly refined using Phenix refine (136)

2.5.6 Protein structure validation and deposition

All atom contacts and geometry of the atomic model was evaluated using Molprobity server (137). The crystal structure of GABARAPL2 will be deposited in PDB when the manuscript, which is currently in preparation, will be accepted.

3. Results

3.1 Development of SILAC assay to identify interaction partners of GIMAPs

3.1.1 Interaction partners of GIMAP7

To understand the biological function of GIMAP7, I systematically screened for interaction partners in Jurkat T cells using a SILAC-based approach (Figure 14). To this end, in a forward experiment, I used GST-tagged GIMAP7 as bait in pull-down experiments using heavy Jurkat T cell lysates as protein source whereas GST protein treated with light Jurkat cell lysate served as a control. The proteins pulled down by bait and control in both heavy and light lysate was mixed in 1:1 ratio and the eluted protein complexes are subjected to Mass spectrometry based quantitation. A label swap strategy (crossover experiment) was adopted in which forward and reverse experiments were conducted to compensate for potential differences in protein expression levels between light and heavy labelled cells.

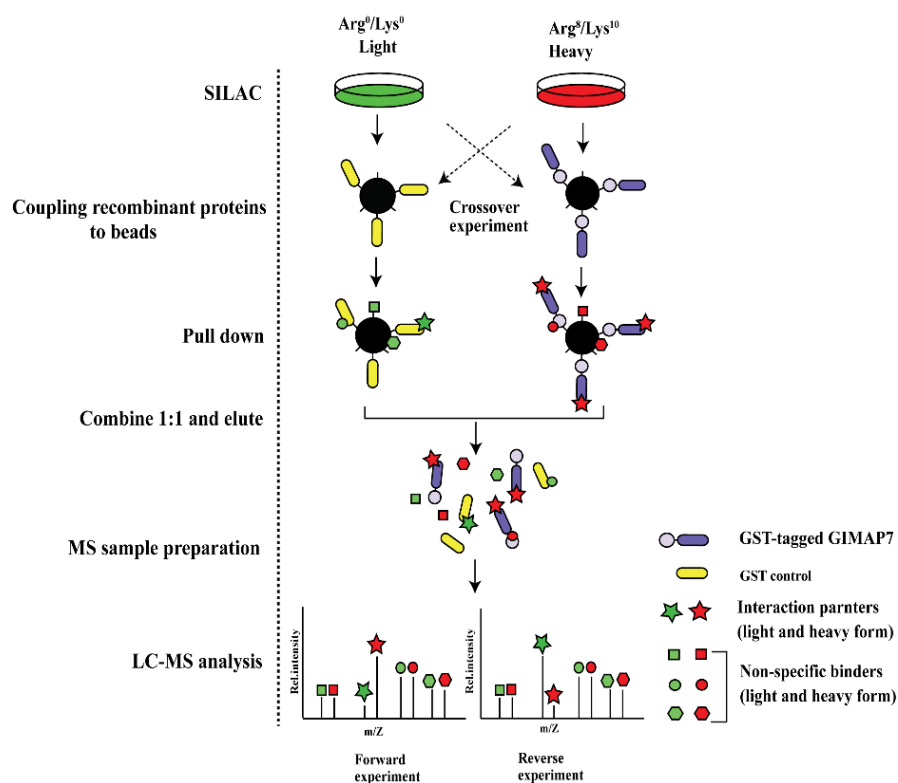


Figure 14: Experimental workflow for identification of interaction partners of GIMAP.

Schematic depiction of pull-down experiment with recombinant GIMAP7 and GST as bait and control respectively. Either light or heavy cell lysate is incubated with GST-tagged GIMAP7

or GST which is coupled to the beads. Post pull-down, beads are mixed in 1:1 ratio and the eluting complexes are analysed by LC-MS. Crossover experiments are performed by swapping the lysate. Specific interaction partners have high heavy-to-light ratios in the straight and low heavy-to-light-ratios in the reverse experiments, whereas non-specific binders have 1:1 heavy-to-light ratio in both forward and reverse experiments.

The forward experiment was performed as described in 2.4.2.3. GIMAP6, GABARAPL2 and PPM1A were identified as possible interactors of GIMAP7 (Figure 15). These binders appeared in both forward and reverse experiments with either positive or negative log₂ fold changes of heavy to light ratios. Additionally, proteins were considered as GIMAP7 specific binders if their log₂ fold change of normalized ratio was a significant positive or negative outlier for the forwards and reverse experiments respectively.

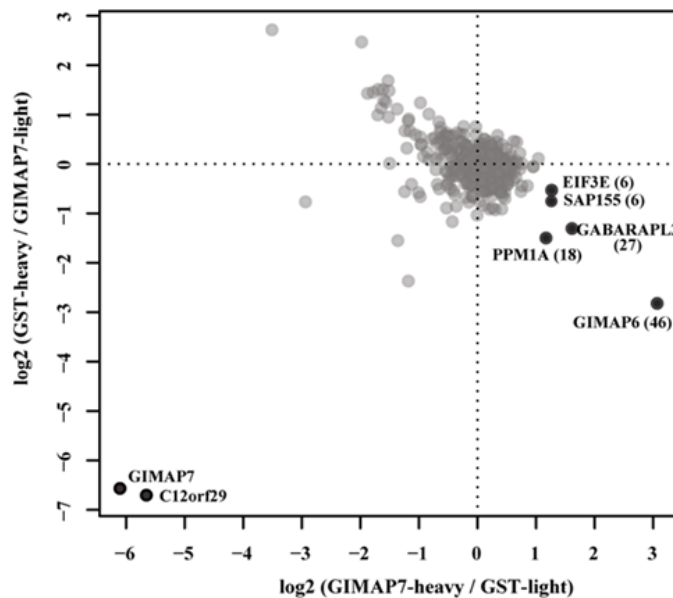


Figure 15: Interaction partners of GIMAP7. SILAC based pull down assay with GST-GIMAP7 (L100Q) and GST (control). The log₂ fold changes of heavy to light ratio from forward and reverse experiments are plotted in x and y axis respectively. The proteins for which at least 6 identified peptide are plotted in the graph. The total number of peptides from specific interaction partners used for quantification in both forward and reverse experiments are indicated in brackets. Specific GIMAP7-interactors found in both experiments are located in the right lower corner.

GIMAP6 is a highly specific interaction partner of GIMAP7 with a total of 46 unique peptides quantified. GIMAP6 is a poorly characterized GIMAP GTPase whose cellular

function is not known. GABARAPL2 (Gamma-aminobutyric acid receptor-associated protein-like 2) is an autophagy-related homolog of ATG8 from yeast and is conjugated to autophagosomes during autophagy (138). PPM1A (Protein phosphatase, Mg²⁺/Mn²⁺ dependent 1A) is member of PP2C family of Ser/Thr protein phosphatases that are known to negatively regulate cellular stress response pathways (139). False positives (grey dots in Figure 15) that non-specifically bound to column matrix or GST tag were differentially enriched in heavy or light lysate and could thus be easily discriminated from the true binders.

3.1.2 Interaction partners of GIMAP2

The SILAC strategy was also applied to identify the interaction partners of GIMAP2. In the forward experiment, recombinantly expressed and immobilized GST tagged GIMAP2 was used to pull down natively expressed interaction partners from SILAC labelled Jurkat T cells. GST protein was used as control, and the binders were identified by mass spectrometry. The forward experiment was performed as described in 2.4.2.3. AIF, ERP44 and DYNLRB1 were identified as possible interactors of GIMAP2 (Figure 16). These binders appeared in both forward and reverse experiments with either positive or negative log₂ folds changes of heavy to light ratios.

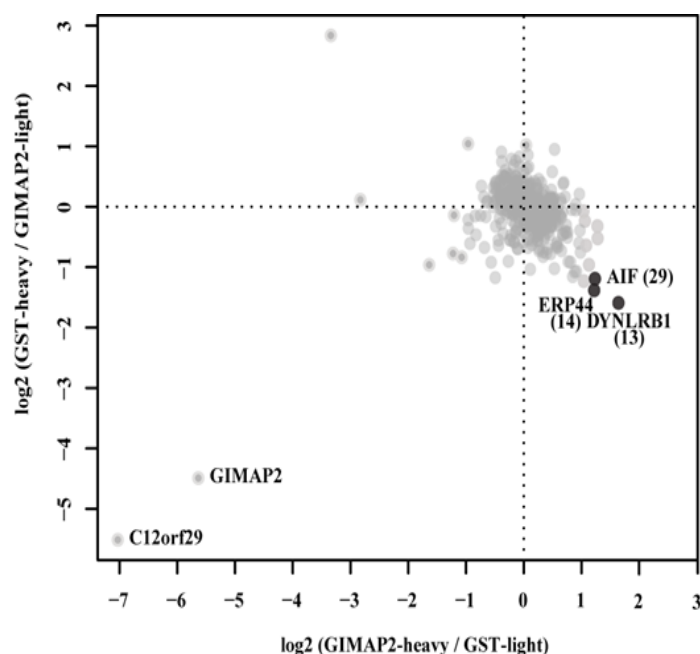


Figure 16: Interaction partners of GIMAP2. SILAC based pull down assay with GST-GIMAP2 and GST (control). The log₂ fold changes of heavy to light ratio from forward and reverse experiments are plotted in x and y axis respectively. See legend of Figure 15 for details.

Specific GIMAP2-interactors found in both experiments are located in the right lower corner. As seen in Figure 16, AIF, ERP44 and DYNLRB1 are significant outliers from the other non-specific binders. AIF (Apoptosis- inducing factor) is a mitochondrial intermembrane protein that after apoptosis induction, translocates to the nucleus and trigger chromatin condensation and DNA fragmentation (140). ERP44 (Endoplasmic reticulum resident protein 44) is thioredoxin domain containing protein assisting protein folding in ER (141). DYNLRB1 (Dynein light chain roadblock-type 1) is involved in motility of vesicles and organelles along microtubules (142).

To confirm interaction partners found for GIMAP2 and GIMAP7 both reverse and forward experiments were performed with recombinant GST-GIMAP2 and GST-GIMAP7 (L100Q). The interaction partners of GIMAP7 found with GST as control (Figure 15) could also be identified when GIMAP7 and GIMAP2 were tested as pairs in pull down assay (Figure 17). Additionally, the identified interaction partners of GIMAP2 (Figure 16) were also identified in this assay (Figure 17). These results confirms the strong reliability of the developed SILAC assay.

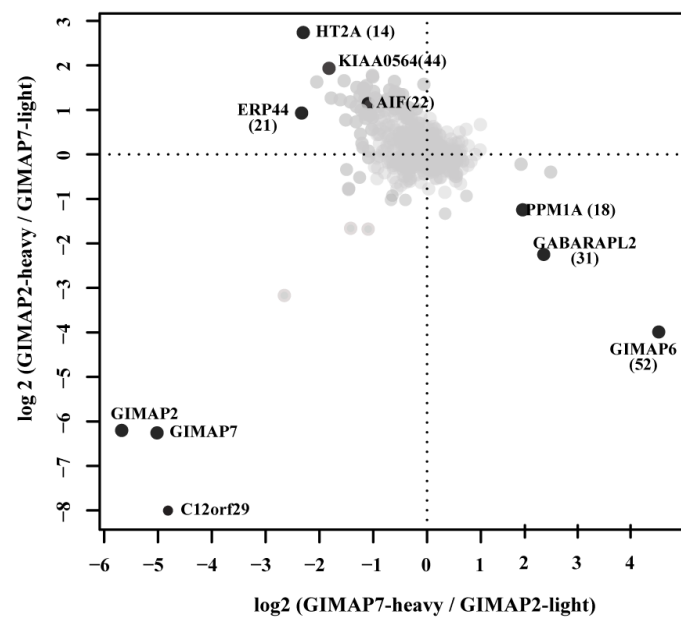


Figure 17: Interaction partners of GIMAP7 and GIMAP2. SILAC based pull down assay with GST-GIMAP2 and GST-GIMAP7. The log₂ fold changes of heavy to light ratio from forward and reverse experiments are plotted in x and y axis respectively. Specific GIMAP7-interactors found in both experiments are located in the right lower corner, whereas GIMAP2-interactors are expected at the top left corner. See legend of Figure 15 for details.

3.2 Purification of GIMAP6 and GABARAPL2

Two of the identified interaction partners of GIMAP7 were further biochemically analysed. To this end, the genes of GIMAP6 and GABARAPL2 were cloned into bacterial expression vectors and solubility screens were conducted (see section 2.3.7). The proteins were produced in large amounts suitable for biochemical and structural studies. To this end, purification protocols were developed (see section 2.3.9). GST-tagged wild type GIMAP6 and GABARAPL2 were purified in a two-step protocol that included GSH-sepharose affinity chromatography, followed by on-column cleavage of the protein and size-exclusion chromatography (see section 2.3.8 and 2.3.9). A typical purification procedure for GIMAP6 and GABARAPL2 is shown in Figure 18.

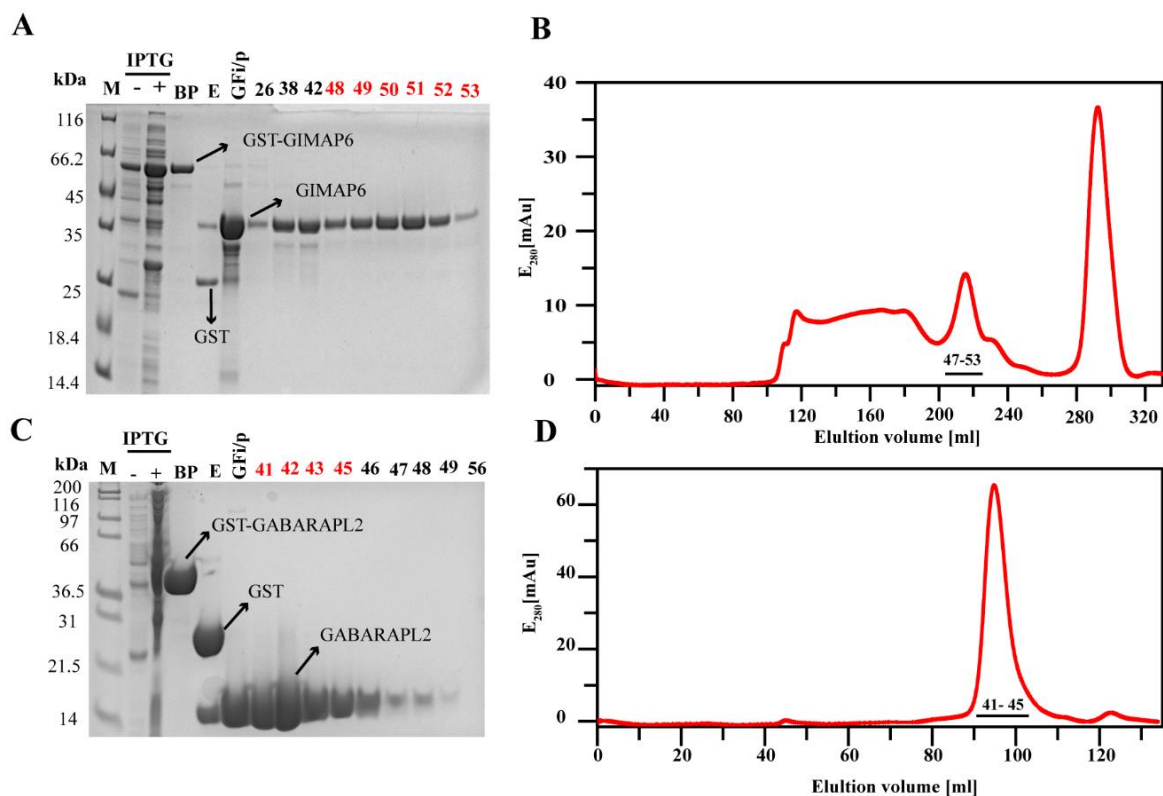


Figure 18: Typical GIMAP6 and GABARAPL2 purification procedure. A) 4-12% SDS PAGE of various samples taken during the GIMAP6 purification. Protein Marker, M; -/+ IPTG, whole-cell bacteria lysates before and after induction; BP, protein bound to the GSH sepharose beads after washing steps, E, GSH elution showing GST and remaining GIMAP6 which bound unspecifically to the column. GF/p, sample loaded on the S200 16-600; 26, 38, 42, 48, 49, 50, 51, 52, 53 fractions collected during size exclusion chromatography. Fractions used for further studies are marked in red. B) Superdex200 size-exclusion chromatogram. Fractions (48-53) pooled and concentrated for further experiments are indicated C) Typical GABARAPL2

purification procedure. 4-12% SDS PAGE of various samples taken during the purification. Protein Marker, M; +/- IPTG, whole-cell bacteria lysates before and after induction; BP, protein bound to the GSH sepharose beads after washing steps, E, GSH elution showing GST. GF_i/p, sample loaded on the S200 16-600; 41, 42, 43, 44, 45, 46, 47, 48, 49, 56 fractions collected during size exclusion chromatography. D) Superdex200 size-exclusion chromatogram. Fractions (41-45) pooled and concentrated for further experiments are indicated.

It is to be noted that yield of wild type GIMAP6 was very poor and remained the bottleneck of the study. The yield of GIMAP6 from 20 lit of *E.coli* culture was only 3-4 mg. Furthermore, the majority of the soluble GIMAP6 aggregated and formed higher order oligomers in gel filtration (Figure 18B) that could not be used for further studies. The peak at the elution volume of 300 ml did not contain any protein and could be explained as the contribution from the nucleotide present in the buffer in the gel filtration input sample. Extensive optimization of buffer composition could not prevent aggregation of GIMAP6. Varying of concentration of NaCl, MgCl₂, glutamine, inclusion of glycerol in all buffers, gel filtration in presence of nucleotide and MgCl₂, purification after denaturation with GnHCl and refolding, short duration of expression at 37 °C with high concentration of IPTG induction could not improve the yield. GIMAP6 was also cloned in pMAL-C2X expression vector for expression as a maltose-binding protein (MBP) fusion to improve the solubility and yield. The MBP-tagged GIMAP6 co-purified with many contaminants which could not be eliminated after gel filtration. This construct was therefore not suitable for further experiments (data not shown). Attempts were also made to purify GIMAP6 fused to MBP for crystallization studies. A construct of GIMAP6 starting at residue 39 (residue 1-38, disordered) was cloned to the C-terminal end of MBP in the pMAL-C2X vector to crystallize it as an MBP-fusion. Even though expression in pMAL-C2X vector dramatically increased the solubility of GIMAP6, it resulted in highly impure GIMAP6 which could not be used for crystallization studies. To increase the purity of this construct, a C-terminal His-tag was cloned and a second affinity purification was performed after elution from MBP column. But this strategy also did not improve the purity of the sample and did not prevent aggregation of GIMAP6 during the purification process (data not shown).

3.3 Nucleotide binding properties of GIMAP6

In order to quantify the affinity of purified GIMAP6 towards guanine nucleotides, ITC measurements were performed. HPLC analysis showed that GIMAP6 was free of nucleotides post purification (data not shown).

GDP was titrated against GIMAP6 (see section 2.3.6). No binding signal was observed in two repeated runs (Figure 19A). Considering that GIMAP6 might selectively bind only to GTP, the non-hydrolysable guanine nucleotide analog, GTP- γ -S, was tested for its ability to bind to GIMAP6. Surprisingly, GTP- γ -S also did not show appreciable binding towards GIMAP6, despite retaining all G motifs responsible for guanine nucleotide binding (Figure 19B). This leads to categorisation of GIMAP6 into a group of G proteins which do not bind nucleotides or involve nucleotide in their reaction (143).

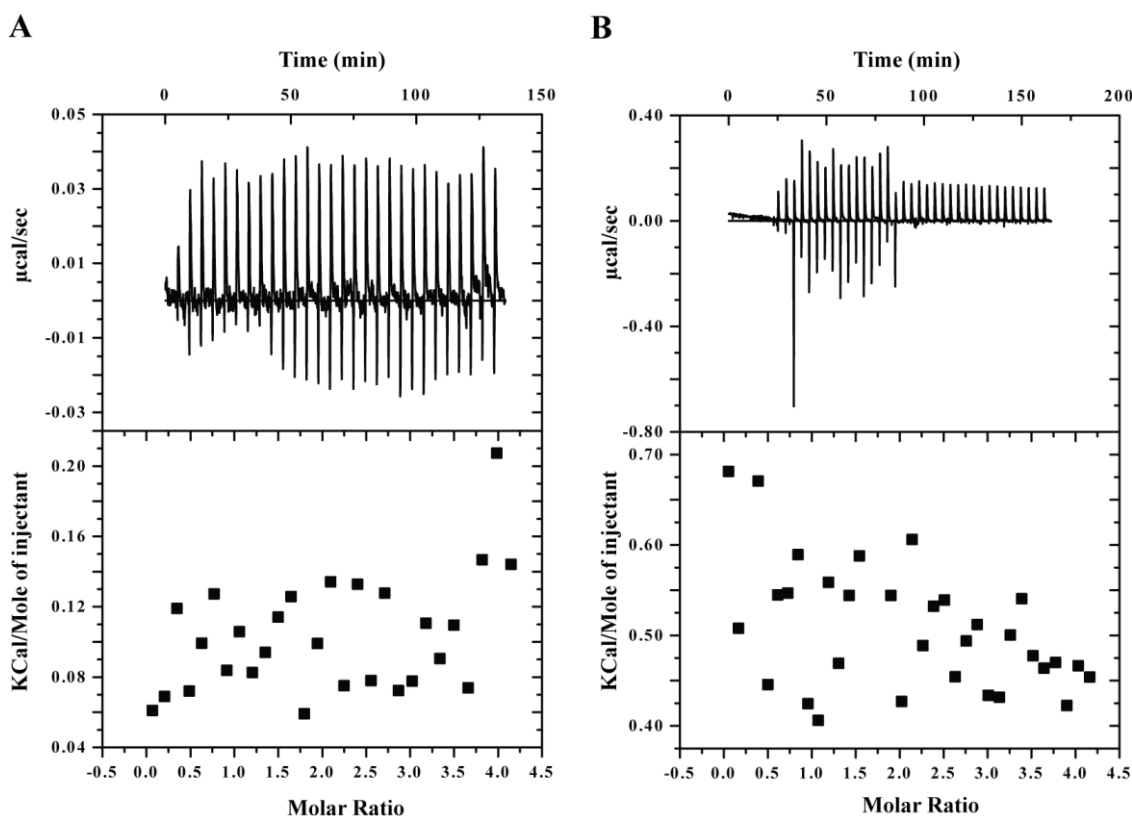


Figure 19: ITC experiment for nucleotide binding of GIMAP6. A) GDP did not show binding to GIMAP6 since no change in the heat signal was observed upon GDP titration. B) GTP γ S also did not show a binding signal to GIMAP6 since no change in the heat signal was observed upon GDP titration. Since there was no binding observed in either case, data fitting is not applicable.

3.4 GIMAP6 inhibits the GTPase activity of GIMAP7

Based on identified interaction between GIMAP6 and GIMAP7 in SILAC pull down assay (section 3.1.1), the ability of GIMAP6 to influence the GTPase reaction of GIMAP7 was tested. HPLC based GTP hydrolysis assays was used for this purpose (see section 2.3.4-2.3.5)

In agreement with the lack of GTP binding, GIMAP6 did not show any GTP hydrolysis, even after 1 hour of incubation with GTP. In contrast, 2.5 μ M GIMAP7 hydrolysed GTP efficiently, with a K_{Obs} of $\sim 0.9 \text{ min}^{-1}$. Interestingly, when GIMAP6 was incubated with GIMAP7 in the presence of GTP, the GTPase reaction of GIMAP7 was completely inhibited (Figure 20A). This suggest a role of GIMAP6 in controlling the GTPase activity of GIMAP7.

To determine if the observed inhibition is a concentration-dependent process, different concentrations of GIMAP6 (2.5, 5, 10, 25, 50, 100 μ M) were tested against a constant concentration of GIMAP7 in a mixed GTPase assay. As shown in Figure 20B, GIMAP6 effectively inhibited GIMAP7 at all concentrations tested. It is interesting to note that a concentration of GIMAP6 as low as 2.5 μ M efficiently blocked the GTPase activity of GIMAP7. This suggest that GIMAP6 inhibits GIMAP7 at an equimolar concentration.

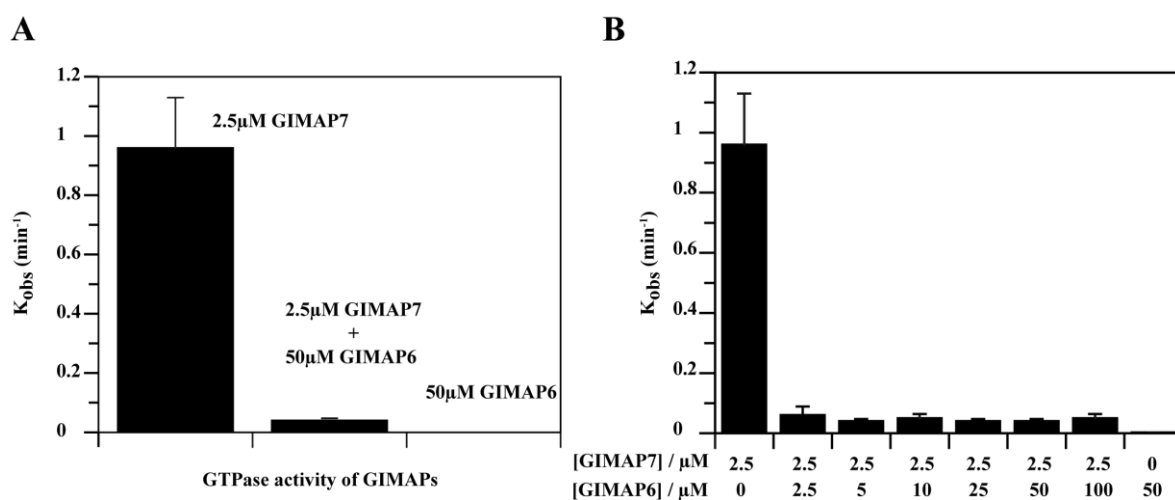


Figure 20: GIMAP6 inhibits GIMAP7. GTP hydrolysis was carried out in buffer 6 (section 2.1.9) at 20°C and nucleotide hydrolysis was measure by HPLC. A) GIMAP6 at a concentration of 50 μ M inhibits the GTPase activity of 2.5 μ M GIMAP7. B) Varying concentration of GIMAP6 was reacted with constant concentration of GIMAP7 (2.5 μ M). GIMAP6 inhibited GIMAP7 in all tested concentrations. 50 μ M GIMAP6 by itself do not hydrolyse GTP.

Since the yield of GIMAP7 from bacterial expression was very low (2 mg / 20 l bacterial culture), the ability of GIMAP6 to inhibit the more soluble GIMAP7 (L100Q) mutant (90) was

also tested. Thus, varying concentrations of GIMAP6 were tested against a constant concentration of GIMAP7 (L100Q) (Figure 21). GIMAP6 efficiently inhibited GIMAP7 (L100Q), with a slightly reduced inhibition rate compared to GIMAP7wt. However, since the inhibition was clearly observed, all experiments were performed with GIMAP7 (L100Q) subsequently.

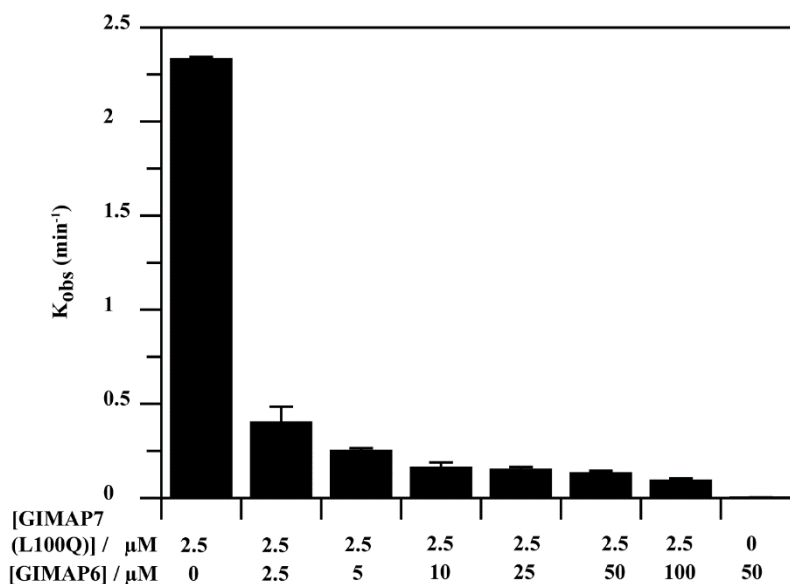


Figure 21: GIMAP6 inhibits GIMAP7 (L100Q). GTP hydrolysis was carried out in buffer 6 (section 2.1.9) at 20°C and nucleotide hydrolysis was measured by HPLC. Varying concentration of GIMAP6 was reacted with constant concentration of GIMAP7 (L100Q) (2.5 μM). GIMAP6 inhibited GIMAP7 in all tested concentrations although with slightly lesser efficiency when compared to GIMAP7wt. 50 μM GIMAP6 by itself do not hydrolyse GTP.

3.5 Modelling the GIMAP6-GIMAP7 interaction

3.4.1 Homology model of GIMAP6

In the absence of a crystal structure, homology models based on a closely related protein can provide useful structural information (144). Since all the efforts to crystallize GIMAP6 did not yield any crystals, a homology model was built based on the structural information of GIMAP7.

The SWISS-MODEL server was used to predict a homology model of GIMAP6, based on the structure of GIMAP7 (L100Q) (PDB:3ZJC) (145). Sequence alignment of GIMAP6 and GIMAP7 was performed using Clustal W sequence alignment (146). The sequence identity

between GIMAP6 and GIMAP7 (L100Q) was found to be 47%. In GIMAP7, the C-terminal helices α_6 , α_7 and the loop connecting them carry high number of charged residues which are lacking in GIMAP6. To account for this difference and the length difference, the C-terminal residues of GIMAP6 were manually aligned to the appropriate sequences in the C-terminal residues of GIMAP7. The resulting sequence alignment file was used as input for making the homology model of GIMAP6. The overall architecture of the predicted model of GIMAP6 is very similar to that of GIMAP7 (Figure 22).

GIMAP6 is a typical G-domain containing protein whose characteristic G motifs are easily identifiable. According to Jpred server (147) the first 39 residues of GIMAP6 are predicted to be highly disordered. Consequently, the model of GIMAP6 lacks the first 39 amino acid residues. Residues 40-226 resemble Ras-like G domain with GIMAP specific helix α_3^* inserted between strand β_5 and helix α_4 . The G domain is followed by helices α_6 and α_7 which folds back on the G-domain as reported for GIMAP2 and GIMAP7. The helix α_7 appears to contact Switch II in the G-domain. The homology model of GIMAP6 suggested that the 3D structure of human GIMAP family members is highly conserved (88, 90). The crystal structure of GDP-bound GIMAP5 (unpublished data from our lab) and structures of GIMAP4 (PDB: 3LXX) and GIMAP1 (PDB: 3V70) supports this inference

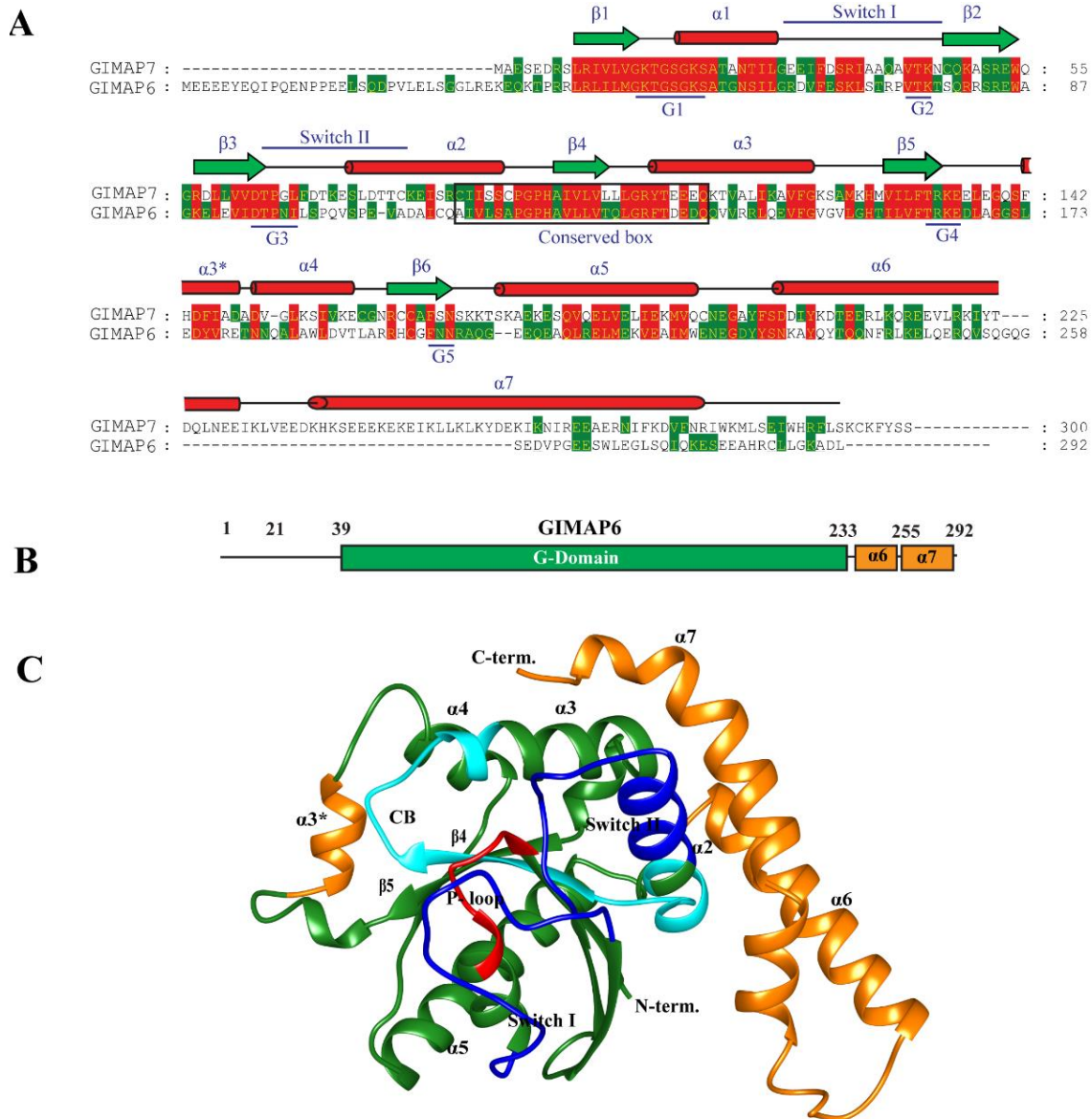


Figure 22: Homology model of GIMAP6. A) Sequence alignment of GIMAP7, GIMAP6. G-motifs (G1-G5) and switch regions are highlighted. The secondary structural elements of GIMAP7 are represented above the sequence with α helices as red barrels, β strands as green arrows and loop regions as black lines. B) Schematic depiction of domain architecture of GIMAP6 with amino acid positions indicated. B) Cartoon representation of homology model of GIMAP6. The G domain is shown in green, switch I and Switch II in blue, the P-loop in red, and the conserved box in cyan. GIMAP specific helix $\alpha 3^*$ and helices $\alpha 6$ and $\alpha 7$ are shown in orange.

3.4.2 GIMAP6:GIMAP7 heterodimer

GIMAP7 showed dimerization-dependent GTP hydrolysis and stimulated the GTPase reaction of GIMAP2 (90). The crystal structure of the GTP-bound GIMAP2 and GIMAP7 dimers showed conserved interaction modes. Thus, it was suggested that GIMAP7 and GIMAP2 formed a related heterodimer to stimulate the GTPase activity of GIMAP2 (90). Along this line, I envisaged to model the GIMAP6-GIMAP7 heterodimer in an analogous way, based on the structure of the GIMAP7 homodimer.

The homology model of GIMAP6 was built as described in 3.4.1 and used to create GIMAP6-GIMAP7 heterodimer model (Figure 23). Using this model, putative residues involved in the interaction could be established. GIMAP6 L70, Q131, R134 and D167 were the most promising residues which could possibly interact with residues in the opposing GIMAP7 (Figure 23A and B). Leu70 is located in switch I which could possibly be involved in the stabilization of the heterodimer during the GTPase inhibition of GIMAP7. This would be also in agreement with the role of switch I in GIMAP2 in stabilizing the GIMAP2-GIMAP7 heterodimer.

Gln131 is the terminal residue in the predicted strand β 4 and is located in conserved box. This residue comes in close proximity to the conserved arginine finger of GIMAP7 (R103). Arg134 in GIMAP6, the homologous residue to the arginine finger R103 in GIMAP7, is pointing in the homology model towards the nucleotide binding pocket of GIMAP7 and could possibly interact with switch I to inhibit the GTPase. Finally, Asp167 is predicted to be part of a small α helix in the homology model that could potentially interact with the base of the opposing nucleotide and also with the opposing switch I.

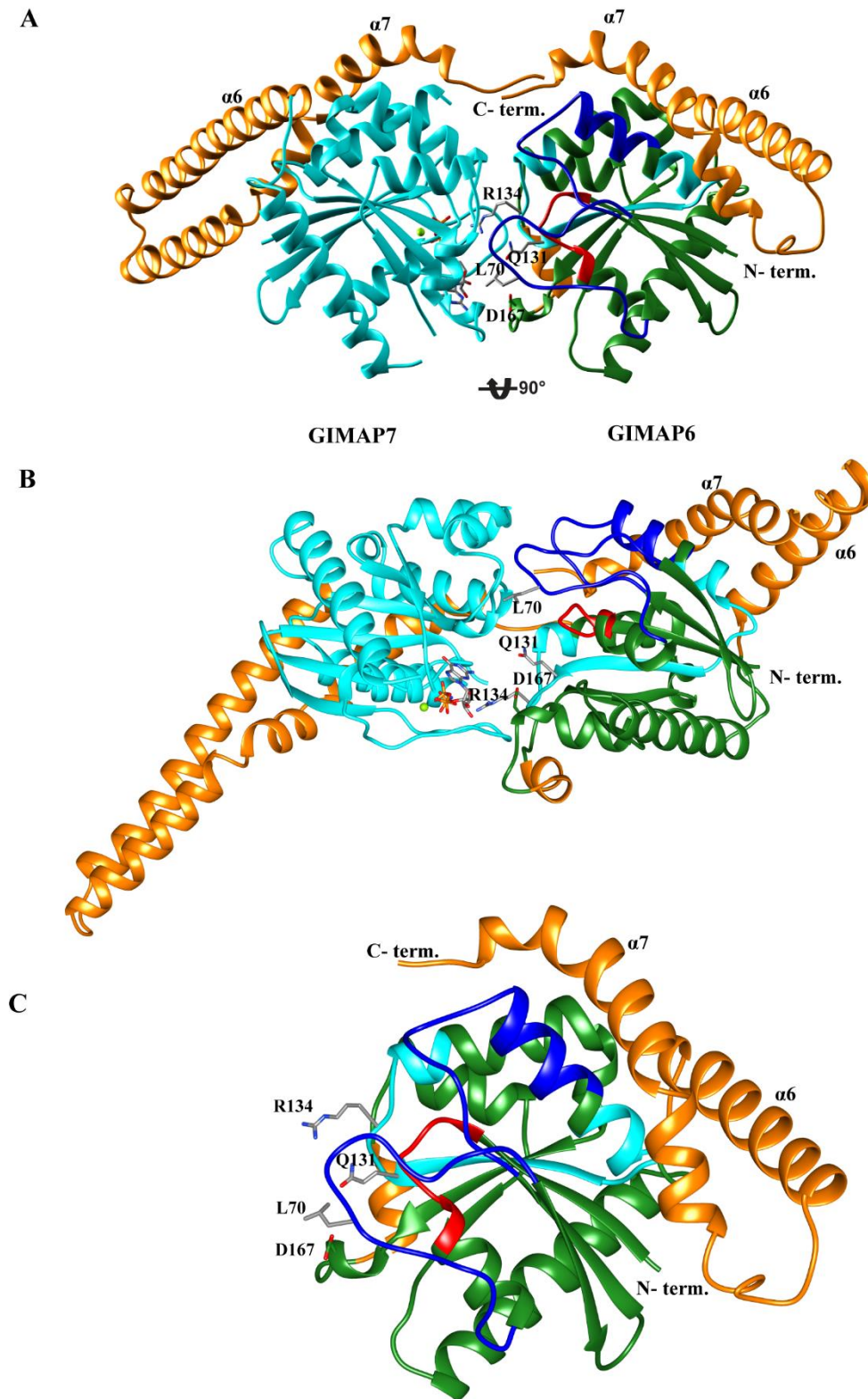


Figure 23: Model of GIMAP6-GIMAP7 heterodimer. A and B) Homology model of GIMAP6 aligned and substituted with one of the monomer in the GMPPNP-bound crystal structure of GIMAP7 homodimer (PDB: 3ZJC). Secondary structural elements and G motifs of GIMAP6 are represented as in Figure 22. The residues of GIMAP6 which could potentially

interact with GIMAP7 are shown in ball and stick model. The G domain of GIMAP7 is represented in cyan and the C terminal helices α_6 and α_7 are depicted in orange C) Residues involved in the inhibition at the GIMAP6:GIMAP7 heterodimer interface are represented as ball and sticks in the isolated GIMAP6 homology model.

To prove the validity of the predicted model, GTPase experiments with GIMAP6 carrying mutations in the predicted interface were carried out. Almost all of the residues (Figure 23C) in the predicted heterodimer model reduced GTPase inhibition of GIMAP6. GIMAP6 L70D, Q131E, R134D, D167W were purified and tested for their ability to influence the GTPase activity of GIMAP7.

The activity of 2.5 μM of GIMAP7 (L100Q) was tested in the presence of 50 μM of the GIMAP6 mutants (Figure 24). GIMAP7 (L100Q) at 2.5 μM concentration hydrolysed GTP at a K_{Obs} of 2 min^{-1} . As shown in Figure 24, all of the predicted mutants showed varying effect on the GTPase activity of GIMAP7. Firstly and most strikingly, D167W mutation had drastic loss of inhibition on GIMAP7. It hydrolysed GTP at a K_{Obs} of 1.6 min^{-1} . Secondly, L70D mutant also exhibited loss of inhibition although lesser than D167W. It showed a K_{Obs} of 1.2 min^{-1} . Thirdly, the conserved arginine finger mutant, R134D retained its inhibitory potential to a larger extent and had a K_{Obs} of 0.2 min^{-1} . Finally, Q131E mutant behaved identical to the wild type protein and completely inhibited the GTPase of GIMAP7.

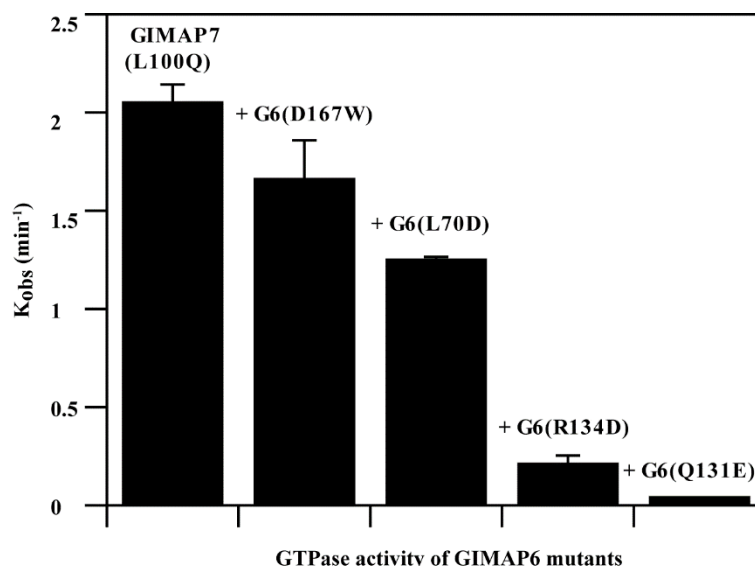


Figure 24: GIMAP6 residues involved in inhibition of GIMAP7. 50 μM GIMAP6 mutant with 2.5 μM GIMAP7 in the presence of 500 μM GTP was assayed for the nucleotide hydrolysis as described in section 2.3.4 and 2.3.5. The assay was carried out at 20°C. D167W showed maximum loss of inhibition whereas Q131E showed least influence on the inhibition.

These results suggest that GIMAP6 mutants L70, R134, D167 are involved in the inhibition reaction of GIMAP7 and support the proposed dimerization model of the GIMAP6-GIMAP7 heterodimer, since these residues are found in the predicted interface.

3.5 Biochemical characterization of inhibition mechanism of GIMAP6

The GTPase activity of GIMAP7 is abrogated in the presence of GIMAP6. Identification of the motif(s) of GIMAP6 which are involved in the inhibition could shed light on the inhibition mechanism. To identify these motifs, various N- and C-terminal deletion constructs were created on the basis of secondary structure and structural homology prediction and tested for their ability to inhibit the GTPase activity of GIMAP7 (Figure 25).

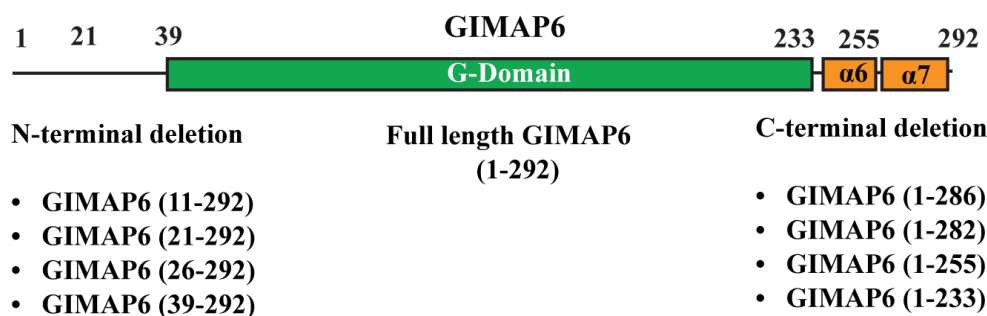


Figure 25: GIMAP6 deletion constructs. Deletion constructs were designed on the basis of secondary structure prediction by JPred server. N terminal deletion constructs are depicted in left whereas the C- terminal deletion constructs are depicted on right. GIMAP6 (1-233) lacked both helices $\alpha 6$ and $\alpha 7$, whereas GIMAP6 (1-255) lacked only $\alpha 7$. The construct GIMAP6 (39-292) starts at the G-domain of the protein.

To decipher the inhibition mechanism, all of the constructs described in Figure 25 were expressed and purified (Section 2.3.9). The yields from the purification were very poor for most of the deletion constructs. Additionally, as the length of the N-terminal was shortened, the yields were further reduced. This suggested that the flexible N-terminal residues acted like a solubility tag. Similar observations were made for the C-terminal deletion constructs.

Coincidentally, the purification of GIMAP6 (R134D) yielded 4-fold higher amounts of protein than that of GIMAP6. A possible reason for this increase in yield could be that the exchange of surface exposed long side chain of arginine with the shorter side chain of aspartate reduced the non-specific interaction among the GIMAP6 molecules and thereby prevented aggregation. Since purified GIMAP6 (R134D) was abundantly available, the GTP hydrolysis assay was

performed to determine its ability to inhibit GIMAP7. Figure 26 shows the inhibition of GIMAP7 by different concentrations of GIMAP6 (R134D). The K_{obs} of GIMAP7 was found to be $\sim 2.4 \text{ min}^{-1}$ at a concentration of $2.5 \mu\text{M}$ and the presence of $2.5 \mu\text{M}$ of GIMAP6 (R134D) could reduce it to nearly half. Furthermore, the mutant showed a concentration-dependent GTPase inhibition. However, compared to GIMAP6wt, GIMAP6 (R134D) inhibited GIMAP7 less efficiently. $50 \mu\text{M}$ GIMAP6 (R134D) was required to equalize the inhibition efficiency exhibited by $2.5 \mu\text{M}$ GIMAP6wt on $2.5 \mu\text{M}$ GIMAP7 (Figure 21). The R136D mutant did not hydrolyse GTP on its own.

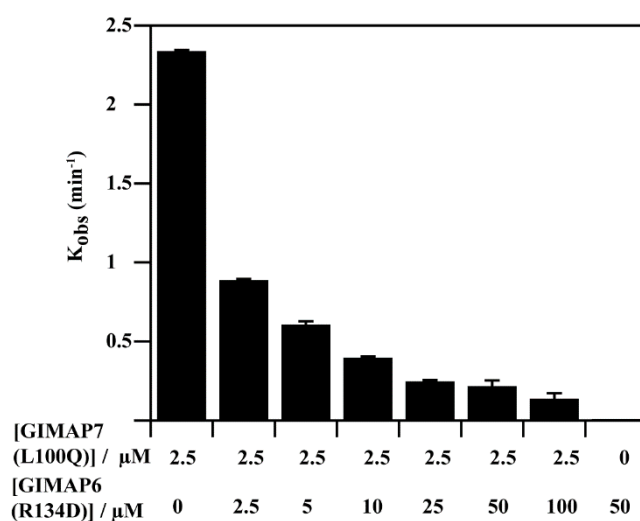


Figure 26: GIMAP6 (R134D) inhibits GIMAP7 (L100Q). GTP hydrolysis was carried out in buffer 6 (see section 2.1.9) at 20°C and nucleotide hydrolysis was measured by HPLC. Varying concentration of GIMAP6 (R134D) was reacted with constant concentration of GIMAP7 (L100Q) ($2.5 \mu\text{M}$). GIMAP6 (R134D) shows concentration dependent inhibition

Since the R134D mutant greatly increased the yield, it was introduced in other deletion constructs of GIMAP6. All the constructs with R134D mutation gave higher yields of protein when compared to that of wildtype and were used in GTPase assays with GIMAP7. Figure 27 shows the results from the assay wherein $50 \mu\text{M}$ of each GIMAP6 deletion constructs (Figure 25) was mixed with $2.5 \mu\text{M}$ GIMAP7. Full length GIMAP6 was used as a control. N-terminal deletion constructs starting at residue 11, 21, 26, 39 inhibited GIMAP7 as efficiently as full length GIMAP6. This suggested that the first 38 residues are not involved in the interaction leading to inhibition of GIMAP7. GIMAP6 C-terminal deletion constructs were still efficiently inhibiting the GIMAP7 reaction, although some of them showed slightly reduced efficiency. Thus, constructs ending at residue 255 (lacking helix $\alpha 7$) and 233 (lacking both helices $\alpha 6$ and $\alpha 7$) were less effective in inhibiting the GTPase reaction of GIMAP7 compared to GIMAP6

wt. Also constructs terminating at residue 282 and 286 showed slightly reduced inhibition efficiency although lesser than the constructs terminating at residue 255 and 233. In agreement with the homology model, these findings suggest that the core G domain is the main determinant of GTPase inhibition of GIMAP6 for GIMAP7. Helices $\alpha 6$ and $\alpha 7$, but not the first 38 N-terminal residues, may have a minor role in the inhibition reaction.

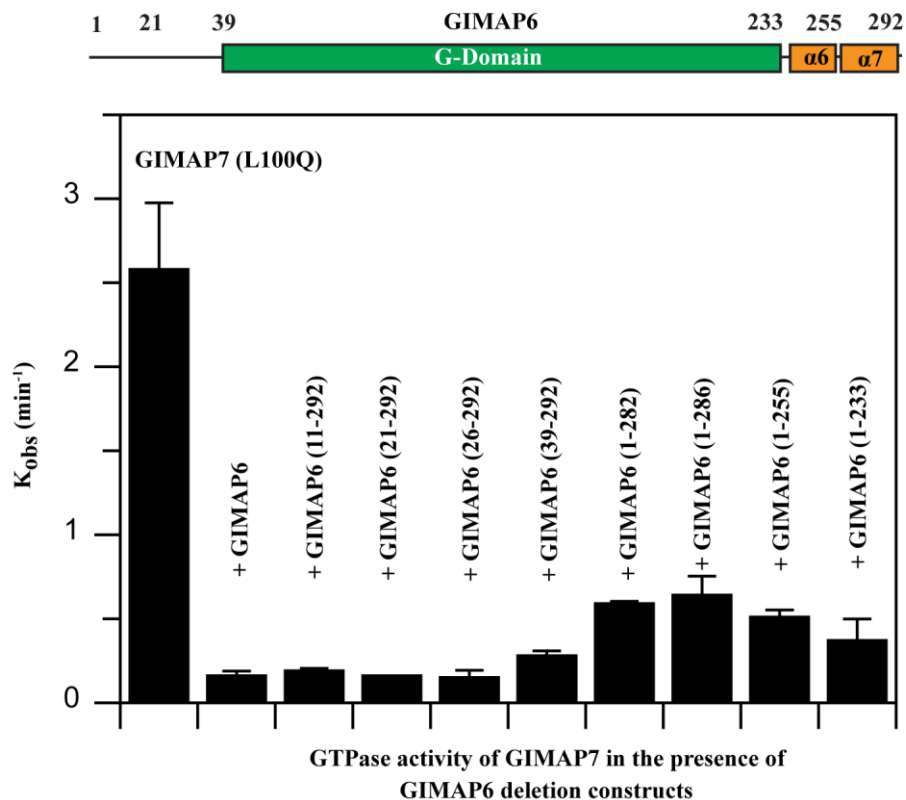


Figure 27: Identification of GIMAP6 motif responsible for inhibition of GIMAP7. A) Predicted domain architecture of GIMAP6 with the domain marked by the residue numbers. B) GTPase activity of GIMAP7 (L100Q) in the presence of deletion constructs of GIMAP6. GTP hydrolysis assay and nucleotide detection was performed as mentioned in sections 2.3.4 and 2.3.5.

3.6 Biochemical characterization of GIMAP6 and GABARAPL2 interaction

GABARAPL2 was identified as specific interaction partner of GIMAP7 in the SILAC pull down assays (Figure 15). To biophysically characterize this interaction, ITC was used to measure the binding affinity of GABARAPL2 to GIMAP7. Surprisingly, no binding was observed in this assay (Figure 28A). Based on this finding, it was hypothesized that GABARAPL2 might interact indirectly with GIMAP7 via GIMAP6 which may act as a

molecular bridge. To test this possibility, a combination of ITC and Bio-Layer Interferometry (BLI) were used. In agreement with the SILAC pull down assays, GABARAPL2 interacted with GIMAP6 (R134D) with high affinity (K_D of 223 nM) (Figure 28B), although the binding stoichiometry was less than 1. A probable explanation could be that a high proportion of GIMAP6 (R134D) in the reaction cell was unfolded and thus unavailable for binding. Additionally, the importance of the last 10 C-terminal residues for GABARAPL2 binding were determined by ITC. As previously reported (124), GIMAP6 (1-282, R134D) did not bind to GABARAPL2, suggesting that the C-terminus of GIMAP6 is involved in the interaction (Figure 28C). It was therefore hypothesized that a peptide comprising the last 10 C-terminal amino acids of GIMAP6 (HRCLLGKADL) may interact with GIMAP6. Surprisingly, the peptide also did not show any binding in ITC (Figure 28D) suggesting that elements other than the C-terminus of GIMAP6 might be involved in the GABARAPL2 interaction.

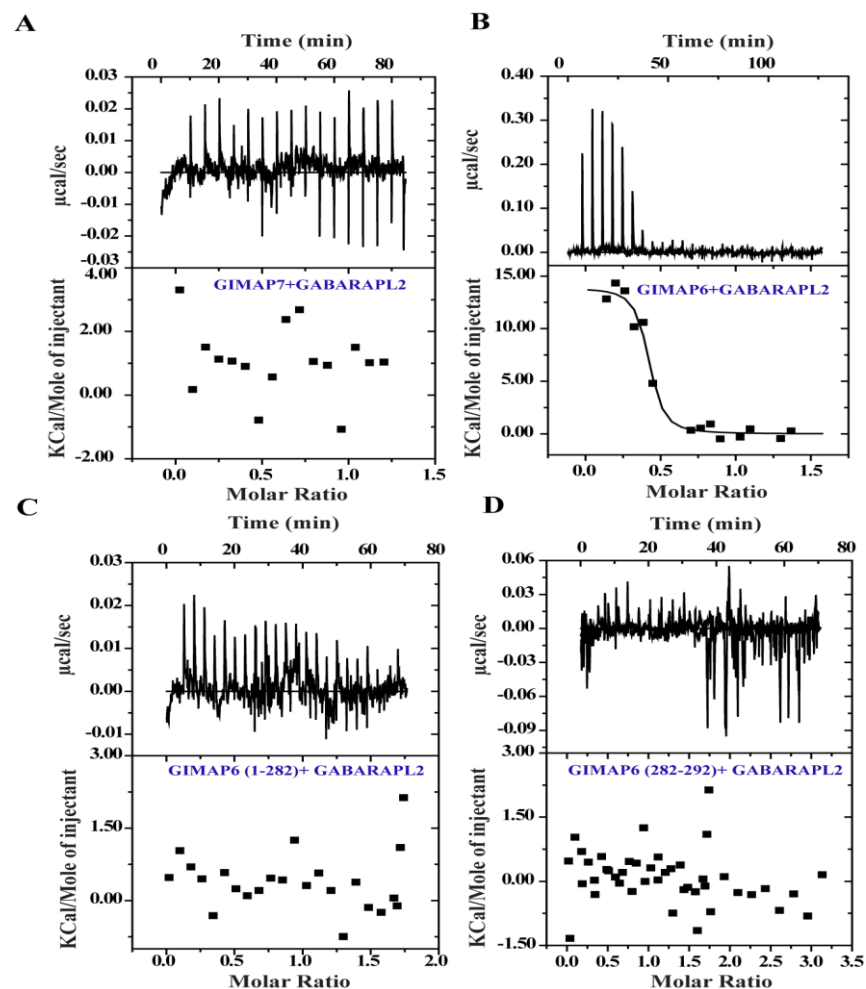


Figure 28: Biochemical characterization of GIMAP6-GABARAPL2 interaction. ITC measurements were performed as described in section 2.3.6 to identify the interaction affinities. A) GABARAPL2 did not bind to GIMAP7 (L100Q) in ITC run. B) GABARAPL2 bound to

GIMAP6 (R134D) with a high affinity. C) As previously reported, GIMAP6 (1-282, R134D) did not bind to GABARAPL2. D) A peptide comprising the last 10 C-terminal amino acids (HRCLLGKADL) of GIMAP6 also did not show any binding reaction. Peptide was dissolved in buffer but with 50mM HEPES, pH 7.5.

To further confirm this interaction, Bio-layer Interferometry (BLI) was performed to characterize the interaction between GIMAP6 and GABARAPL2. Advantages of using BLI in characterizing protein-protein interaction are that the sample volume and concentration requirement is very less when compared to the requirement in ITC. Importantly, the time required to characterize a protein-protein interaction is relatively short as the BLI measurement

GST-GABARAPL2 (Ligand) and GIMAP6 (Analyte) were purified to homogeneity for the BLI measurements. Anti-GST biosensors coated with anti-GST antibody were used in order to immobilize GST-GABARAPL2 and to study its interaction with GIMAP6. The advanced kinetic assay platform in the BLItz software suite was used for carrying out the experiment as described in 2.3.11. The global fitting on the BLI response obtained with 5 different concentrations of GIMAP6 yielded a K_D of 22.8 nM, K_a of $3.91 \times 10^3 \text{ M}^{-1}\text{S}^{-1}$ and K_d of $8.95 \times 10^{-5} \text{ S}^{-1}$ (Figure 29). As observed in Figure 29, since the affinity between GIMAP6 and GABARAPL2 is high, the dissociation of GIMAP6 as observed in the BLI response is very low.

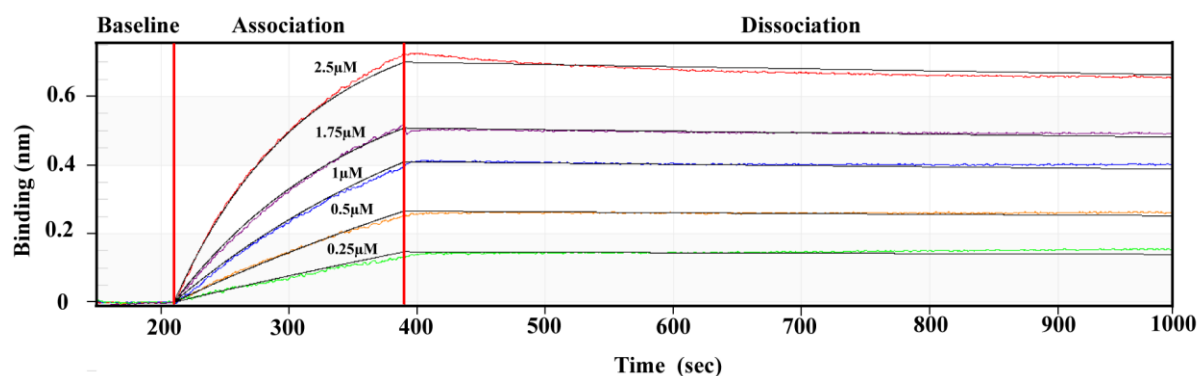


Figure 29: GIMAP6 interacts with GABARAPL2 in Bio-Layer interferometry. The interaction is measured in terms of binding response (in nm) on the y axis during the bio-layer interferometry measurement. Indicated concentrations of GMAP6 were allowed to associate with GABARAPL2 for 3 minutes, followed by dissociation for 10 minutes.

The interaction between GABARAPL2 and GIMAP6 confirmed by both ITC and BLI conclusively proved that GABARAPL2 interact with GIMAP6. Even though the exact region responsible for the interaction is yet to be characterized, current biochemical findings reveal a

high affinity interaction among them. The fact that GIMAP6 also interacts with GIMAP7 suggests that GABARAPL2 might co-exists as heterotrimeric complex in a yet to be identified cellular pathway.

3.7 Structure of GABARAPL2

To obtain insights from the crystal structure of GABARAPL2, crystallization trials were set at both 20 °C and 4 °C with the purified GABARAPL2 at a concentration of 15mg/ml. GABARAPL2 crystallised in many conditions as shown in Figure 30. In most of the conditions, crystals appeared after two days. Crystals were cryo-protected by the addition of 20% glycerol and flash frozen in liquid nitrogen. The crystal in the drop from Figure 30A was used for data collection at BESSY BL 14.1.

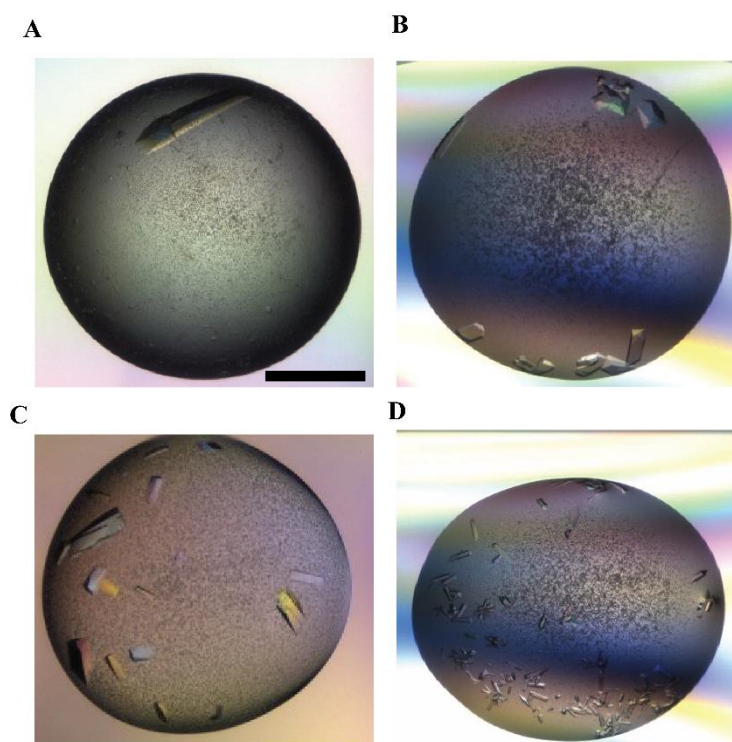


Figure 30: Crystals of GABARAPL2. Crystals appeared in A) 30 % w/v PEG 4000, 200 mM MgCl₂, 100 mM Tris-HCl pH 8.5 at 20°C, B) 2.00 M NaCl, 100 mM Sodium Acetate pH 4.6 at 20 °C. C) 20% w/v PEG 3350, 200 mM ammonium dihydrogen phosphate at 4 °C. D) 5% (w/v) PEG 6000, 1.0 M NaCl at 20 °C. The bar represents 200µm.

Diffraction data was collected as described in section 2.5.3, and crystals diffracted to a maximum resolution of 0.99 Å which is the highest resolution structure of GABARAPL2 available so far. The structure was solved by molecular replacement with GABARAP1 (PDB:

2R2Q) as search model. The structure of GABARAPL2 at atomic resolution features a compact ellipsoid fold belonging to the $\alpha+\beta$ class of protein (SCOP database) (Figure 31). It exhibited striking similarity to the ubiquitin superfamily fold in the C-terminal subdomain of the polypeptide. It is composed of four-stranded ellipsoid central β -sheet with the helices $\alpha 1$ and $\alpha 2$ packing against the convex side of the ellipsoid sheet whereas helices $\alpha 3$ and $\alpha 4$ faces the concave face of the sheet.

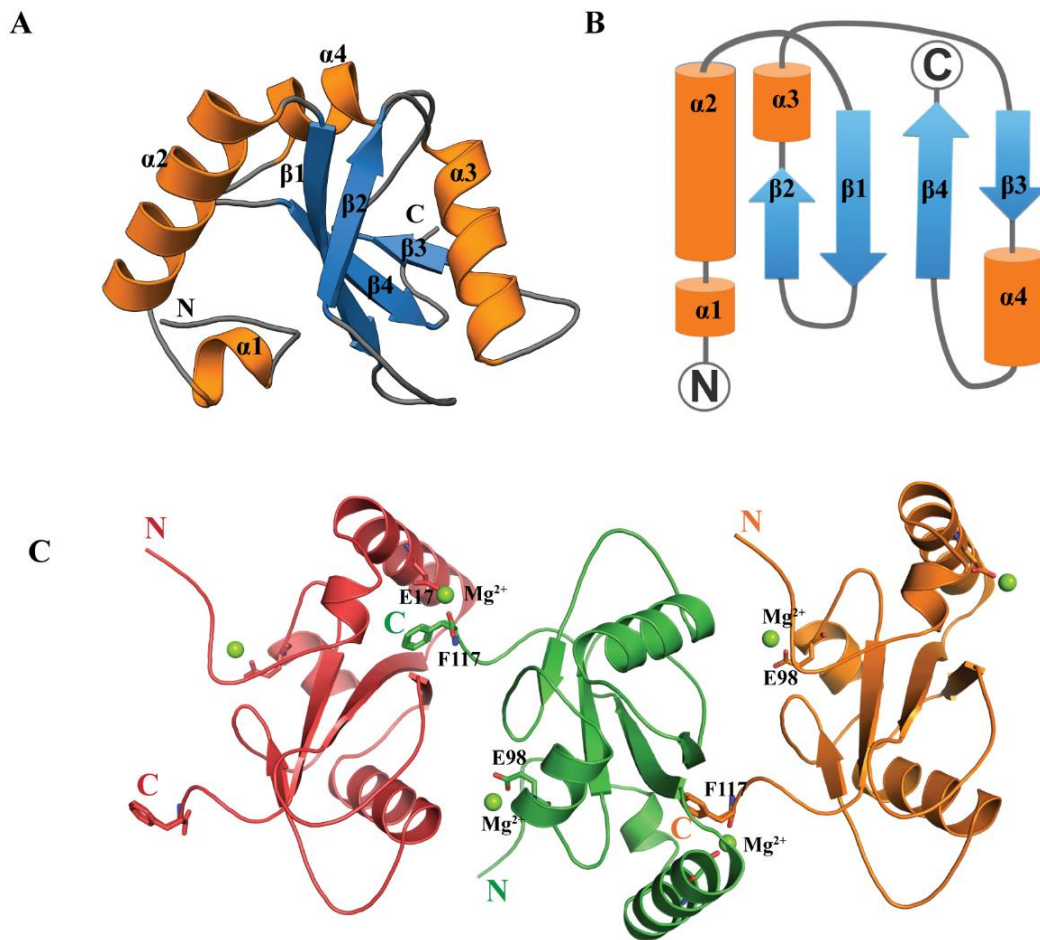


Figure 31: Crystal structure of GABARAPL2. A) Cartoon representation of 3D structure of GABARAPL2. The secondary structural elements are labelled. B) Topology diagram of GABARAPL2 representing an ubiquitin superfamily fold at the C terminus with GABARAPL2 specific helices $\alpha 1$ and $\alpha 2$ at the N-terminus. C) GABARAPL2 oligomerized in the crystals in a head to tail manner via Mg^{2+} ion coordination. Mg^{2+} is represent as green ball with the side chains of the coordinating amino acid represented as sticks.

GABARAPL2 oligomerized in the crystals in a head to tail fashion. The N-terminal of one monomer is in contact with the C terminal of the neighbouring monomer which is flipped

backwards by 180° (Figure 31C). GABARAPL2 exhibited a surface containing partially solvent-accessible hydrophobic residues, which are flanked by basic side chains. The boundary of the region is marked by basic residues on helix $\alpha 2$ and helix $\alpha 3$ flanking the central β -sheet carrying hydrophobic residues. The residues constituting this basic/hydrophobic face are highly conserved among Atg8 family proteins, and were proposed to mediate protein-protein interactions (148). In crystals, this region is involved in the formation of lattice contacts. The last C-terminal Phe117 appears to make contact with the Glu17 located in helix $\alpha 2$ in the opposing monomer via Mg^{2+} ion coordination (Figure 31C). Furthermore, Glu98, the last residue of helix $\alpha 4$ coordinates Mg^{2+} ion. It could be speculated that such oligomerization mode could occur on the surface of autophagosomes, as reported in a model where Atg8 is used as a protein scaffold by the Rab33B-GAP OATL1 (149). Data collection and refinement statistics for the dataset are given in Table 2 and Table 3, respectively.

Data collection	GABARAPL2
Beamline	BESSY 14.1
Wavelength [Å]	0.9184
Space group	P 2 ₁ 2 ₁ 2 ₁
Cell dimensions	
a, b, c [Å]	35.603, 53.991, 59.757
α , β , γ [°]	90, 90, 90
Resolution [Å] *	26.14 - 0.99 (1.03-0.99)
No. obs. reflections	571744 (20478)
No. unique reflections	63434 (5266)
R_{sym} (%)	4.6 (114.6)
I/ σ	24.95 (1.21)
Completeness (%)	0.98 (0.83)
Redundancy	9.0 (3.9)

Table 2: Data collection statistics of GABARAPL2. * Numbers in parentheses apply for the highest resolution shell.

Refinement	GABARAPL2
Resolution [Å]	(1.026- 0.99)
No. Reflection used	63432 (5266)
R _{work} /R _{free}	0.1489 (0.2747)/ 0.1673 (0.2986)
Protein molecules / asymmetric unit	1
No. of Protein atoms	2216
B-factor protein [Å ²]	12.36
R.m.s deviations	
Bond lengths [Å]	0.011
Angles [°]	1.16
Residues in favored region of the Ramachandran plot (%)	98

Table 3: Refinement statistics of GABARAPL2

3.8 Purification and crystallization of GIMAP6-GABARAPL2 complex.

Since GABARAPL2 and GIMAP6 showed a high affinity interaction, a crystal structure of the complex would shed light on the structural elements responsible for the interaction. In order to obtain crystal structure of GIMAP6-GABARAPL2 complex, extensive crystallization trials by mixing the purified proteins were carried out which did not yield crystals. However, since only a fraction of GIMAP6 bound to GABARAPL2 (see section 2.3.10), I sought to establish a purification protocol to obtain a homogenous GIMAP6:GABARAPL2 complex for crystallization trials. Initially, the purified proteins were tested for their ability to run as a heterodimeric complex in analytical gel filtration (Figure 32). As observed in Figure 32A, GIMAP6 (R134) and GABARAPL2 eluted at a volume of approximately 14 ml (fractions B4, B5, B6 and B7, in green) and 17 ml (fractions B8 and B9 in red), respectively. In the sample of complex, there is no apparent shift of GIMAP6 peak corresponding to the molecular size of GIMAP6-GABARAPL2 heterodimer. However, on analysing the fractions of the complex sample on SDS-PAGE (Figure 32B), a significant amount of GABARAPL2 co-migrated with GIMAP6 (R134D) in this peak. Fractions B3, B4, B5, B6 and B7, (in blue) from the complex sample contained GABARAPL2 in addition to GIMAP6 (R134D). Thus, it was confirmed that GIMAP6 and GABARAPL2 runs as a complex in gel filtration and could be purified on large scale for structural studies

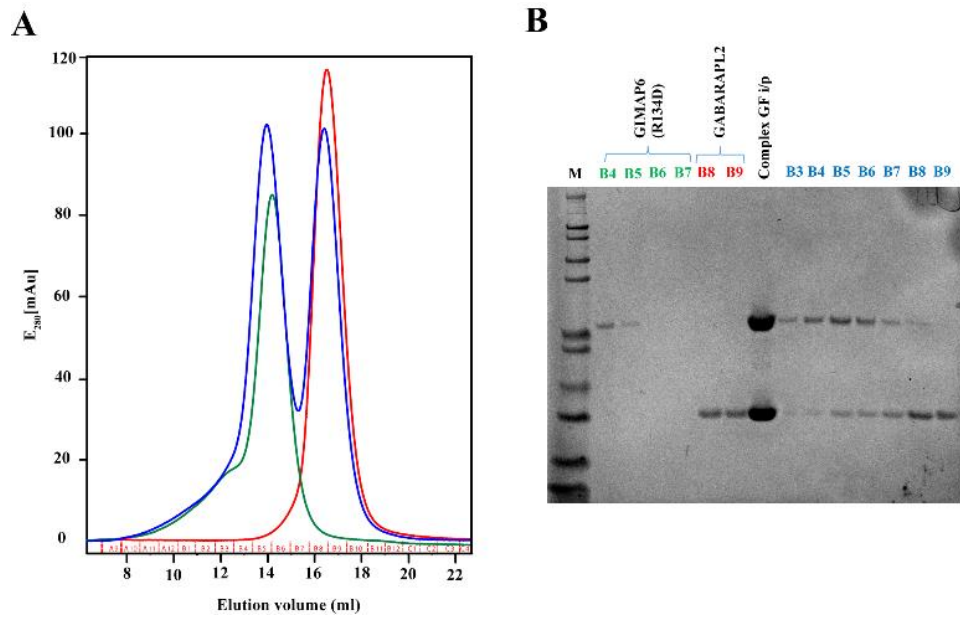


Figure 32: Analytical gel filtration of GABARAPL2-GIMAP6 (R134D) complex. A) 3mg each of GIMAP6 (R134D) (green), GABARAPL2 (red) and GIMAP6 (R134D)-GABARAPL2 mixture (blue) was injected onto a S200 10/300 Superdex column. B) A SDS-PAGE gel of the resulting fractions from the analytical gel filtration. Protein Marker, M (200, 116, 97, 66, 55, 36.5, 31, 21.5, 14, 6, 3.5 in KDa, from top to bottom)

Various purification strategies were adopted to obtain the active GIMAP6:GABARAPL2 and are detailed in section 2.3.10. A typical complex purification procedure by co-transformation strategy is shown in Figure 33. The yields obtained from this strategy were considerably higher than when the isolated proteins were purified. Thus, 10 litres of *E.coli* culture yielded 14-15 mg of purified GIMAP6-GABARAPL2 complex

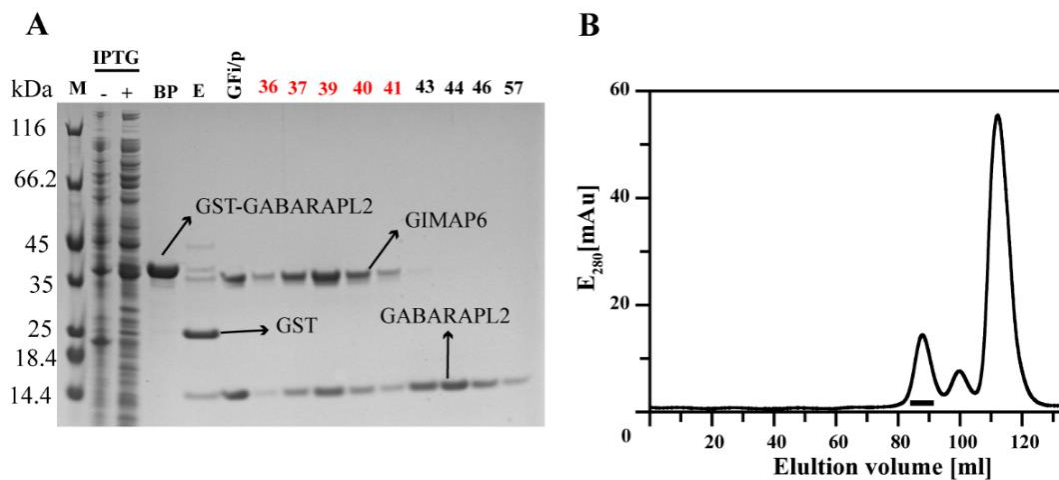


Figure 33: Typical GIMAP6wt-GABARAPL2 complex purification procedure. A) 4-12% SDS PAGE of various samples taken during the purification. Protein Marker (KDa) ; -/+ IPTG,

whole-cell bacteria lysates before and after induction; BP, protein bound to the GSH sepharose beads after washing steps; E, GSH elution showing (top to bottom) preScission protease, uncleaved GST-GABARAPL2, non-specifically bound GIMAP6, GST and non-specifically bound GABARAPL2; GF*i/p*, sample loaded on the S200 16-600; 36, 37, 39, 40, 41, 43, 44, 46, 57 fractions collected during size exclusion chromatography. Fractions used for further studies are highlighted in red. b) Superdex200 size-exclusion chromatogram. Fractions pooled (36-41) and concentrated for further experiments are indicated.

The GIMAP6:GABARAPL2 complex eluted as a single peak on a size exclusion column (Figure 33). This complex was concentrated to 12.5 mg/ml and directly used for crystallization screening using various crystallization screens at both 4 °C and 22 °C. Initial crystal hits of GIMAP6-GABARAPL2 were obtained in 8% PEG 4000, 800 mM LiCl₂ and 100 mM Tris-HCl pH 8.5 after 4 weeks at 4 °C (Figure 34A).

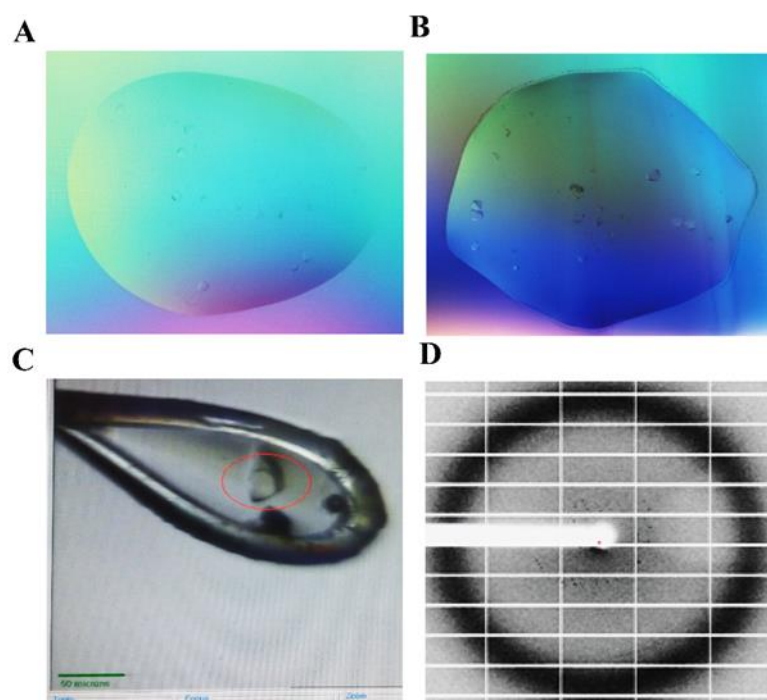


Figure 34: Crystallization of GIMAP6wt-GABARAPL2 complex. A) & B) crystals of GIMAP6-GABARAPL2 complex. C) Crystal used for data collection at BL14.1, BESSY. The size of the crystals is about 25 μ m in length. d) Diffraction image obtained from the crystal shown in C.

These crystals were cryoprotected in 20% ethylene glycol in mother liquor and flash frozen in liquid nitrogen. However, these crystals diffracted only to 8 Å under synchrotron radiation, which did not allow for structure determination. Fine screens of the previous

conditions was made with a fresh batch of GIMAP6wt-GABARAPL2 complex. Surprisingly, the crystals appeared (Figure 34B) within 2 weeks in 8% PEG 4000, 1.4 M LiCl₂ and 100mM Tris-HCl pH 8.0 at 4 °C. The crystals were flash frozen in liquid nitrogen with 20% ethylene glycol as the cryo protectant. Crystals (Figure 34C) diffracted up to 6.49 Å. The diffraction pattern obtained from the crystal can be seen in Figure 34D. A complete data set was collected from this crystal to gain insights about the orientation of GIMAP6 or GABARAPL2 in the crystals. It was attempted to solve the structure of the complex by molecular replacement, using the homology model of GIMAP6 or GABARAPL2 as search models. However, no clear molecular replacement solution was found.

Efforts are ongoing to obtain crystals of the complex. Crystallization trials for GIMAP6 (26-292, R134D):GABARAPL2 and GIMAP6 (39-292, R134D):GABARAPL2 complexes were made with no success. Seeding experiment were performed using the tiny crystals obtained from the full length complex with no or little success.

3.9 GIMAP6:GABARAPL2 complex inhibits GIMAP7

Based on identified interaction between GIMAP6, GABARAPL2 and GIMAP7 in SILAC pull down assay (section 3.1.1), the ability of purified GIMAP6:GABARAPL2 complex to influence the GTPase reaction of GIMAP7 was tested. HPLC based GTP hydrolysis assays were used for this purpose (see section 2.3.4-2.3.5)

To determine the influence of GIMAP6:GABARAPL2 complex on GIMAP7, different concentrations of complex (2.5, 5, 10, 25, 50 µM) were tested against a constant concentration of 2.5µM GIMAP7 in the presence of 500µM GTP at 20°C in a mixed GTPase assay. GIMAP7 had a K_{Obs} of $\sim 1.1 \text{ min}^{-1}$ and GIMAP6:GABARAPL2 complex did not lead to detectable levels of nucleotide hydrolysis. However, as shown in Figure 35, GIMAP6:GABARAPL2 complex effectively inhibited GIMAP7 at all concentrations tested. This suggest that GIMAP6:GABARAPL2 is an active inhibitory complex of GIMAP7. It can also be inferred that the observed inhibition is not dependent on concentration of the inhibitory complex. Similar to GIMAP6 (Figure 20B), GIMAP6:GABARAPL2 complex effectively inhibited GIMAP7 at equimolar concentration. These results further strengthens the findings of SILAC pull down assay that GIMAP6, GABARAPL2 and GIMAP7 co-exist as a complex.

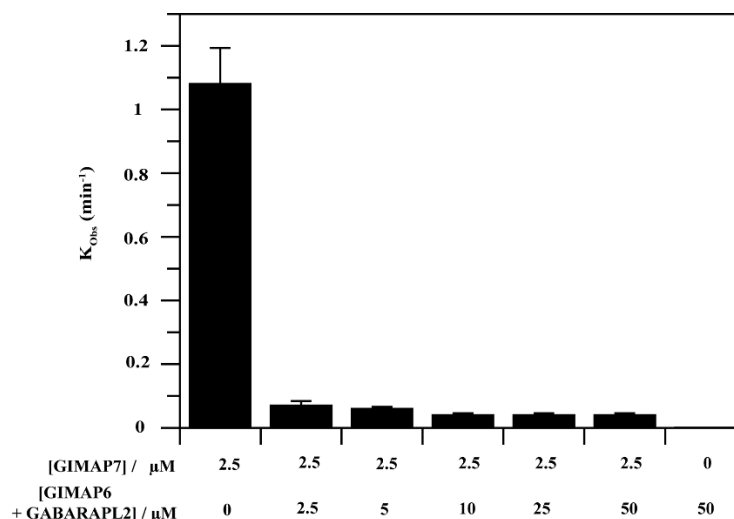


Figure 35: GIMAP6:GABARAPL2 complex inhibits GIMAP7. GTP hydrolysis was carried out in buffer 6 (section 2.1.9) at 20°C and nucleotide hydrolysis was measured by HPLC. Varying concentration of GIMAP6:GABARAPL2 complex was reacted with constant concentration of GIMAP7 (2.5 μM). The complex inhibited GIMAP7 in all tested concentrations. 50 μM GIMAP6:GABARAPL2 complex did not hydrolyse GTP.

3.10 Influence of GTPase activity within GIMAP family

GIMAP7 stimulated the GTPase activity of GIMAP2 which was inherently incapable of hydrolysing GTP (90). It was also observed that GIMAP6 inhibited the GTPase activity of GIMAP7. This led to the hypothesis that cytosolic members of the GIMAP family (e.g. GIMAP4 and GIMAP7) influence the GTPase activity of membrane-associated GIMAP members (GIMAP1, GIMAP2 and GIMAP5). In order to address this hypothesis, GTP hydrolysis assays were performed across cytosolic and membrane associated members of GIMAPs.

Initially, increasing concentrations of GIMAP2 were tested against a constant concentration of GIMAP7 to further support the observed stimulated GTPase reaction. As shown in Figure 36A, increasing concentration of GIMAP2 increased the overall GTPase activity of the GIMAP2-GIMAP7 mixture. It could be suggested that the elevated GTPase activity was due to the contribution of GIMAP2 as GIMAP2 (R117D), a mutant in the dimerization interface, could not elevate the overall GTPase activity as wild type GIMAP2. This suggested that R117 of GIMAP2 is required for the concentration-dependent stimulation of the GTPase reaction by GIMAP7.

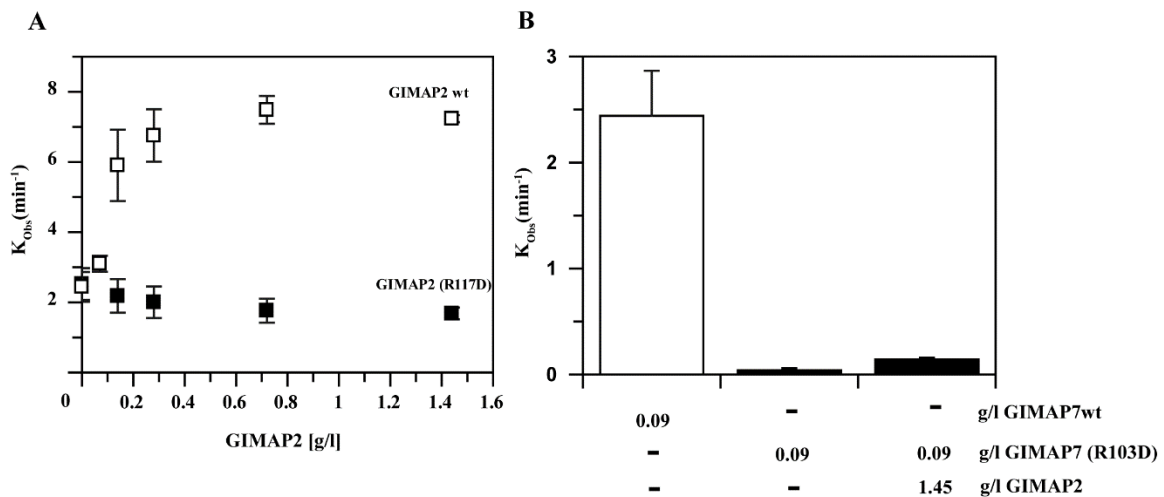


Figure 36: Arginine fingers of GIMAP2 and GIMAP7 are required for the stimulated GTPase reaction. A) Concentration dependency of GIMAP2 on the stimulation of GTPase activity. B) The conserved arginine finger of GIMAP7, R103, is required for GTPase stimulation.

Further on, it was confirmed that the arginine finger of GIMAP7, Arg103 is indeed provided in trans to stimulate GIMAP2. GTPase assays with GIMAP7 (R103D) and GIMAP2 showed a complete loss of GTPase activity (Figure 36B). Neither GIMAP7 (R103D) nor GIMAP2 together with GIMAP7 (R103D) showed GTP hydrolysis. Individual GTPase reactions of both GIMAP7 and GIMAP7 (R103D) served as controls. These results prove that the arginine finger of GIMAP7 is donated in trans to GIMAP2 to stimulate its GTPase activity.

A possible influence of GIMAP6 on the GTPase reaction of GIMAP5 was also tested. At first, the GTPase activity of GIMAP5 (1-276) was determined (Figure 37A). As can be observed in Figure 37A, GIMAP5 did not hydrolyse GTP, even after an extended incubation time of over 10 hrs. To determine the influence of GIMAP6 on GIMAP5, equimolar concentrations of GIMAP5 and GIMAP6 were incubated with GTP and analysed for GTP hydrolysis. As can be seen in Figure 37B, GIMAP6 did not influence the activity of GIMAP5 (red triangle). 50 μ M of each GIMAP6 and GIMAP5 with 500 μ M GTP were used as controls in separate reactions.

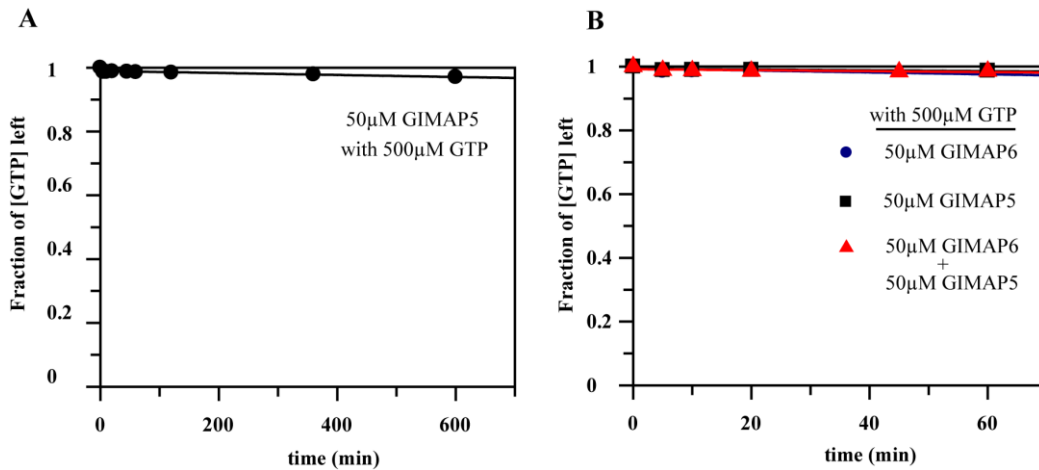


Figure 37: GIMAP6 did not influence GIMAP5 in GTP hydrolysis assay. A) GTP hydrolysis assay of GIMAP5 with GTP over a period of 10hrs. No detectable GTP hydrolysis was observed. B) No detectable hydrolysis observed in GTP hydrolysis assay of GIMAP5 in the presence of GIMAP6. Catalytically silent GIMAP6 and GIMAP5 separately served as control. Data points represent mean values \pm range of two independent experiments

GIMAP6 was tested against GIMAP2. It was speculated that cytosolic GIMAP6 could interact with free GIMAP2 on the surface of lipid droplet and could influence its GTPase activity. But as shown in Figure 38A, GIMAP6 did not influence the GTPase reaction (inverted blue triangles). Catalytically silent GIMAP2 and GIMAP 5 were used as controls.

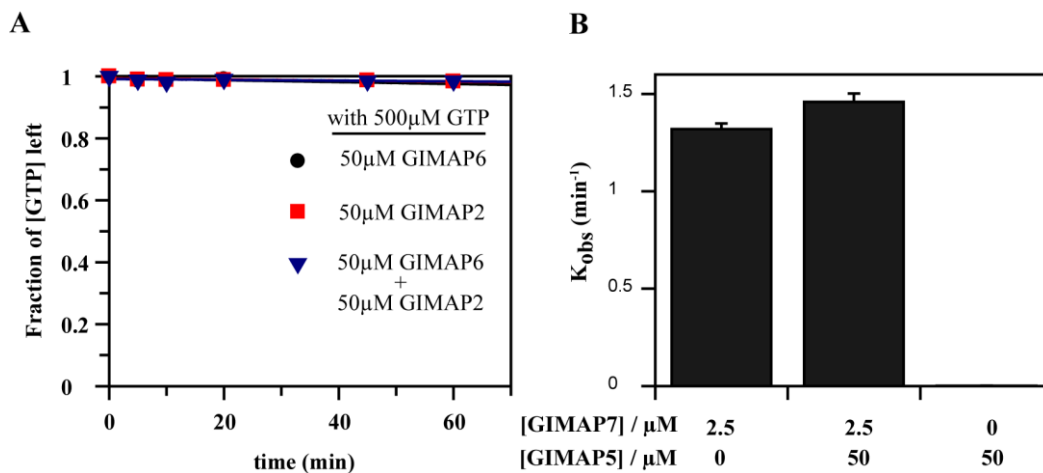


Figure 38: GIMAP6 and GIMAP7 did not influence GIMAP2 and GIMAP5 respectively in GTP hydrolysis assays. A) GTP hydrolysis assay of GIMAP2 in the presence of GIMAP6 showed no detectable GTP hydrolysis. GIMAP6 and GIMAP2 separately served as control. B) 50 μ M GIMAP5 did not influence the GTPase activity of 2.5 μ M GIMAP7. As shown in Figure

37A, GIMAP5 did not possess GTP hydrolytic activity. Data points represent mean values \pm range of two independent

Finally, the possibility of GIMAP5 influencing the GTPase activity of GIMAP7 was also determined. 2.5 μ M of GIMAP7 had a K_{Obs} of $\sim 1.3 \text{ min}^{-1}$. The activity of 2.5 μ M GIMAP7 was not affected significantly in the presence of 50 μ M GIMAP5. As expected, GIMAP5 was catalytically silent with no detectable GTP hydrolysis. To conclude, the experiments suggest that GIMAPs interact among the family members in a selective manner. It should also be considered that GIMAPs could interact with a variety of other proteins in cells which are yet to be identified and characterized.

3.11 Cellular localization and function of GIMAPs in Jurkat T cells

GIMAPs are abundantly expressed in tissue of immune system like spleen, lymph node, and the subcellular localization of GIMAPs vary based on the presence or absence of stretches of hydrophobic sequence in the C-terminal helices (see section 1.6.1). Cell biological experiment were carried out to understand the role of GIMAPs in Jurkat T cells. Subcellular localization, role in autophagy and apoptosis and the involvement in regulation of lipid droplet numbers in Jurkat T cells were tested.

The subcellular localization of all human GIMAPs were previously determined except for GIMAP6. As shown in Figure 39, EGFP tagged GIMAP6 is cytosolic which is in agreement with the lack of hydrophobic sequence at the C-terminus. It was previously determined that GIMAP1 localizes to the Golgi apparatus and GIMAP5 to lysosomes (see Table 1). Live cell imaging was performed in Jurkat T cells to determine if overexpressed GIMAP1 and GIMAP5 localized to LDs. As observed in Figures 39C and D, the fluorescence signal emerging from BODIPY and the mCherry-tagged GIMAP1 and GIMAP5 are from distinct region in the cell, thus proving that neither GIMAP1 nor GIMAP5 localized to lipid droplets. An observation was also made in the previous studies that the number of lipid droplet per cell doubled upon over expression of GIMAP2 (88). Based on the finding that GIMAP2 and GIMAP7 interacted and co-localized on LDs, the effect of overexpression of GIMAP7 on LD numbers in Jurkat cells was determined. Unlike GIMAP2, overexpression of GIMAP7 did not seem to have an effect on the lipid droplet numbers (Figure 39B)

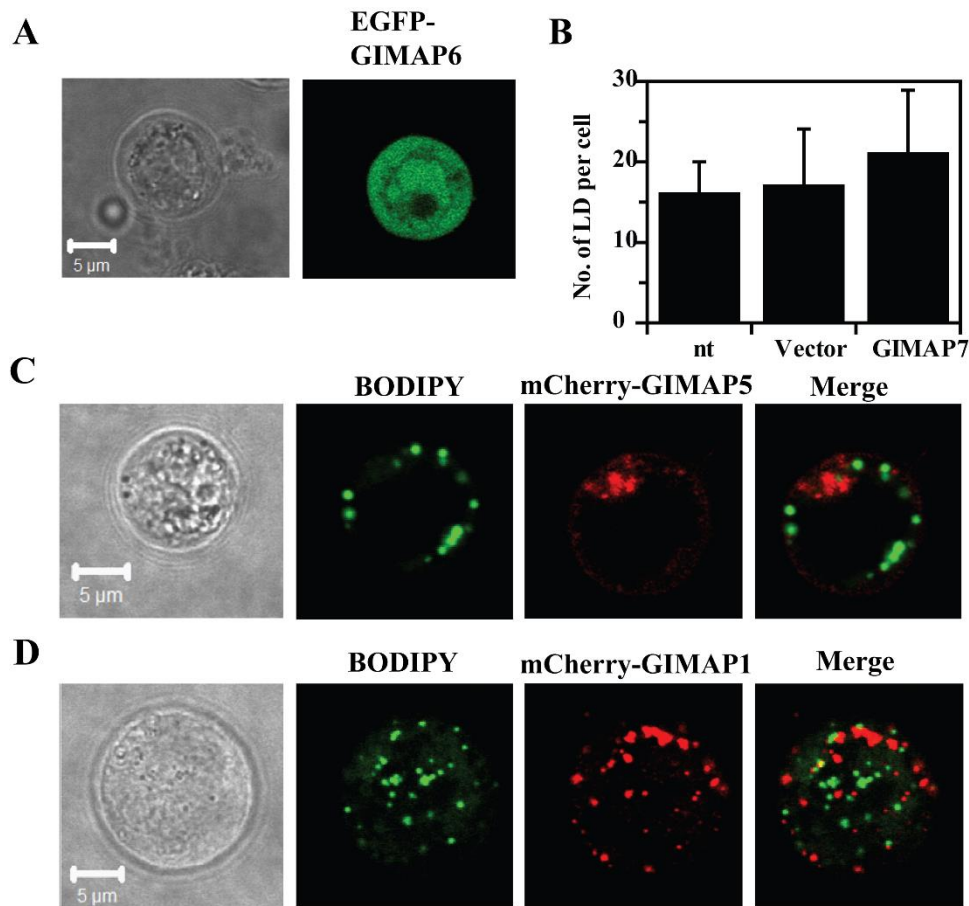


Figure 39: Localization screen of GIMAP1, GIMAP5 and GIMAP6 in Jurkat T cells. A) EGFP-GIMAP6 was cytosolic upon its overexpression in Jurkat T cells. B) Overexpression of GIMAP7 did not influence the LD numbers. 24 h after transfection with the GIMAP7, lipid droplets were stained with BODIPY 495/503 and counted in two independent experiments. The mean lipid droplet number and standard deviation are shown. Non transfected (nt) cells and empty mCherry vector transfected cells served as controls. C and D) Overexpressed mCherry tagged GIMAP1 and GIMAP5 did not localize to BODIPY 495/503 stained LDs.

Despite the lack of a hydrophobic sequence, GIMAP7 co-localized on LDs along with GIMAP2. Based on the co-localization, it could be speculated that GIMAP7 interacted with GIMAP2 on the surface of lipid droplets. This led to the hypothesis that GIMAP7 might change its sub-cellular locality under certain physiological condition. Apoptosis and autophagy were used to examine this hypothesis.

Apoptosis was induced by anti-CD95 antibody in Jurkat T cells transfected with mCherry tagged GIMAP7 and its localization was observed by fluorescence microscopy. In the control cells, GIMAP7 localized to LDs as seen in Figure 40A (upper panel). 24 hours post

transfection, mCherry-positive cells were sorted and apoptosis was induced and later confirmed by the nuclear staining with DAPI. It should be noted that the nucleus of healthy Jurkat T cells does not get stained by the DAPI dye, whereas the nucleus of a dying or apoptotic cell can take up the DAPI stain. Nuclear fragmentation, a mark of apoptosis was also observed. 6 hours post induction of apoptosis, cells were stained for lipid droplets with BODIPY 493/503 and observed under the microscope. It was found that, GIMAP7 still remained on the surface of lipid droplets (Figure 40B, lower panel) suggesting that the process of apoptosis does not alter the localization of GIMAP7.

Similarly, localization of GIMAP7 was studied in Jurkat T cells undergoing autophagy. The cells were co-transfected with both EGFP-LC3B and mCherry-GIMAP7 and the cells were treated with Suberoylanilide Hydroxamic Acid (SAHA) to induce autophagy. SAHA induced autophagy by triggering the production of reactive oxygen species (ROS) (88) Microtubule-associate light chain 3B (LC3B) is a marker of autophagy (150). Under physiological conditions, LC3B is cytosolic but upon induction of autophagy, LC3B is cleaved to form an intermediate called LC3II which in turn localizes to the autophagosomes. As seen in Figure 40B, autophagy was successfully induced in Jurkat T cells which is observed as a speckled pattern of EGFP-LC3B. In non-autophagic cells, LC3B was cytosolic. mCherry- tagged GIMAP7 also showed localization to lipid droplets by forming circular rings around them. The localization of GIMAP7 was indeed on the surface of lipid droplet which was confirmed in an independent experiment (data not shown). This clearly suggested that localization of GIMAP7 did not change upon induction of autophagy. These preliminary cell biological experiments lay foundation for a more thorough understanding of the GIMAPs in the cellular context.

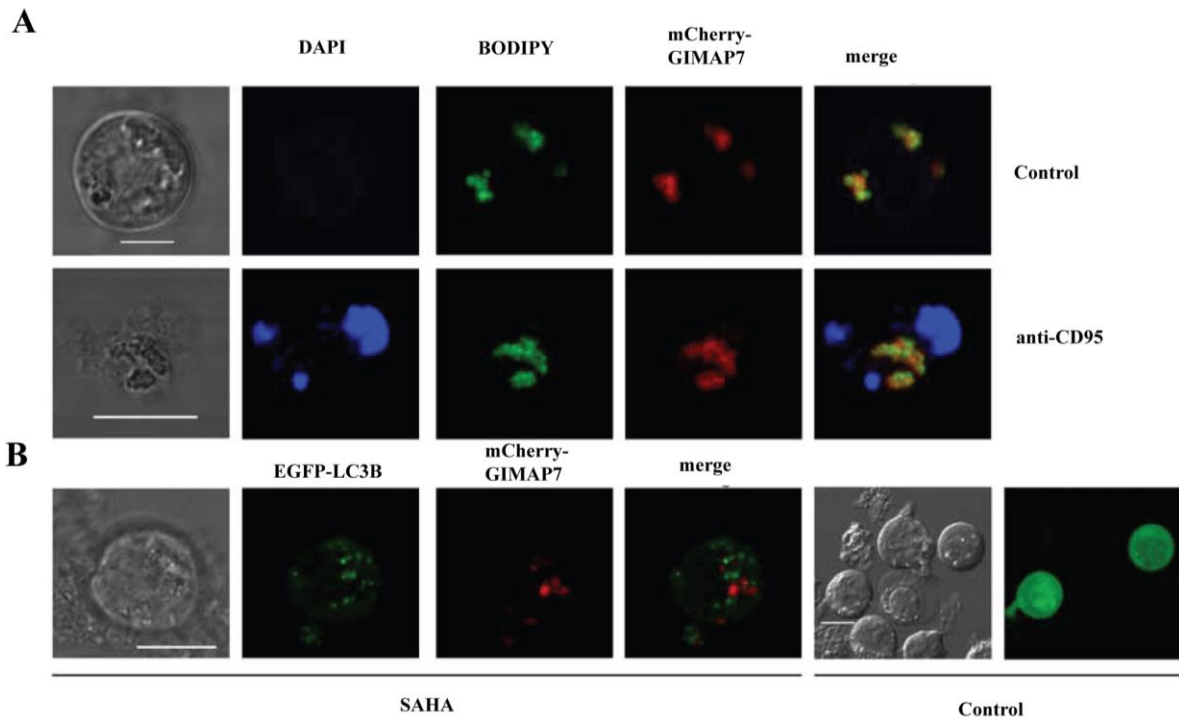


Figure 40: Effect of apoptosis and autophagy on the localization of GIMAP7. A) mCherry-tagged GIMAP7 was expressed in healthy control Jurkat cells (upper panel) or in Jurkat cells where apoptosis was induced (lower panel) using anti-CD95 antibody, as described in section 2.4.3. LDs were stained with BODIPY 493/503. Nuclear DNA was stained with DAPI. DAPI only stains the nuclei of apoptotic cells and appeared fragmented. B) mCherry-tagged GIMAP7 was expressed in Jurkat cells treated with the autophagy-inducer SAHA, as described in section 2.4.4. Induction of autophagy was confirmed by following the relocalization of EGFP-tagged microtubule associated protein 1 light chain 3B (LC3B) from the cytosol to autophagic membranes (compare to control cells on the right side). GIMAP7 in autophagic cells still localized to regular spherical compartments resembling lipid droplets.

5. Discussion

5.1 GIMAP6 homology model and GIMAP6-GIMAP7 structural interface

GIMAP6 was identified as a specific interaction partner of GIMAP7 in SILAC pull down assays. Considering the high degree of confidence in its detection using mass spectrometric analysis, the definitive biochemical function of GIMAP6 has been characterized in this doctoral work. GIMAP6 exhibited an inhibitory function on the GTPase activity of GIMAP7. Since GIMAP6 did not yield crystals despite extensive crystallization trials, a homology model was built with GIMAP7 as the template in the modelling process. Accordingly, the obtained homology model of GIMAP6 had high resemblance to that of GIMAP7 (Figure 22C). The model featured all the highly conserved G motifs, and in addition it also carried the antiparallel β -strand at one end of the sheet which is a typical feature of the TRAFAC class of GTPases (63). The β -strand (β_2) begins with a serine which is adjacent to the switch I region (Figure 22A). Sequence alignment of GIMAP7, GIMAP6 and GIMAP2 also showed high sequence similarity except in the regions of the C-terminal extensions (Figure 41A). As expected, GIMAP6 not only resembled GIMAP7 but also GIMAP2 on its overall structure, as evident from the alignment of their structures (Figure 41B). With such a confident homology structures, the modes of interactions of both GIMAP2 and GIMAP6 with GIMAP7 could be compared.

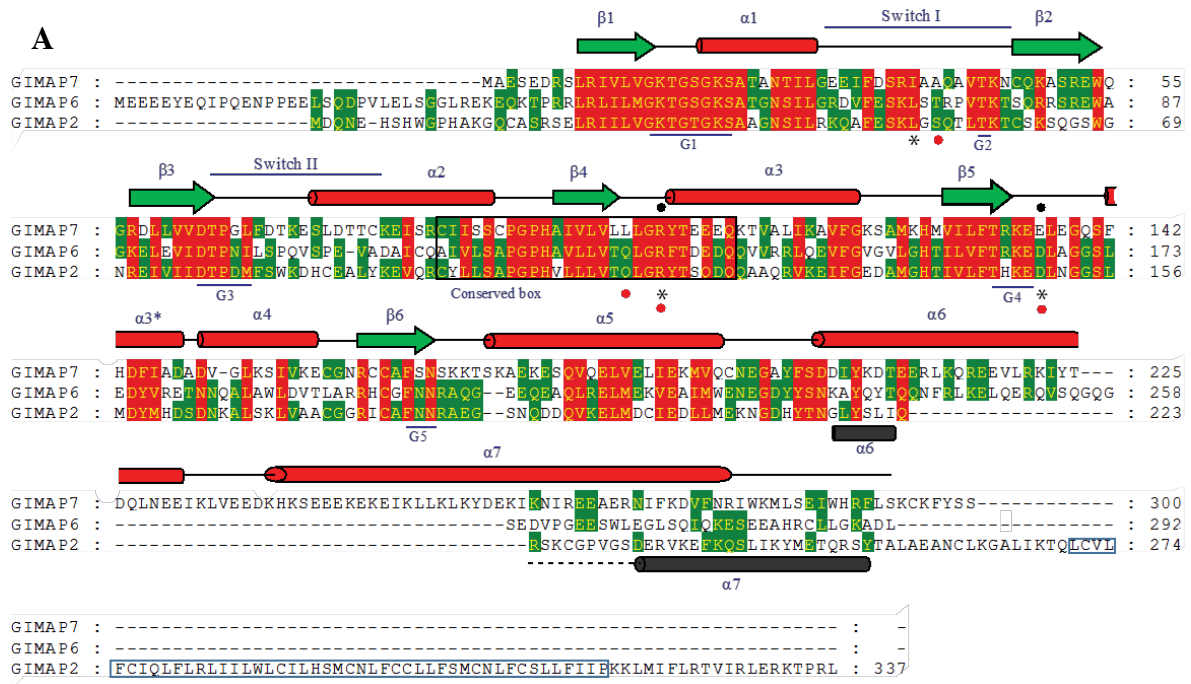
It was shown that GIMAP7 stimulated the GTPase activity of GIMAP2 via the G interface. The catalytic arginine fingers R103 and R117 in GIMAP7 and GIMAP2, respectively are indispensable for the interaction (Figure 36). Residues involved in homodimerization, such as Ser54 in switch I of GIMAP2 and Gln136 adjacent to the G4 motif of GIMAP7 were also shown to be necessary for efficient GTPase stimulation (90). Interestingly, corresponding conserved residues and motifs in GIMAP6 were also crucial for the inhibition of GIMAP7 (Figure 24). For instance, the mutation of Leu70 in GIMAP6 in the centre of switch I to Asp significantly reduced the ability of GIMAP6 to block the GTPase reaction in GIMAP7. It is probable that switch I of GIMAP6 stabilizes the GIMAP6-GIMAP7 heterodimeric complex.

Strikingly, Asp167 adjacent to G4 motif in GIMAP6, was found to be the most important residue for heterodimer formation. The D167W mutant had only a minimal effect on

the GTPase activity of GIMAP7 revealing the importance of this residue. It should also be noted that the corresponding conserved residue Asp150 in GIMAP2 (Figure 41A) was involved in stabilization of GIMAP2 homodimer by forming hydrogen bond with the exocyclic amino group of the guanine base in the opposing monomer. Similar interactions has also been shown in the dynamin G domain dimer where Asp211 in G4 motif interacts with nucleotide in trans (151). It should be recollected that the corresponding residue Glu136 (adjacent to G4 motif) in GIMAP7 played a crucial role for both homodimerization and for the stimulation of the GTPase activity in GIMAP2. All of these observations suggest that Asp167 in GIMAP6 plays a crucial role in stabilization of GIMAP6-GIMAP7 complex and subsequently prevent GTP hydrolysis in GIMAP7.

The conserved arginine residue of GIMAP6, Arg134, had a strikingly different function when compared to that of other canonical G proteins (Figure 26). For example, in the Ras superfamily, GTP hydrolysis is stimulated by GTPase-activating proteins (GAPs) which supply an arginine finger in trans into the catalytic site (65). In case of the GIMAP7-GIMAP2 heterodimer, Arg103 in GIMAP7 and Arg117 in GIMAP2 are thought to be delivered into the opposing catalytic site during hetero-dimerization, leading to an overall increase of GTP hydrolysis (Figure 36). However, Arg134 in GIMAP6 appears to play an entirely different role for the regulation of GTP hydrolysis in GIMAP7. The mutation R134D in GIMAP6 significantly interfered with the inhibition of the GTPase activity in GIMAP7 (Figure 26) in a yet to be identified mechanism. The above observations suggest that the arginine fingers in G proteins has multiple functions, stimulation of GTPase activity in GIMAP7, inhibition of GTPase activity in case of GIMAP6 and the formation of a regular scaffold in GIMAP2. Finally, Gln131 in GIMAP6 did not influence the GTPase reaction of GIMAP7, whereas the corresponding conserved residue Gln114 in GIMAP2 is involved in the stabilization of the GIMAP2 homodimer by forming hydrogen bond with Arg117 in the opposing monomer (88).

Apart from the G domain residues in GIMAP6, the GIMAP-specific C-terminal extension also has a partial role in the inhibition of GIMAP7 (Figure 27). Based on the homology model, helix $\alpha 7$ appears to be in contact with switch II and could possibly stabilize this region for the formation of a catalytically silent GIMAP6-GIMAP7 complex. A similar interaction was shown for GIMAP2, where $\alpha 7$ is in direct contact with the switch II, but only in the GDP-bound form. On the contrary, the highly disordered N-terminal region of GIMAP6 did not contribute to the inhibition. Thus, the GIMAP6 mutants based on the homology model and truncated variants establishes the mode of interaction between GIMAP6 and GIMAP7.



B **GIMAP6** **GIMAP7**
GIMAP2

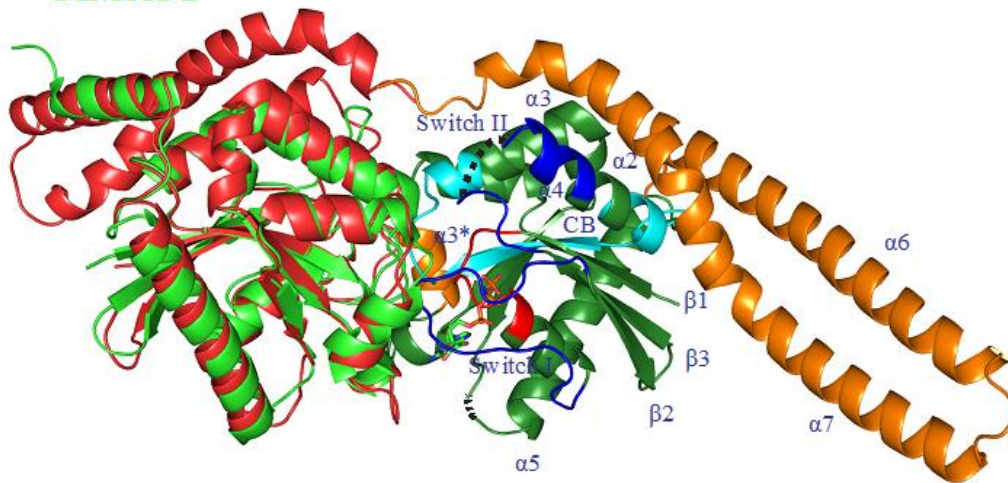


Figure 41: Modes of interaction in GIMAP6-GIMAP7 heterodimer. A) Sequence alignment of GIMAP7, GIMAP6 and GIMAP2 using ClustalW. The G motifs (G1-G5) and switch regions are highlighted. The secondary structural elements of GIMAP7 are represented above the sequence with α helices as red barrels, β strands as green arrows and loop regions as black lines. GIMAP6 mutants described in this study are marked with an (*). The residues of GIMAP2 involved in the homodimerization and stimulation of GTPase activity are marked with pink dots. The GIMAP7 residues responsible for catalysis and homodimerization are marked with black dots. The C terminal extension of GIMAP2 consisting of helices $\alpha 6$ and $\alpha 7$

are depicted as black barrels. Also the hydrophobic segment of GIMAP2 are highlighted in blue box. B) Superimposition of GIMAP2 (green) on the GIMAP6:GIMAP7 heterodimer homology model. GIMAP6 is shown in red whereas GIMAP7 is coloured based on motifs and secondary structural elements. The G domain is shown in green, switch I and Switch II in blue, the P-loop in red, and the conserved box in cyan. GIMAP specific helix $\alpha 3^*$ and helices $\alpha 6$ and $\alpha 7$ are shown in orange.

5.2 GIMAP6-GABARAPL2 interaction

GABARAPL2, the mammalian homologue of yeast Atg8, was found to interact with GIMAP6 in a SILAC-based pull down assays (Figure 15). The interaction was confirmed by both ITC and Bio-layer interferometry. The identified interaction was of high affinity in the nanomolar range (Figures 28B and 29). It was reported that GIMAP6 is recruited to autophagosome upon induction of autophagy (124). Subsequently, both the cytosolic GIMAP6 and GABARAPL2 formed punctate structures. It was shown that GABARAPL2 interacts with GIMAP6 and subsequently guides it to the autophagosomes for degradation.

Since GIMAP6 is a G protein, it was speculated that the interaction with GABARAPL2 is nucleotide-dependent. However, it was revealed in this study that GIMAP6 bound neither GTP- γ -S nor GDP, despite featuring all of the consensus sequence motifs for nucleotide binding (Figure 19). A plausible explanation for GIMAP6 not binding to nucleotide could be related to G1 motif. It was reported that in a group of G proteins that did not bind or involve nucleotide in their function had the three dimensional conformation of variable residues (XXXX) in the GXXXGKT(S) motif widely different in crystal structures when compared to nucleotide binding G proteins (143). In addition to that, GIMAP6 bound GABARAPL2 in a buffer devoid of nucleotide in ITC experiments, suggesting that the interaction is nucleotide-independent (Figure 28B). Despite this nucleotide independent interaction, mutations in the G motifs (G1, G2 and G3) were shown to prevent the interaction (124) suggesting some involvement of the G domain in the interaction surface. Additionally, a construct of GIMAP6 lacking the 20 N-terminal residues bound GABARAPL2 with equal affinity compared to that of full length GIMAP6 (data not shown). This is in agreement with a recent publication reporting that introducing a mutation in a putative LIR motif in the N-terminal residues of GIMAP6 did not affect the interaction with GABARAPL2 (124). It was also demonstrated that last 10 residues in the C-terminus are responsible for the interaction (Figure 28C). Surprisingly,

a peptide consisting of those 10 residues also did not bind GABARAPL2 (Figure 28D). Furthermore, the N-terminal 10 residues in GABARAPL2 were shown to be necessary for the interaction. These observations suggest that three structural components namely, N-terminal of GABARAPL2, C-terminal of GIMAP6 and G1-G3 motifs in GIMAP6 are essential for the interaction. Such a large interaction interface involving motifs on both GIMAP6 and GABARAPL2 is in strong agreement with the observation that GIMAP6 and GABARAPL2 interact with nanomolar affinities.

The crystal structure of GABARAPL2 solved independently in this study has the highest resolution (0.99 Å) among structures available to date for mammalian homologues of Atg8 (Figure 31). It featured a closed conformation where the N-terminal helix α 1 is packed onto C-terminal ellipsoid β -sheet. Even though the structure of GABARAPL2 was reported earlier, the arrangement of GABARAPL2 molecules in the crystals obtained in this study are different (152). GABARAPL2 appears to form head to tail oligomers in the crystals. Due to the atomic resolution obtained in this study, an interaction between Glu16 in helix α 2 and Phe117 (terminal residue) in the neighbouring molecule in the crystal via Mg^{2+} ion coordination is suggested (Figure 31C). Consistent with this observation there is a report on crystal structures of GABARAP, a homologue of GABARAPL2 where the N-terminal helix α 1 folds outwards of the C-terminal subdomain and forms close contact with the β -sheet of the neighbouring molecule in the crystal (153). The same study also reported two different conformation of GABARAP in crystals. Firstly, it featured a closed conformation, as observed in structure of GABARAPL2 (Figure 42B).

Superimposition of crystal structures of GABARAP (PDB: 2R2Q) and GABARAPL2 revealed a similar structure with differences in conformation of loop region. It should also be noted that the C-terminus of GABARAP and GABARAPL2 are pointing in opposite direction. Secondly, an open conformation with helix α 1 contacting the neighbouring molecule was reported in GABARAP1. Interestingly, GABARAPL2 possibly formed oligomers despite having a closed conformation in the crystals unlike GABARAP which formed oligomers only in open conformation. Moreover, the reported crystallisation condition for the open conformation is consistent with some of the other conditions in which GABARAPL2 crystallized (Figure 30B and D, data still to be collected). X-ray diffraction data obtained from the crystals grown in high salt concentration may reveal GABARAPL2 in an open conformation consistent with the open conformation of GABARAP. Although the unfolding of helix α 1 observed in the open conformation may have been induced by the crystallization

conditions favouring a peculiar lattice contact, NMR studies on GABARAP had confirmed that the N-terminal portion of GABARAP exhibits an equilibrium of two or more conformations (154, 155).

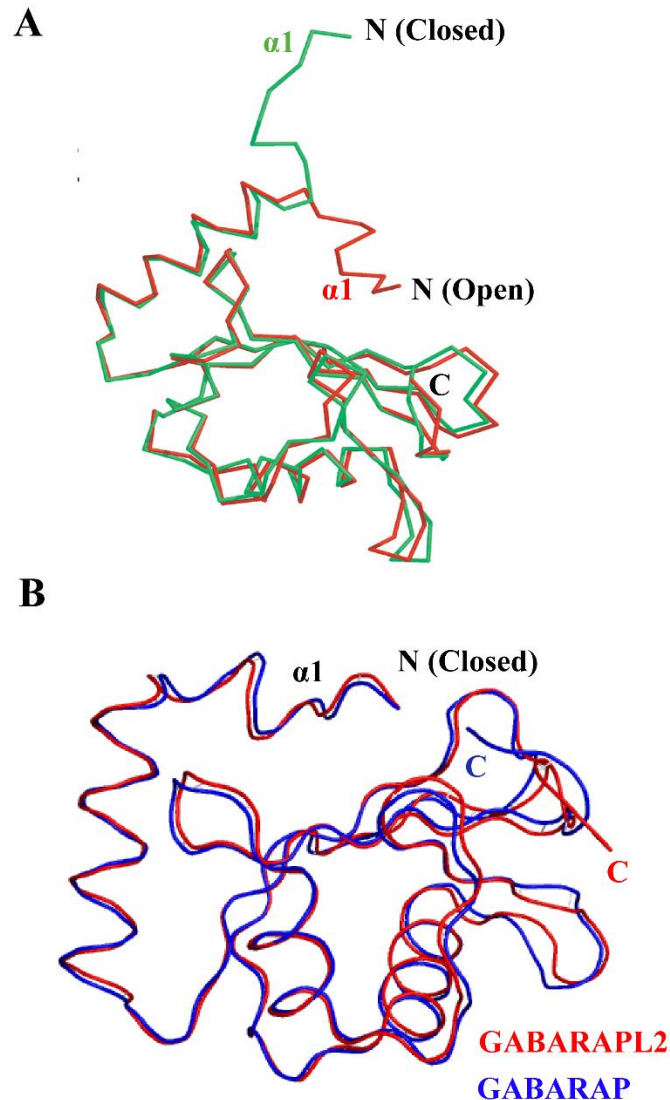


Figure 42: Structural superimposition of GABARAPL2 and GABARAP. A) Overlay of closed conformation and open conformation of GABARAP. In closed conformation, N-terminal helix $\alpha 1$ is facing outward to the rest of the molecule whereas in closed conformation, it is facing C-terminal domain. Figure modified from (153). B) Superimposition of structures of GABARAPL2 (red) and GABARAP (blue) (PDB: 1GNU) revealing a closed conformation with helices $\alpha 1$ facing the C-terminal domain (156). Structural difference are observed in the loop regions connecting the β -strands in the C-terminal domain.

Interestingly, the structure of Ras Interacting Domain in RalGDS (RalGDS-RID) in complex with Ras might give insights into the interaction between GABARAPL2 and GIMAP6. This is based on the fact that RalGDS-RID showed strong structural similarity to the ubiquitin like C-terminal subdomain of GABARAPL2 and GIMAP6 featured significant structural similarity towards Ras. Ras1GDS is an effector of Ras and interacts by forming a pseudo-continuous β -sheet using its strand β 2 with the switch I region of Ras (Figure 43). It is tempting to speculate that the GABARAPL2 and GIMAP6 might interact in the same manner.

Moreover, the basic surface with exposed hydrophobic patches is found on the face of GABARAPL2 resembling the Ras binding face in Ras1GDS-RID (152, 157).

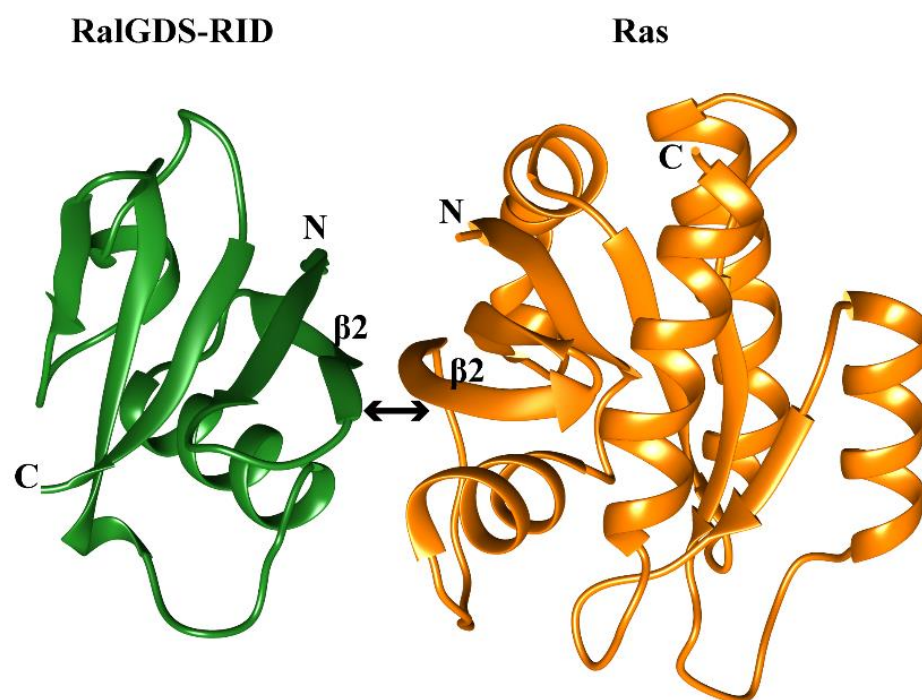


Figure 43: Structure of Ras:RalGDS-RID complex. Ras and RalGDS interacted via β 2 strands on both their structures (indicated by double headed arrow) (PDB: 1LFD). The Ras interacting domain is similar to the structure of GABARAPL2 except that it lacks the N-terminal helices α 1 and α 2. The structure of Ras featured canonical G domain with central β sheet flanked by α helices. Only β 2 strands which are involved in the interaction are marked in the figure.

In conclusion, an experimentally obtained crystal structure of the GIMAP6-GABARAPL2 complex would give a clear picture of the interaction mechanism between the proteins. Additionally, model based mutagenesis both in GIMAP6 and GABARAPL2 could be performed to address the interaction interface in detail.

5.3 GIMAPs a master regulator of apoptosis, autophagy and lymphoid cell development.

As described in section 1.4.2.1, apoptosis plays a crucial role in the maintenance of lymphocytes. It was shown that GIMAPs interacted with both anti-apoptotic and pro-apoptotic Bcl-2 machinery located in mitochondria. Pro-apoptotic function has been ascribed for GIMAP4 as it interacted with pro-apoptotic members of the Bcl2-family such as BAX. GIMAP5 and GIMAP3 were determined to have anti-apoptotic functions since they interacted with Bcl-2 and Bcl-x1. Additionally, GIMAP5 knockout in mice led to severe T cell lymphopenia (91). Hence it was proposed that GIMAPs control the survival of lymphocytes by regulating the intrinsic pathway of apoptosis through mitochondria. Contradicting this finding, genetic deficiency of Bim (pro-apoptotic member) which can potentially restore the T cell compartment did not prevent lymphopenia caused by GIMAP5 sphinx mutation (116). Furthermore, the identification of endogenous GIMAP5 at lysosomes further challenged the mitochondrial model adapted by GIMAPs in T cell maintenance.

Even though the role of GIMAPs on mitochondria for lymphocyte survival cannot be entirely ruled out, a role for GIMAPs in regulating autophagy appears more likely, given the observed GABARPL2-GIMAP6 interaction. Such a function would also be consistent with a role of GIMAPs in the maintenance of lymphocytes, since autophagy is a crucial process for lymphocyte survival. In support of this hypothesis, it was established that the phenotype of GIMAP5-deficient mice resembled the phenotype of *Atg5/7* deficient mice (108, 117) with depleted peripheral T lymphocytes. An impaired mitophagy was proposed to be responsible for this phenotype in both GIMAP5 and *Atg5/7* knockout. Moreover, localization of GIMAP2 on LDs also speculatively linked autophagy to GIMAPs. It was reported that LDs are subjected to autophagy (158) and subsequently regulated lipid metabolism. It was demonstrated that the inhibition of autophagy increased triglycerides (TG) and LDs both *in vivo* (*Atg5* deficient hepatocytes and *Atg5* knock out mice) and *in vitro* (inhibition with 3-methyladenine). This also led to increased lipid droplet number per cell and size.

In agreement with a recent report (124), GIMAP6 interacted with GABARAPL2, a mammalian homologue of autophagy protein Atg8 which linked GIMAPs to the process of autophagy. Even though a direct role of GIMAP6 in mediating autophagy is not established, it was shown that GABARAPL2 regulated the GIMAP6 expression levels over time possibly recruiting and degrading them in autophagosomes. Furthermore, the localization of GIMAP7

was determined in healthy Jurkat T cells and the in cells undergoing autophagy and apoptosis as GIMAPs are implied in both the pathways. Moreover, GIMAP7 showed partial localization to LD in Jurkat T cells despite lacking hydrophobic sequence unlike other membrane associating GIMAPs. These observation lead to the selection of GIMAP7 as a candidate to investigate its subcellular localization upon induction of autophagy and apoptosis. As shown in Figure 40, both autophagy and apoptosis did not influence localization of GIMAP7 thereby leading to an observation that the process of autophagy and apoptosis can function successfully with GIMAP7 localized on LDs. Furthermore, cell biological experiments involving GIMAP6, GIMAP7 and GABARAPL2 would shed light on their possible involvement or regulation of autophagy and apoptosis.

5.4 GIMAPs-Current understanding and a working model

Research over the last decade has conclusively established GIMAPs to be the part of the immune system in mammals. The discovery of GIMAP (GIMAP4) in plants as a protein overexpressed during the bacterial infection led to the association of the term “immunity” to the family (76). Later, genes encoding for GIMAPs were identified and characterized in humans, mice and rats. The genes were found to be tightly clustered in a single autosome in which it was found (91). In particular, human possesses 7 functional *GIMAP* genes, listed as *GIMAP1-GIMAP8* (*GIMAP3* is a pseudo gene). Even though biochemical functions of GIMAPs are still poorly understood, animal models have strongly established the role of GIMAPs in survival and maintenance of lymphocytes (78). It has been demonstrated that GIMAPs play a crucial role in the regulating both T and B cell numbers. GIMAPs are also implicated in human diseases, such as systemic lupus erythematosus and diabetes (118, 159). Additionally, GIMAPs were shown to interact with proteins involved in apoptotic Bcl-2 machinery for lymphocytes maintenance (91). In addition to that, the finding in this thesis linked one of the GIMAP member (GIMAP6) to an autophagy protein (GABARAPL2), consistent with an independent study (124). Although with contradictory findings in the beginning, the cellular localization of all the GIMAPs have been assessed carefully now (Table 1) (90). As a result, it was revealed that GIMAPs exhibited differential cellular localization based on the presence of a hydrophobic amino acid sequence stretch at their C-terminal extensions. GIMAPs with hydrophobic sequence at their C-terminus associate with membranous organelles like lipid droplet and lysosomes (88, 89). Considering the domain

architecture of GIMAPs, they were found to be closely related to the septin superfamily in the TRAFAC subclass of G proteins (see section 1.5.2) (63). Albeit possessing some GIMAP specific structural and sequence elements, GIMAPs resembled largely the canonical G proteins (see section 1.5.1). Structural studies carried out on human GIMAP2 and GIMAP7 had revealed interesting structural and biochemical functions of these proteins. GIMAPs also exhibit differential binding towards guanine nucleotides (84, 88, 90) with the exception of GIMAP6 which does not bind to nucleotide (Figure 19). Interestingly, not all GIMAPs hydrolysed GTP. GIMAP2, GIMAP5 and GIMAP6 (Figure 37) were catalytically silent whereas GIMAP7 (Figure 20) and GIMAP4 exhibited GTPase activity (84). In addition to that, GIMAP7 which co-localized with GIMAP2 stimulated the GTPase activity of GIMAP2 which is otherwise catalytically inactive. Interestingly, it was discovered in this study that GIMAP6 interacted with both GIMAP7 and GABARAPL2 (Figure 15) Further investigation on this discovery lead to the identification that GIMAP6 simultaneously inhibited the GTPase activity of GIMAP7 and interacted with GABARAPL2 (Figure 20, 28 and 35). Consistent with an independent report (124), the interaction identified between GIMAP6 and GABARAPL2 links the GIMAP family to the autophagy pathway.

With this current understanding, GIMAPs can be classified into a cytosolic and membrane-associated subfamily on the basis of possessing C-terminal hydrophobic sequence stretches or not. In humans, GIMAP1, GIMAP2 and GIMAP5 comprise the membrane-associated members whereas GIMAP4, GIMAP6, GIMAP7 and GIMAP8 form the cytosolic members. Based on the current findings, it has been suggested that the cytosolic subfamily regulates the membrane associated GIMAP subfamily members. A similar working model of interaction among a G protein family have been reported for the members of the immunity-related GTPases (IRG). IRG members are interferon-inducible G proteins against a broad spectrum of intracellular pathogens including *Toxoplasma gondii*. IRGs are classified into subgroups based on the sequence feature of the G1 motif they carry. Group with sequence of GxxxxGMS and GxxxxGKS (canonical) in the G1 motifs are named as GMS and GKS subgroup, respectively. IRG members are involved in nucleotide dependent regulatory interactions among the family members. GMS members regulate the localization of GDP-bound inactive GKS member both prior and post infection with *T.gondii*. It has been suggested that upon infection, GTP-bound GKS members form higher order oligomer on the surface of parasitophorous vacuole membrane (PVM) containing the parasite and ultimately lead to the rupture of vacuole conferring immunity against the infection (160, 161).

Based on the current understanding of GIMAPs, a model of their function in Jurkat T cell is proposed (Figure 44). It was shown that GIMAP2 is recruited to lipid droplets by its hydrophobic sequences (HS) to form a stable scaffold in the GTP bound state (88). As a typical scaffold, it could, for example, recruit effector proteins to LD. The putative cytosolic GIMAP7 associates with GIMAP2 on the surface of lipid droplet and stimulates its GTPase activity (90).

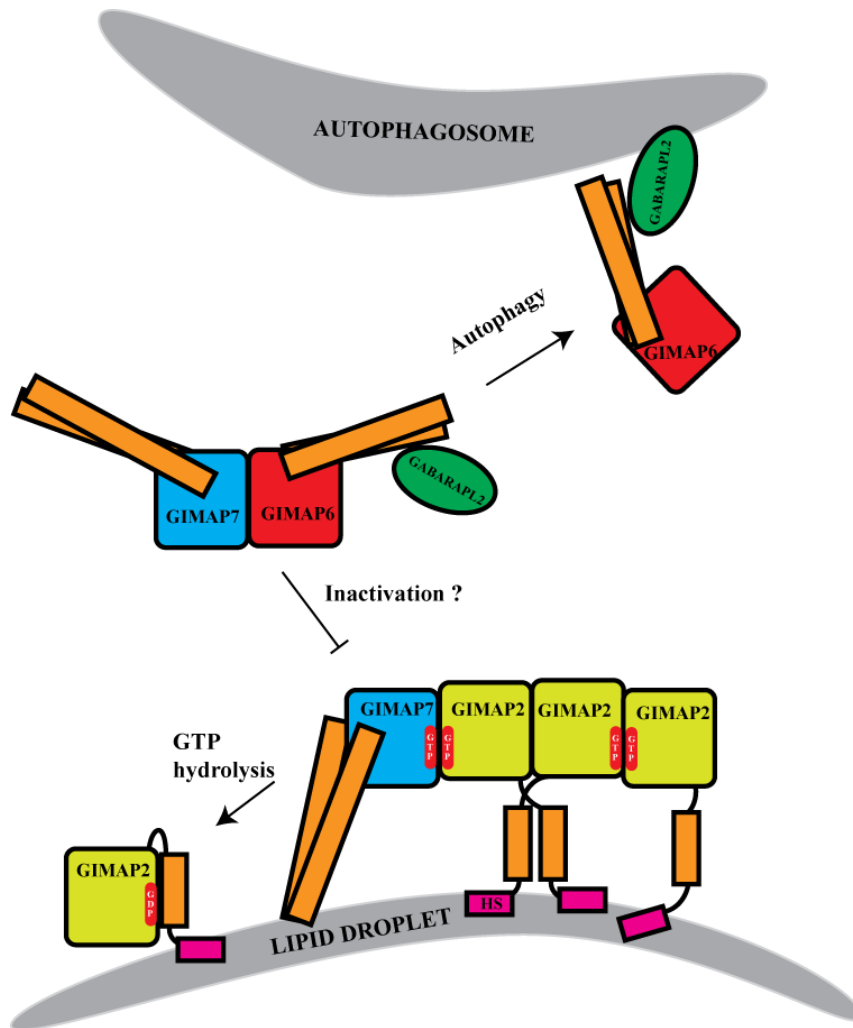


Figure 44: Model of GIMAP function in Jurkat cell. Under physiological condition, cytosolic GIMAP7 is in equilibrium interaction state with both GIMAP6 and GIMAP2. Part of GIMAP7 population disassembles GIMAP2 scaffold on LDs by stimulating its GTPase activity and other part is interacting with GIMAP6 which in turn is interacting with GABARAPL2. Upon induction of autophagy, GABARAPL2 recruits GIMAP6 to autophagosomes leading to the shift of interaction equilibrium of GIMAP7 towards LDs leading to higher rate of GIMAP2 scaffold disassembly.

This stimulation could result in the disassembly of the GIMAP2 scaffold since the scaffold disassembles in the GDP-bound state. Further upstream of this process, a cytosolic and pre-

existing complex of GIMAP6 and GABARAPL2 interact with GIMAP7 and inhibit its GTPase activity (Figure 35). In this way, it may sequester GIMAP7 making it unavailable for disassembly of the GIMAP2 scaffold on lipid droplets. Under physiological condition, it is proposed that GIMAP7 is in equilibrium between GIMAP2 and GIMAP6 interaction state. Interestingly, upon induction of autophagy, GIMAP6 is recruited to autophagosome for degradation (124) and the equilibrium of GIMAP7 may shift towards GIMAP2 in the vicinity of lipid droplets. I therefore suggest that a sophisticated interplay among the GIMAP family members involving homo- and hetero-dimerization contributes to the regulation of scaffold assembly. Further study needs to clarify which molecules may be assembled on GIMAP scaffolds and what is the exact function of the GIMAP scaffold.

APPENDIX A- G motifs in GIMAPs

Human GIMAP	G1 motif GXXXXGKS	G2 motif XTX	G3 motif DXXG	Conserved Box (CB) LSXPGPHALLL VXQLG-ΘTXEψ	G4 motif NKXD	G5 motif XCAX
GIMAP1	GRTGAGKS 34-41	VIK 44-46	DTPD 82-85	LSAPGPHALLL VTQLG_RFTAQD 107-128	RKED 153-156	VCAF 185-188
GIMAP2	GKTGTGKS 93-100	VTR 121-123	DTPD 141-144	LSAPGPHVLLL VTQLG_RYTSQD 165-188	HKED 213-216	ICAF 242-245
GIMAP4	GKTGAGKS 37-44	ITK 65-67	DTPG 85-88	LTSPGPHALLL VVPLG_RYTEEE 109-130	RKDT 155-158	YCAL 186-189
GIMAP5	GKTGCGKS 34-41	VTR 62-64	DTPS 82-85	LSAPGPHVLLL VIQLG_RFTAQD 106-127	HKED 152-155	YCAF 184-187
GIMAP6	GKTGSGKS 47-54	VTK 75-77	DTPN 95-98	LSAPGPHAVLLTQ LGRFTDED 118-139	RKED 164-167	HCGF 196-199
GIMAP7	GKTGSGKS 15-22	VTK 43-45	DTPG 63-66	SSCPGPHAIVLV LLLG_RYTEEE 87-108	RKEE 133-136	CCAF 164-167
GIMAP8	GKCRSGKS 17-24	VIK 44-46	DTPG 64-67	LSAPSLHALLL VIAIG_HFTRED 89-111	RKDD 136-139	YCIF 165-168
	GKTGAGKS 254-261	VTQ 281-289	DAPD 101-104	TGPHAFLLV TPLG_FYTKND 322-340	RKED 465-468	YSAF 396-399
	GRSGTGKS 445-452	VTK 473-475	DTPS 493-496	CCEKGDTEFFVLV FQLG_RFTEED 520-541	RKED 566-569	VCAF 598-601

Appendix A: G motifs and conserved sequence elements in GIMAPs. All the motifs G1-G5 along with conserved box of GIMAPs are listed. The corresponding amino acid sequence number belonging to the specific GIMAP is mentioned at the bottom of the conserved sequence. Θ refers to an aromatic and ψ refers to an acidic residue.

APPENDIX B – Instruments

Instrument	Manufacturer
24-well crystallization plates	Hampton Research, Aliso Viejo, USA
35 mm glass bottom dishes	MatTek, Ashland, USA
45 Ti rotor	Beckman Coulter, Krefeld, D
96 well 107rilliant107ation plates	Sigma-Aldrich, Steinheim, D
Agarose Gel Electrophoresis System	OLS, Bremen, D
Amicon centrifugal filter device	Millipore, Billerica, USA
An 50-Ti rotor	Beckman Coulter, Krefeld, D
Automated imaging and storing system Rock Imager	Formulatrix, Waltham, USA
Benchtop Centrifuge 5415 R	Eppendorf, Hamburg, D
Benchtop Centrifuge 5804 R	Eppendorf, Hamburg, D
Block Heater Rotilabo H250	Roth, Karlsruhe, D
Cell culture incubator CB150	Binder, Tuttlingen, D
Cell culture microscope Leica DM IL	Leica, Wetzlar, D
Centrifuge Avanti J-26 XP	Beckman Coulter, Krefeld, D
Chromatography columns Superdex 200 16/60,26/60	GE Healthcare, Piscataway, USA
Chromatography columns Superdex 75 16/60, 26/60	GE Healthcare, Piscataway, USA
Chromatography columns XK 16/20, XK 26/20	GE Healthcare, Piscataway, USA
Cryo-Fridge VIP Series -86°C	Sanyo, Moriguchi, J
CryoLoops, various sizes	Hampton Research, Aliso Viejo, USA
Double-sector flow-through centerpiece AUC cell	Beckman Coulter, Krefeld, D
Fluidizer M-110 L Pneumatic	Microfluidics, Newtown, USA
FPLC Äkta Prime Plus / Purifier	GE Healthcare, Piscataway, USA
Fridge N3956 4°C/-20°C	Liebherr, Biberach an der Riss, D
HPLC system 1260 Infinity LC	Agilent Technologies, Santa Clara, USA
Imaging system LAS4000 mini	FujiFilm, Düsseldorf, D
Isothermal Titration Calorimeter (MicroCal VP-ITC)	GE Healthcare, Piscataway, USA
Isothermal Titration Calorimeter (MicroCal iTC200)	Malvern Instruments, Worcestershire, U.K
JLA 8.100 rotor	Beckman Coulter, Krefeld, D
Laminar flow cabinet Herasafe HS12	Thermo Scientific, Dreieich, D
Microscope FluoView FV1000	Olympus, Hamburg, D
NanoDrop 2000	Thermo Scientific, Wilmington, USA
Nucleosil 100 C18 HPLC precolumn	Knauer, Berlin, D
Optima MAX-XP benchtop ultracentrifuge	Beckman Coulter, Krefeld, D
PCR thermocycler T-Gradient thermoblock	Biometra, Göttingen, D
Peristaltic pump ISM 827 B	Ismatec, Wertheim, D
pH-Meter	Mettler-Toledo, Gießen, D
Pipettes Eppendorf Research vario	Eppendorf, Hamburg, D
Pipetting robot Hydra-plus-One	Thermo Scientific, Dreieich, D
Precision scales	Mettler-Toledo, Gießen, D
RALS 270 dual detector	Malvern Instruments, Worcestershire, U.K.
Refractive index detector VE 3580	Malvern Instruments, Worcestershire, U.K.
Reversed-phase ODS-2 hypersil HPLC column	Thermo Scientific, Dreieich, D
SDS PAGE System Xcell Sure Lock	Life Technologies, Karlsruhe, D
Shaker Incubator Innova 44 R	New Brunswick Scientific, Enfield, USA

Soundssystem Inspire T3030
Thermoblock MKR13
TLA 100 rotor S.N. 899
Ultracentrifuge Optima L-100 K
Vacuum pump
Vortex Genie 2
Water quench Julabo TW20
Western Blot Module Xcell II
XLI analytical ultracentrifuge

Creative Labs, Dublin, IRL
HLC Biotech, Bovenden, D
Beckman Coulter, Krefeld, D
Beckman Coulter, Krefeld, D
Vacuubrand, Wertheim, D
Bender+Hobien, Zurich, CH
Julabo, Seelbach, D
Life Technologies, Karlsruhe, D
Beckman Coulter, Krefeld, D

APPENDIX C- Chemicals

Chemical / Enzyme / Kit	Cat.-No.	Manufacturer
10 x cloned Pfu reaction buffer	600153-82	Stratagene, La Jolla, USA
2-Log DNA ladder	N3200S	NEB, Frankfurt a. M., D
Acetic Acid	3783.5	Roth, Karlsruhe, D
Acetone	9372.2	Roth, Karlsruhe, D
Acetonitrile	CN20.2	Roth, Karlsruhe, D
Additive Screen	HR2-428	Hampton Research, Aliso Viejo, USA
Agarose	2267.3	Roth, Karlsruhe, D
Ammonium acetate	9689	Sigma-Aldrich, Steinheim, D
Ammonium chloride	9700	Sigma-Aldrich, Steinheim, D
Ammonium citrate dibasic	9833	Sigma-Aldrich, Steinheim, D
Ammonium fluoride	9737	Sigma-Aldrich, Steinheim, D
Ammonium formate	9735	Sigma-Aldrich, Steinheim, D
Ammonium iodide	9874	Sigma-Aldrich, Steinheim, D
Ammonium nitrate	9889	Sigma-Aldrich, Steinheim, D
Ammonium phosphate monobasic	9709	Sigma-Aldrich, Steinheim, D
Ammonium sulfate	9212.2	Roth, Karlsruhe, D
Autoinduction medium	71491-5	Novagen, Darmstadt, D
BamHI	R0136S	NEB, Frankfurt a. M., D
Boric acid	5935.2	Roth, Karlsruhe, D
Calcium acetate Hydrate	21056	Sigma-Aldrich, Steinheim, D
Calcium chloride	A119.1	Roth, Karlsruhe, D
Chloramphenicol	3886.3	Roth, Karlsruhe, D
Coomassie 108rilliant blue R 250 (C.I. 42660)	3862.2	Roth, Karlsruhe, D
di-Ammonium hydrogen phosphate	9839	Sigma-Aldrich, Steinheim, D
di-Potassium hydrogen phosphate anhydrous	P749.2	Roth, Karlsruhe, D
di-Sodium hydrogen phosphate anhydrous	P030.2	Roth, Karlsruhe, D
DMEM	E15-877 04 716 728	PAA, Pasching, A
DNase I	001	Roche, Mannheim, D
DpnI	R0176S	NEB, Frankfurt a. M., D
DTT	6908.2	Roth, Karlsruhe, D
EcoRI	R0101S	NEB, Frankfurt a. M., D
EDTA	8040.2	Roth, Karlsruhe, D
Ethanol	5054.2	Roth, Karlsruhe, D
Ethidium bromide	2218.1	Roth, Karlsruhe, D
Fetal bovine serum	A11-211	PAA laboratories, Pasching, A
GDP	NU-1172S	Jena Bioscience, Jena, D

GeneAmp© dNTPs	N8080007	Roche Molecular, Branchburg, USA
Glutathione Sepharose™ 4B	27-4574-01	Amersham, Piscataway, USA
Glycerol	3783.1	Roth, Karlsruhe, D
GSH reduced	3541	Calbiochem, Darmstadt, D
GTP	NU-1012-1G	Jena Bioscience, Jena, D
Guanidinehydrochloride	37.1	Roth, Karlsruhe, D
HEPES	9105.4	Roth, Karlsruhe, D
HindIII	R0104S	NEB, Frankfurt a. M., D
Imidazole	3899.3	Roth, Karlsruhe, D
Isopropanol	9866.5	Roth, Karlsruhe, D
Kanamycinsulfate	T823.4	Roth, Karlsruhe, D
Lithium acetate Dihydrate	62393	Sigma-Aldrich, Steinheim, D
Lithium citrate tribasic Tetrahydrate	62484	Sigma-Aldrich, Steinheim, D
Lithium nitrate	62574	Sigma-Aldrich, Steinheim, D
Magnesium acetate Tetrahydrate	63049	Sigma-Aldrich, Steinheim, D
Magnesium chloride Hexahydrate	63065	Sigma-Aldrich, Steinheim, D
Magnesium formate Dihydrate	793	Sigma-Aldrich, Steinheim, D
Magnesium nitrate	237175-100G	Sigma-Aldrich, Steinheim, D
Magnesium sulfate Heptahydrate	63138	Sigma-Aldrich, Steinheim, D
Malonic acid	63290	Sigma-Aldrich, Steinheim, D
Mark12™ unstained standard	LC5677	Life Technologies, Karlsruhe, D
Methanol	4627.5	Roth, Karlsruhe, D
MPD	68340	Sigma-Aldrich, Steinheim, D
Ni Sepharose HP	71-5027-67 AD	GE Healthcare, München, D
NuPAGE© LDS Sample Buffer (4x)	NP0007	Life Technologies, Karlsruhe, D
NuPAGE© MES SDS Buffer Kit	NP0060	Life Technologies, Karlsruhe, D
NuPAGE© MOPS SDS Buffer Kit	NP0050	Life Technologies, Karlsruhe, D
NuPAGE© Novex 4-12% Bis-Tris Gel 1,5 mm, 10 / 15 well	NP0335BOX /NP0336BOX	Life Technologies, Karlsruhe, D
PBS	H15-002	PAA, Pasching, A
Pefabloc© SC-Protease inhibitor	A154.2	Roth, Karlsruhe, D
PEG 1000	81188	Sigma-Aldrich, Steinheim, D
PEG 2000MME	81321	Sigma-Aldrich, Steinheim, D
PEG 3350	88276	Sigma-Aldrich, Steinheim, D
PEG 400	91893	Sigma-Aldrich, Steinheim, D
PEG 4000	95904	Sigma-Aldrich, Steinheim, D
PEG 500MME	71578	Sigma-Aldrich, Steinheim, D
PEG 8000	89510	Sigma-Aldrich, Steinheim, D
Penicillin-Streptomycin, liquid, 100x	15140-122	Life Technologies, Karlsruhe, D
Pfu DNA polymerase	600153	Stratagene, La Jolla, USA
pGEX-6-P1	27-4597-01	GE Healthcare, München, D

Potassium acetate	60035	Sigma-Aldrich, Steinheim, D
Potassium chloride	6781.3	Roth, Karlsruhe, D
Potassium citrate tribasic monohydrate	25107	Sigma-Aldrich, Steinheim, D
Potassium dihydrogen phosphate	3904.1	Roth, Karlsruhe, D
Potassium fluoride	60239	Sigma-Aldrich, Steinheim, D
Potassium formate	60246	Sigma-Aldrich, Steinheim, D
Potassium iodide	60400	Sigma-Aldrich, Steinheim, D
Potassium nitrate	60414	Sigma-Aldrich, Steinheim, D
Potassium phosphate	3904.3	Roth, Karlsruhe, D
Potassium sulfate	60528	Sigma-Aldrich, Steinheim, D
Potassium thiocyanate	60517	Sigma-Aldrich, Steinheim, D
PreScission™ Protease	27-0843-01	GE Healthcare, München, D
QIAprep™ Spin Miniprep Kit	27106	Qiagen, Hilden, D
QIAquick gel extraction kit	28704	Qiagen, Hilden, D
Roti©Fect transfection kit	P001.3	Roth, Karlsruhe, D
Sodium acetate Trihydrate	71188	Sigma-Aldrich, Steinheim, D
Sodium chloride	9265.2	Roth, Karlsruhe, D
Sodium citrate tribasic Dihydrate	71402	Sigma-Aldrich, Steinheim, D
Sodium di-hydrogen phosphate 2-hydrate	T879.1	Roth, Karlsruhe, D
Sodium fluoride	71519	Sigma-Aldrich, Steinheim, D
Sodium hydroxide	6771.1	Roth, Karlsruhe, D
Sodium nitrate	71755	Sigma-Aldrich, Steinheim, D
Sodium sulfate Decahydrate	71969	Sigma-Aldrich, Steinheim, D
Sodium tartrate dibasic dihydrate	71994	Sigma-Aldrich, Steinheim, D
Sodium thiocyanate	71938	Sigma-Aldrich, Steinheim, D
T4 DNA ligase	M0202S	NEB, Frankfurt a. M., D
Terrific-Broth medium	HP61.1	Roth, Karlsruhe, D
Tetrabutylammonium bromide	86860-500G	Sigma-Aldrich, Steinheim, D
The Classics II Suite	130723	Qiagen, Hilden, D
The Classics Suite	130701	Qiagen, Hilden, D
The JSCG+ Suite	130720	Qiagen, Hilden, D
The MPD Suite	130706	Qiagen, Hilden, D
The pHClear II Suite	130710	Qiagen, Hilden, D
Trichloromethane	6340.2	Roth, Karlsruhe, D
Tryptone/peptone	8952.2	Roth, Karlsruhe, D
Uranyl acetate dihydrate	73943	Sigma-Aldrich, Steinheim, D
Western Blotting Detection Reagent Amersham ECL Prime	RPN2232	GE Healthcare, München, D
XhoI	R0146L	NEB, Frankfurt a. M., D
Yeast extract	2363.2	Roth, Karlsruhe, D
Zinc acetate Dihydrate	96459	Sigma-Aldrich, Steinheim, D

APPENDIX D- List of Clones

Construct (primer number, FW/REV)	Forward primer
	Reverse primer
hsGIMAP6 (R134D) C990/C991	5'- ctg gtg aca caa ctg ggc GAC ttc acg gat gag- 3'
	5'- ctc atc cgt gaa GTC gcc cag ttg tgt cac cag- 3'
hsGIMAP6 (L70D) (D702/703)	5'-gac gtc ttc gag tet aaa GAC agc acc aga ccc gtg acc-3'
	5'-ggg cac ggg tet ggt gct GTC ttt aga ctc gaa gac gtc-3'
hsGIMAP6 (Q131E) (D704/705)	5'- gcc gtg ctc ctg gtg aca GAA ctg ggc cgg ttc acg gat g-3'
	5'- c atc cgt gaa ccg gcc cag TTC tgt cac cag gag cac ggc-3'
hsGIMAP6 (D167W) (D700/701)	5'- gtg ttc acc cgg aag gaa TGG ctg gct ggc gcc tcc ctg -3'
	5'- cag gga gcc gcc agc cag CCA ttc ctt ccg ggt gaa cac -3'
hsGIMAP6 (1-292) Full length EcoRI/Xho (A13 /A25)	5'-ggc GAA TTC atg gag gaa gaa gaa tat gaa caa att c -3'
	5'- ggc CTC GAG tca tca aag gtc agc ctt ccc cag cag-3'
hsGIMAP6 (11-292) EcoRI/XhoI (D374/A13)	5'- gcc GAA TTC cag gag aat ccc cca gaa gag -3'
	5'- Ggc CTC GAG tca tca aag gtc agc ctt ccc cag cag-3'
hsGIMAP6 (21-292) EcoRI/XhoI (D375/A13)	5'- gcc GAA TTC gat cct gtg ctg gag ctg tca gg -3'
	5'- Ggc CTC GAG tca tca aag gtc agc ctt ccc cag cag -3'
hsGIMAP6 (39-292) EcoRI/XhoI (D049/A13)	5'- gcc GAA TTC agg aga ctg agg ctc att ctc-3'
	5'- Ggc CTC GAG tca tca aag gtc agc ctt ccc cag cag -3'
hsGIMAP6 (232-292) EcoRI/XhoI (D619/A13)	5'- gcc GAA TTC agc aac aag gct tac caa tat acc cag -3'
	5'- Ggc CTC GAG tca tca aag gtc agc ctt ccc cag cag -3'
hsGIMAP6 (1-255) EcoRI/XhoI (A13/D078)	5'- ggc gaa ttc atg gag gaa gaa gaa tat gaa caa att c -3'
	5'- ggc CTC GAG tca tca ctg gct tac ttg cct ttc ctg -3'
hsGIMAP6 (1-233) EcoRI/XhoI (A13 /D077)	5'- ggc gaa ttc atg gag gaa gaa gaa tat gaa caa att c -3'
	5'- ggc CTC GAG tca tca gtt gct gta ata atc tcc ttc -3'
hsGIMAP6 (1-282) EcoRI/XhoI (A13 /D379)	5'- ggc GAA TTC atg gag gaa gaa gaa tat gaa caa att c -3'
	5'- ggc CTC GAG tca tca ggc ttc ctc aga ttc ctt ctg gat ctg g-3'
hsGIMAP6 (1-286) EcoRI/XhoI (A13 /D378)	5'- ggc gaa ttc atg gag gaa gaa gaa tat gaa caa att c -3'
	5'- ggc CTC GAG tca tca cag gca tet gtg ggc ttc ctc aga ttc-3'
hsGIMAP6 (11-286) EcoRI/XhoI (D374/D378)	5'- gcc GAA TTC cag gag aat ccc cca gaa gag -3'
	5'- ggc CTC GAG tca tca cag gca tet gtg ggc ttc ctc aga ttc-3'

hsGIMAP6 (11-282) EcoRI/XhoI (D374/D379)	5'- gcc gaa ttc cag gag aat ccc cca gaa gag -3'
	5'- ggc CTC GAG tca tca ggc ttc ctc aga ttc ctt ctg gat ctg g-3'
hsGIMAP6 (21-286) EcoRI/XhoI (D375/D378)	5'-gcc GAA TTC gat cct gtg ctg gag ctg tca gg -3'
	5'- ggc CTC GAG tca tca cag gca tct gtg ggc ttc ctc aga ttc-3'
hsGIMAP6 (21-282) EcoRI/XhoI (D375/D379)	5'- gcc GAA TTC gat cct gtg ctg gag ctg tca gg -3'
	5'- ggc CTC GAG tca tca ggc ttc ctc aga ttc ctt ctg gat ctg g-3'
hsGABARAPL2 EcoRI/XhoI (D142/D143)	5'- ggc gaa ttc atg aag tgg atg ttc aag gag gac cac -3'
	5'- ggc CTC GAG tca tca gaa gcc aaa agt gtt ctc tcc -3'
hsGIMAP6 (39-292) in pMAL- C2X vector with-out linker between MBP and insert	5'- cag act aat tcg agc tcg agg aga ctg agg ctc att ctc -3'
	5'- gag aat gag cct cag tct cct cga get cga att agt ctg -3'

APPENDIX E- List of Abbreviations

Abbreviation	Expansion
Amp	Ampicillin
ATP	Adenosine-5'-triphosphate
AIG1	AvrRpt2-induced gene 1
ALCL	Anaplastic large cell lymphoma
BAFF	B cell activating factor belonging to the TNF family
BBDP	Biobreeding diabetes-prone
BCR	B cell receptor
BESSY	Berliner Elektronenspeicherring-Gesellschaft für Synchrotronstrahlung
BODIPY	Boron-dipyrrromethene
cDNA	complementary deoxyribonucleic acid
CHAPS	3-[(3-cholamidopropyl)dimethylammonio]-1-propanesulfonate
C-terminus	Carboxy-terminus
CB	Conserved box
CD	Cluster of differentiation
DC	Dendritic cell
DN	Double negative
DP	Double positive
DTT	Dithiothreitol
<i>EcoRI</i>	<i>Escherichia coli R I</i>
EDTA	Ethylenediaminetetraacetic acid
e.g.	exempli gratia
EGFP	Enhanced green fluorescent protein
ER	Endoplasmic reticulum
G domain	Guanine nucleotide binding domain
G protein	Guanine nucleotide binding protein
GAP	GTPase-activating protein
GDP	Guanosine-5'-diphosphate
GEF	Guanine nucleotide exchange factor
GIMAP	GTPase of immunity-associated proteins
GMP	Granulocyte/monocyte precursor
GMP-PNP	Guanosine-5'-[β,γ -imido]triphosphate
GSH	Reduced glutathione
GST	Glutathione-S-transferase
GTP	Guanosine-5'-triphosphate
HEPES	(4-(2-hydroxyethyl)-1-piperazineethanesulfonic acid
<i>hs</i>	<i>Homo sapiens</i>
HPLC	High pressure liquid chromatography
HS	Hydrophobic segment
HSC	Hematopoietic stem cell

IAN	Immunity-associated nucleotide binding protein
Ig	Immunoglobulin
IL	Interleukine
IPTG	Isopropyl- β -D-1 thiogalactopyranoside
ITC	Isothermal titration calorimetry
IRG	Immunity-related GTPases
Kan	Kanamycin
LD	Lipid droplet
MDC	Max-Delbrück-Centrum für Molekulare Medizin Berlin-Buch
MES	2-(N-morpholino)ethanesulfonic acid
MHC	Major histocompatibility complex
MOPS	3-(N-morpholino)propanesulfonic acid
NK cell	Natural killer cell
NP-40	4-Nonylphenyl poly(ethylene glycol)
N-terminus	Amino-terminus
PAGE	polyacrylamide gel electrophoresis
P-loop	Phosphate-binding loop
PCR	Polymerase chain reaction
PDB	Protein Data Bank
PEG	Polyethylene glycol
Ras	Rat sarcoma
RPMI	Roswell Park Memorial Institute medium
RT-PCR	Reverse transcriptase polymerase chain reaction
SDS PAGE	Sodiumdodecylsulfate polyacrylamide gel electrophoresis
SEC	Size-exclusion chromatography
SP	Single positive
TB	Terrific broth
TCR	T cell receptor
TNF	Tumor necrosis factor
Toc	Translocon at the outer envelope membrane of chloroplasts
TRAFAC	Translation factor associated
VDJ	Variable, diversity, joining segments

Amino acid abbreviations:

For amino acids, the one and three letter codes were used: A, Ala: alanine; C, Cys: cysteine; D, Asp: aspartate; E, Glu: glutamate; F, Phe: phenylalanine; G, Gly: glycine; H, His: histidine; I, Ile: isoleucine; K, Lys: lysine; L, Leu: leucine; M, Met: methionine; N, Asn: asparagine; P, Pro: proline; Q, Gln: glutamine; R, Arg: arginine; S, Ser: serine; T, Thr: threonine; V, Val: valine; W, Trp: tryptophane; Y, Tyr: tyrosine; x: any amino acid.

References

1. Paul WE. *Fundamental Immunology*. 2013(7th Edition).
2. Orkin SH, Zon LI. Hematopoiesis: an evolving paradigm for stem cell biology. *Cell*. 2008;132(4):631-44.
3. Kuby. *Immunology*. 2013;7th edition.
4. Mogensen TH. Pathogen recognition and inflammatory signaling in innate immune defenses. *Clinical microbiology reviews*. 2009;22(2):240-73, Table of Contents.
5. O'Neill LA, Golenbock D, Bowie AG. The history of Toll-like receptors - redefining innate immunity. *Nature reviews Immunology*. 2013;13(6):453-60.
6. Boehm T. Design principles of adaptive immune systems. *Nature reviews Immunology*. 2011;11(5):307-17.
7. Kenneth M. Murphy PT, and Mark Walport. *Janeways Immunobiology*. Garland Science. 2007(7th edition).
8. Litman GW, Rast JP, Fugmann SD. The origins of vertebrate adaptive immunity. *Nat Rev Immunol*. 2010;10(8):543-53.
9. Burnet FM. *The Clonal Selection Theory of Acquired Immunity*. Cambridge University Press. 1959.
10. Gellert M. V(D)J recombination: RAG proteins, repair factors, and regulation. *Annu Rev Biochem*. 2002;71:101-32.
11. Tonegawa S. Somatic generation of antibody diversity. *Nature*. 1983;302(5909):575-81.
12. Sohn SJ, Rajpal A, Winoto A. Apoptosis during lymphoid development. *Current opinion in immunology*. 2003;15(2):209-16.
13. Guo P, Hirano M, Herrin BR, Li J, Yu C, Sadlonova A, et al. Dual nature of the adaptive immune system in lampreys. *Nature*. 2009;459(7248):796-801.
14. Dias S, Xu W, McGregor S, Kee B. Transcriptional regulation of lymphocyte development. *Current opinion in genetics & development*. 2008;18(5):441-8.
15. Sakano H, Huppi K, Heinrich G, Tonegawa S. Sequences at the somatic recombination sites of immunoglobulin light-chain genes. *Nature*. 1979;280(5720):288-94.
16. Anderson G, Jenkinson EJ. Lymphostromal interactions in thymic development and function. *Nat Rev Immunol*. 2001;1(1):31-40.
17. Starr TK, Jameson SC, Hogquist KA. Positive and negative selection of T cells. *Annu Rev Immunol*. 2003;21:139-76.
18. van Ewijk W. T-cell differentiation is influenced by thymic microenvironments. *Annual review of immunology*. 1991;9:591-615.

19. Robey E, Fowlkes BJ. Selective events in T cell development. *Annu Rev Immunol.* 1994;12:675-705.
20. von Boehmer H, Teh HS, Kisielow P. The thymus selects the useful, neglects the useless and destroys the harmful. *Immunology today.* 1989;10(2):57-61.
21. Matzinger P, Guerder S. Does T-cell tolerance require a dedicated antigen-presenting cell? *Nature.* 1989;338(6210):74-6.
22. Nagasawa T. Microenvironmental niches in the bone marrow required for B-cell development. *Nat Rev Immunol.* 2006;6(2):107-16.
23. Rolink AG, Schaniel C, Andersson J, Melchers F. Selection events operating at various stages in B cell development. *Current opinion in immunology.* 2001;13(2):202-7.
24. Kurosaki T, Shinohara H, Baba Y. B cell signaling and fate decision. *Annu Rev Immunol.* 2010;28:21-55.
25. von Boehmer H, Melchers F. Checkpoints in lymphocyte development and autoimmune disease. *Nat Immunol.* 2010;11(1):14-20.
26. Tiegs SL, Russell DM, Nemazee D. Receptor editing in self-reactive bone marrow B cells. *The Journal of experimental medicine.* 1993;177(4):1009-20.
27. Yorimitsu T, Klionsky DJ. Autophagy: molecular machinery for self-eating. *Cell Death Differ.* 2005;12 Suppl 2:1542-52.
28. Yang Z, Klionsky DJ. Eaten alive: a history of macroautophagy. *Nature cell biology.* 2010;12(9):814-22.
29. Nakatogawa H, Suzuki K, Kamada Y, Ohsumi Y. Dynamics and diversity in autophagy mechanisms: lessons from yeast. *Nat Rev Mol Cell Biol.* 2009;10(7):458-67.
30. Itakura E, Mizushima N. Characterization of autophagosome formation site by a hierarchical analysis of mammalian Atg proteins. *Autophagy.* 2010;6(6):764-76.
31. Suzuki K, Kubota Y, Sekito T, Ohsumi Y. Hierarchy of Atg proteins in pre-autophagosomal structure organization. *Genes to cells : devoted to molecular & cellular mechanisms.* 2007;12(2):209-18.
32. Mizushima N, Komatsu M. Autophagy: renovation of cells and tissues. *Cell.* 2011;147(4):728-41.
33. Li C, Capan E, Zhao Y, Zhao J, Stolz D, Watkins SC, et al. Autophagy is induced in CD4+ T cells and important for the growth factor-withdrawal cell death. *Journal of immunology (Baltimore, Md : 1950).* 2006;177(8):5163-8.
34. Pua HH, Dzhagalov I, Chuck M, Mizushima N, He YW. A critical role for the autophagy gene Atg5 in T cell survival and proliferation. *The Journal of experimental medicine.* 2007;204(1):25-31.
35. Nedjic J, Aichinger M, Emmerich J, Mizushima N, Klein L. Autophagy in thymic epithelium shapes the T-cell repertoire and is essential for tolerance. *Nature.* 2008;455(7211):396-400.

36. Wang R, Dillon CP, Shi LZ, Milasta S, Carter R, Finkelstein D, et al. The transcription factor Myc controls metabolic reprogramming upon T lymphocyte activation. *Immunity*. 2011;35(6):871-82.
37. Kyewski B, Klein L. A central role for central tolerance. *Annu Rev Immunol*. 2006;24:571-606.
38. Nicholson DW, Thornberry NA. Caspases: killer proteases. *Trends in biochemical sciences*. 1997;22(8):299-306.
39. Rathmell JC, Thompson CB. The central effectors of cell death in the immune system. *Annu Rev Immunol*. 1999;17:781-828.
40. Ashkenazi A, Dixit VM. Death receptors: signaling and modulation. *Science*. 1998;281(5381):1305-8.
41. Sprick MR, Weigand MA, Rieser E, Rauch CT, Juo P, Blenis J, et al. FADD/MORT1 and caspase-8 are recruited to TRAIL receptors 1 and 2 and are essential for apoptosis mediated by TRAIL receptor 2. *Immunity*. 2000;12(6):599-609.
42. Enari M, Sakahira H, Yokoyama H, Okawa K, Iwamatsu A, Nagata S. A caspase-activated DNase that degrades DNA during apoptosis, and its inhibitor ICAD. *Nature*. 1998;391(6662):43-50.
43. Green DR, Reed JC. Mitochondria and apoptosis. *Science*. 1998;281(5381):1309-12.
44. Willis SN, Adams JM. Life in the balance: how BH3-only proteins induce apoptosis. *Current opinion in cell biology*. 2005;17(6):617-25.
45. Opferman JT. Apoptosis in the development of the immune system. *Cell death and differentiation*. 2008;15(2):234-42.
46. Wei MC, Lindsten T, Mootha VK, Weiler S, Gross A, Ashiya M, et al. tBID, a membrane-targeted death ligand, oligomerizes BAK to release cytochrome c. *Genes & development*. 2000;14(16):2060-71.
47. Li P, Nijhawan D, Budihardjo I, Srinivasula SM, Ahmad M, Alnemri ES, et al. Cytochrome c and dATP-dependent formation of Apaf-1/caspase-9 complex initiates an apoptotic protease cascade. *Cell*. 1997;91(4):479-89.
48. Cheng EH, Wei MC, Weiler S, Flavell RA, Mak TW, Lindsten T, et al. BCL-2, BCL-X(L) sequester BH3 domain-only molecules preventing BAX- and BAK-mediated mitochondrial apoptosis. *Molecular cell*. 2001;8(3):705-11.
49. Zong WX, Lindsten T, Ross AJ, MacGregor GR, Thompson CB. BH3-only proteins that bind pro-survival Bcl-2 family members fail to induce apoptosis in the absence of Bax and Bak. *Genes & development*. 2001;15(12):1481-6.
50. Willis SN, Fletcher JI, Kaufmann T, van Delft MF, Chen L, Czabotar PE, et al. Apoptosis initiated when BH3 ligands engage multiple Bcl-2 homologs, not Bax or Bak. *Science*. 2007;315(5813):856-9.

51. Owen JJ, Jenkinson EJ. Apoptosis and T-cell repertoire selection in the thymus. *Annals of the New York Academy of Sciences*. 1992;663:305-10.
52. Berg LJ, Kang J. Molecular determinants of TCR expression and selection. *Current opinion in immunology*. 2001;13(2):232-41.
53. Nemazee D. Receptor editing in lymphocyte development and central tolerance. *Nat Rev Immunol*. 2006;6(10):728-40.
54. Bouillet P, Metcalf D, Huang DC, Tarlinton DM, Kay TW, Kontgen F, et al. Proapoptotic Bcl-2 relative Bim required for certain apoptotic responses, leukocyte homeostasis, and to preclude autoimmunity. *Science*. 1999;286(5445):1735-8.
55. Mandal M, Borowski C, Palomero T, Ferrando AA, Oberdoerffer P, Meng F, et al. The BCL2A1 gene as a pre-T cell receptor-induced regulator of thymocyte survival. *The Journal of experimental medicine*. 2005;201(4):603-14.
56. McCarty N, Paust S, Ikizawa K, Dan I, Li X, Cantor H. Signaling by the kinase MINK is essential in the negative selection of autoreactive thymocytes. *Nat Immunol*. 2005;6(1):65-72.
57. Mackay F, Woodcock SA, Lawton P, Ambrose C, Baetscher M, Schneider P, et al. Mice transgenic for BAFF develop lymphocytic disorders along with autoimmune manifestations. *The Journal of experimental medicine*. 1999;190(11):1697-710.
58. He B, Chadburn A, Jou E, Schattner EJ, Knowles DM, Cerutti A. Lymphoma B cells evade apoptosis through the TNF family members BAFF/BLyS and APRIL. *Journal of immunology (Baltimore, Md : 1950)*. 2004;172(5):3268-79.
59. Kern C, Cornuel JF, Billard C, Tang R, Rouillard D, Stenou V, et al. Involvement of BAFF and APRIL in the resistance to apoptosis of B-CLL through an autocrine pathway. *Blood*. 2004;103(2):679-88.
60. Scheffzek K, Ahmadian MR. GTPase activating proteins: structural and functional insights 18 years after discovery. *Cellular and molecular life sciences : CMLS*. 2005;62(24):3014-38.
61. Bourne HR, Sanders DA, McCormick F. The GTPase superfamily: a conserved switch for diverse cell functions. *Nature*. 1990;348(6297):125-32.
62. Wittinghofer A, Vetter IR. Structure-function relationships of the G domain, a canonical switch motif. *Annual review of biochemistry*. 2011;80:943-71.
63. Leippe DD, Wolf YI, Koonin EV, Aravind L. Classification and evolution of P-loop GTPases and related ATPases. *Journal of molecular biology*. 2002;317(1):41-72.
64. Wennerberg K, Rossman KL, Der CJ. The Ras superfamily at a glance. *Journal of cell science*. 2005;118(Pt 5):843-6.
65. Bos JL, Rehmann H, Wittinghofer A. GEFs and GAPs: critical elements in the control of small G proteins. *Cell*. 2007;129(5):865-77.
66. Saraste M, Sibbald PR, Wittinghofer A. The P-loop--a common motif in ATP- and GTP-binding proteins. *Trends in biochemical sciences*. 1990;15(11):430-4.

67. Walker JE, Saraste M, Runswick MJ, Gay NJ. Distantly related sequences in the alpha- and beta-subunits of ATP synthase, myosin, kinases and other ATP-requiring enzymes and a common nucleotide binding fold. *The EMBO journal*. 1982;1(8):945-51.
68. Cherfils J, Zeghouf M. Regulation of small GTPases by GEFs, GAPs, and GDIs. *Physiol Rev*. 2013;93(1):269-309.
69. Hartwell LH. Genetic control of the cell division cycle in yeast. IV. Genes controlling bud emergence and cytokinesis. *Experimental cell research*. 1971;69(2):265-76.
70. Byers B, Goetsch L. A highly ordered ring of membrane-associated filaments in budding yeast. *The Journal of cell biology*. 1976;69(3):717-21.
71. Hu Q, Milenkovic L, Jin H, Scott MP, Nachury MV, Spiliotis ET, et al. A septin diffusion barrier at the base of the primary cilium maintains ciliary membrane protein distribution. *Science (New York, NY)*. 2010;329(5990):436-9.
72. Mostowy S, Bonazzi M, Hamon MA, Tham TN, Mallet A, Lelek M, et al. Entrapment of intracytosolic bacteria by septin cage-like structures. *Cell host & microbe*. 2010;8(5):433-44.
73. Mostowy S, Cossart P. Septins: the fourth component of the cytoskeleton. *Nature reviews Molecular cell biology*. 2012;13(3):183-94.
74. Sirajuddin M, Farkasovsky M, Hauer F, Kuhlmann D, Macara IG, Weyand M, et al. Structural insight into filament formation by mammalian septins. *Nature*. 2007;449(7160):311-5.
75. Weirich CS, Erzberger JP, Barral Y. The septin family of GTPases: architecture and dynamics. *Nature reviews Molecular cell biology*. 2008;9(6):478-89.
76. Reuber TL, Ausubel FM. Isolation of Arabidopsis genes that differentiate between resistance responses mediated by the RPS2 and RPM1 disease resistance genes. *The Plant cell*. 1996;8(2):241-9.
77. Poirier GM, Anderson G, Huvar A, Wagaman PC, Shuttleworth J, Jenkinson E, et al. Immune-associated nucleotide-1 (IAN-1) is a thymic selection marker and defines a novel gene family conserved in plants. *Journal of immunology (Baltimore, Md : 1950)*. 1999;163(9):4960-9.
78. Nitta T, Takahama Y. The lymphocyte guard-IANs: regulation of lymphocyte survival by IAN/GIMAP family proteins. *Trends in immunology*. 2007;28(2):58-65.
79. Oreb M, Tews I, Schleiff E. Policing Tic 'n' Toc, the doorway to chloroplasts. *Trends in cell biology*. 2008;18(1):19-27.
80. Douglas LM, Alvarez FJ, McCreary C, Konopka JB. Septin function in yeast model systems and pathogenic fungi. *Eukaryotic cell*. 2005;4(9):1503-12.
81. Wain HM, Bruford EA, Lovering RC, Lush MJ, Wright MW, Povey S. Guidelines for human gene nomenclature. *Genomics*. 2002;79(4):464-70.
82. Sprang SR. G protein mechanisms: insights from structural analysis. *Annu Rev Biochem*. 1997;66:639-78.

83. Krucken J, Schmitt-Wrede HP, Markmann-Mulisch U, Wunderlich F. Novel gene expressed in spleen cells mediating acquired testosterone-resistant immunity to *Plasmodium chabaudi* malaria. *Biochemical and biophysical research communications*. 1997;230(1):167-70.
84. Cambot M, Aresta S, Kahn-Perles B, de Gunzburg J, Romeo PH. Human immune associated nucleotide 1: a member of a new guanosine triphosphatase family expressed in resting T and B cells. *Blood*. 2002;99(9):3293-301.
85. Stamm O, Krucken J, Schmitt-Wrede HP, Benten WP, Wunderlich F. Human ortholog to mouse gene *imap38* encoding an ER-localizable G-protein belongs to a gene family clustered on chromosome 7q32-36. *Gene*. 2002;282(1-2):159-67.
86. Krucken J, Schroetel RM, Muller IU, Saidani N, Marinovski P, Benten WP, et al. Comparative analysis of the human *gimap* gene cluster encoding a novel GTPase family. *Gene*. 2004;341:291-304.
87. MacMurray AJ, Moralejo DH, Kwitek AE, Rutledge EA, Van Yserloo B, Gohlke P, et al. Lymphopenia in the BB rat model of type 1 diabetes is due to a mutation in a novel immune-associated nucleotide (*Ian*)-related gene. *Genome research*. 2002;12(7):1029-39.
88. Schwefel D, Frohlich C, Eichhorst J, Wiesner B, Behlke J, Aravind L, et al. Structural basis of oligomerization in septin-like GTPase of immunity-associated protein 2 (GIMAP2). *Proceedings of the National Academy of Sciences of the United States of America*. 2010;107(47):20299-304.
89. Wong VW, Saunders AE, Hutchings A, Pascall JC, Carter C, Bright NA, et al. The autoimmunity-related GIMAP5 GTPase is a lysosome-associated protein. *Self/nonself*. 2010;1(3):259-68.
90. Schwefel D, Arasu BS, Marino SF, Lamprecht B, Kochert K, Rosenbaum E, et al. Structural insights into the mechanism of GTPase activation in the GIMAP family. *Structure (London, England : 1993)*. 2013;21(4):550-9.
91. Nitta T, Nasreen M, Seike T, Goji A, Ohigashi I, Miyazaki T, et al. IAN family critically regulates survival and development of T lymphocytes. *PLoS biology*. 2006;4(4):e103.
92. Saunders A, Lamb T, Pascall J, Hutchings A, Dion C, Carter C, et al. Expression of GIMAP1, a GTPase of the immunity-associated protein family, is not up-regulated in malaria. *Malaria journal*. 2009;8:53.
93. Dion C, Carter C, Hepburn L, Coadwell WJ, Morgan G, Graham M, et al. Expression of the *Ian* family of putative GTPases during T cell development and description of an *Ian* with three sets of GTP/GDP-binding motifs. *International immunology*. 2005;17(9):1257-68.
94. Kaplan MH, Schindler U, Smiley ST, Grusby MJ. *Stat6* is required for mediating responses to IL-4 and for development of Th2 cells. *Immunity*. 1996;4(3):313-9.
95. Thiam AR, Farese RV, Jr., Walther TC. The biophysics and cell biology of lipid droplets. *Nature reviews Molecular cell biology*. 2013;14(12):775-86.

96. Daheron L, Zenz T, Siracusa LD, Brenner C, Calabretta B. Molecular cloning of Ian4: a BCR/ABL-induced gene that encodes an outer membrane mitochondrial protein with GTP-binding activity. *Nucleic acids research*. 2001;29(6):1308-16.
97. Jokinen R, Lahtinen T, Marttinen P, Myohanen M, Ruotsalainen P, Yeung N, et al. Quantitative changes in Gimap3 and Gimap5 expression modify mitochondrial DNA segregation in mice. *Genetics*. 2015;200(1):221-35.
98. Yano K, Carter C, Yoshida N, Abe T, Yamada A, Nitta T, et al. Gimap3 and Gimap5 cooperate to maintain T-cell numbers in the mouse. *European journal of immunology*. 2014;44(2):561-72.
99. Schnell S, Demolliere C, van den Berk P, Jacobs H. Gimap4 accelerates T-cell death. *Blood*. 2006;108(2):591-9.
100. Carter C, Dion C, Schnell S, Coadwell WJ, Graham M, Hepburn L, et al. A natural hypomorphic variant of the apoptosis regulator Gimap4/IAN1. *Journal of immunology (Baltimore, Md : 1950)*. 2007;179(3):1784-95.
101. Filen JJ, Filen S, Moulder R, Tuomela S, Ahlfors H, West A, et al. Quantitative proteomics reveals GIMAP family proteins 1 and 4 to be differentially regulated during human T helper cell differentiation. *Molecular & cellular proteomics : MCP*. 2009;8(1):32-44.
102. Duthie KA, Osborne LC, Foster LJ, Abraham N. Proteomics analysis of interleukin (IL)-7-induced signaling effectors shows selective changes in IL-7Ralpha449F knock-in T cell progenitors. *Molecular & cellular proteomics : MCP*. 2007;6(10):1700-10.
103. Rahman N, Stewart G, Jones G. A role for the atopy-associated gene PHF11 in T-cell activation and viability. *Immunology and cell biology*. 2010;88(8):817-24.
104. Ramanathan S, Poussier P. BB rat lyp mutation and Type 1 diabetes. *Immunological reviews*. 2001;184:161-71.
105. Hornum L, Romer J, Markholst H. The diabetes-prone BB rat carries a frameshift mutation in Ian4, a positional candidate of Iddm1. *Diabetes*. 2002;51(6):1972-9.
106. Michalkiewicz M, Michalkiewicz T, Ettinger RA, Rutledge EA, Fuller JM, Moralejo DH, et al. Transgenic rescue demonstrates involvement of the Ian5 gene in T cell development in the rat. *Physiological genomics*. 2004;19(2):228-32.
107. Moralejo DH, Park HA, Speros SJ, MacMurray AJ, Kwitek AE, Jacob HJ, et al. Genetic dissection of lymphopenia from autoimmunity by introgression of mutated Ian5 gene onto the F344 rat. *Journal of autoimmunity*. 2003;21(4):315-24.
108. Groen H, Klatter FA, Brons NH, Mesander G, Nieuwenhuis P, Kampinga J. Abnormal thymocyte subset distribution and differential reduction of CD4+ and CD8+ T cell subsets during peripheral maturation in diabetes-prone BioBreeding rats. *Journal of immunology (Baltimore, Md : 1950)*. 1996;156(3):1269-75.

109. Plamondon C, Kottis V, Brideau C, Metroz-Dayer MD, Poussier P. Abnormal thymocyte maturation in spontaneously diabetic BB rats involves the deletion of CD4-8+ cells. *Journal of immunology (Baltimore, Md : 1950)*. 1990;144(3):923-8.
110. Zadeh HH, Greiner DL, Wu DY, Tausche F, Goldschneider I. Abnormalities in the export and fate of recent thymic emigrants in diabetes-prone BB/W rats. *Autoimmunity*. 1996;24(1):35-46.
111. Hernandez-Hoyos G, Joseph S, Miller NG, Butcher GW. The lymphopenia mutation of the BB rat causes inappropriate apoptosis of mature thymocytes. *European journal of immunology*. 1999;29(6):1832-41.
112. Ramanathan S, Norwich K, Poussier P. Antigen activation rescues recent thymic emigrants from programmed cell death in the BB rat. *Journal of immunology (Baltimore, Md : 1950)*. 1998;160(12):5757-64.
113. Whalen BJ, Weiser P, Marounek J, Rossini AA, Mordes JP, Greiner DL. Recapitulation of normal and abnormal BioBreeding rat T cell development in adult thymus organ culture. *Journal of immunology (Baltimore, Md : 1950)*. 1999;162(7):4003-12.
114. Schulteis RD, Chu H, Dai X, Chen Y, Edwards B, Haribhai D, et al. Impaired survival of peripheral T cells, disrupted NK/NKT cell development, and liver failure in mice lacking Gimap5. *Blood*. 2008;112(13):4905-14.
115. Hawkins T, Fuller J, Olson K, Speros S, Lernmark A. DR.lyp/lyp bone marrow maintains lymphopenia and promotes diabetes in lyp/lyp but not in +/+ recipient DR.lyp BB rats. *Journal of autoimmunity*. 2005;25(4):251-7.
116. Barnes MJ, Aksoylar H, Krebs P, Bourdeau T, Arnold CN, Xia Y, et al. Loss of T cell and B cell quiescence precedes the onset of microbial flora-dependent wasting disease and intestinal inflammation in Gimap5-deficient mice. *Journal of immunology (Baltimore, Md : 1950)*. 2010;184(7):3743-54.
117. Cousins L, Graham M, Tooze R, Carter C, Miller JR, Powrie FM, et al. Eosinophilic bowel disease controlled by the BB rat-derived lymphopenia/Gimap5 gene. *Gastroenterology*. 2006;131(5):1475-85.
118. Hellquist A, Zucchelli M, Kivinen K, Saarialho-Kere U, Koskenmies S, Widen E, et al. The human GIMAP5 gene has a common polyadenylation polymorphism increasing risk to systemic lupus erythematosus. *Journal of medical genetics*. 2007;44(5):314-21.
119. Lim MK, Sheen DH, Kim SA, Won SK, Lee SS, Chae SC, et al. IAN5 polymorphisms are associated with systemic lupus erythematosus. *Lupus*. 2009;18(12):1045-52.
120. Shin JH, Janer M, McNeney B, Blay S, Deutsch K, Sanjeevi CB, et al. IA-2 autoantibodies in incident type I diabetes patients are associated with a polyadenylation signal polymorphism in GIMAP5. *Genes and immunity*. 2007;8(6):503-12.

121. Payne F, Smyth DJ, Pask R, Barratt BJ, Cooper JD, Twells RC, et al. Haplotype tag single nucleotide polymorphism analysis of the human orthologues of the rat type 1 diabetes genes *Ian4* (*Lyp/Iddm1*) and *Cblb*. *Diabetes*. 2004;53(2):505-9.
122. Shiao YM, Chang YH, Liu YM, Li JC, Su JS, Liu KJ, et al. Dysregulation of GIMAP genes in non-small cell lung cancer. *Lung cancer (Amsterdam, Netherlands)*. 2008;62(3):287-94.
123. Thirunavukkarasu S, Plain KM, de Silva K, Begg D, Whittington RJ, Purdie AC. Expression of genes associated with cholesterol and lipid metabolism identified as a novel pathway in the early pathogenesis of *Mycobacterium avium* subspecies *paratuberculosis*-infection in cattle. *Veterinary immunology and immunopathology*. 2014;160(3-4):147-57.
124. Pascall JC, Rotondo S, Mukadam AS, Oxley D, Webster J, Walker SA, et al. The immune system GTPase GIMAP6 interacts with the Atg8 homologue GABARAPL2 and is recruited to autophagosomes. *PLoS one*. 2013;8(10):e77782.
125. Kuznetsov SA, Gelfand VI. 18 kDa microtubule-associated protein: identification as a new light chain (LC-3) of microtubule-associated protein 1 (MAP-1). *FEBS letters*. 1987;212(1):145-8.
126. Mann SS, Hammarback JA. Molecular characterization of light chain 3. A microtubule binding subunit of MAP1A and MAP1B. *The Journal of biological chemistry*. 1994;269(15):11492-7.
127. Oliver H. Weiergräber JMdaDW. Atg8 Family Proteins — Autophagy and Beyond. Chapter 2 in book, *Autophagy - A Double-Edged Sword - Cell Survival or Death?* . Bailly DY, editor 2013.
128. Krucken J, Epe M, Benten WP, Falkenroth N, Wunderlich F. Malaria-suppressible expression of the anti-apoptotic triple GTPase mGIMAP8. *Journal of cellular biochemistry*. 2005;96(2):339-48.
129. Wilkins MR, Gasteiger E, Bairoch A, Sanchez JC, Williams KL, Appel RD, et al. Protein identification and analysis tools in the ExPASy server. *Methods in molecular biology (Clifton, NJ)*. 1999;112:531-52.
130. Lenzen C, Cool RH, Wittinghofer A. Analysis of intrinsic and CDC25-stimulated guanine nucleotide exchange of p21ras-nucleotide complexes by fluorescence measurements. *Methods in enzymology*. 1995;255:95-109.
131. Yang W, Zhang L, Lu Z, Tao W, Zhai Z. A new method for protein coexpression in *Escherichia coli* using two incompatible plasmids. *Protein expression and purification*. 2001;22(3):472-8.
132. Leslie AG. The integration of macromolecular diffraction data. *Acta crystallographica Section D, Biological crystallography*. 2006;62(Pt 1):48-57.
133. Hahn T, et al. *International tables for crystallography*. 1984;A, A1, B, C, E, G
134. Taylor G. The phase problem. *Acta crystallographica Section D, Biological crystallography*. 2003;59(pt 4).
135. Emsley P, Cowtan K. Coot: model-building tools for molecular graphics. *Acta crystallographica Section D, Biological crystallography*. 2004;60(Pt 12 Pt 1):2126-32.

136. Adams PD, Afonine PV, Bunkoczi G, Chen VB, Davis IW, Echols N, et al. PHENIX: a comprehensive Python-based system for macromolecular structure solution. *Acta crystallographica Section D, Biological crystallography*. 2010;66(Pt 2):213-21.
137. Davis IW, Leaver-Fay A, Chen VB, Block JN, Kapral GJ, Wang X, et al. MolProbity: all-atom contacts and structure validation for proteins and nucleic acids. *Nucleic acids research*. 2007;35(Web Server issue):W375-83.
138. Shpilka T, Weidberg H, Pietrokovski S, Elazar Z. Atg8: an autophagy-related ubiquitin-like protein family. *Genome biology*. 2011;12(7):226.
139. Brautigan DL. Protein Ser/Thr phosphatases--the ugly ducklings of cell signalling. *The FEBS journal*. 2013;280(2):324-45.
140. Susin SA, Lorenzo HK, Zamzami N, Marzo I, Snow BE, Brothers GM, et al. Molecular characterization of mitochondrial apoptosis-inducing factor. *Nature*. 1999;397(6718):441-6.
141. Anelli T, Alessio M, Mezghrani A, Simmen T, Talamo F, Bachi A, et al. ERp44, a novel endoplasmic reticulum folding assistant of the thioredoxin family. *The EMBO journal*. 2002;21(4):835-44.
142. Jin Q, Liu G, Domeier PP, Ding W, Mulder KM. Decreased tumor progression and invasion by a novel anti-cell motility target for human colorectal carcinoma cells. *PloS one*. 2013;8(6):e66439.
143. Ramakrishnan C, Dani VS, Ramasarma T. A conformational analysis of Walker motif A [GXXXXGKT (S)] in nucleotide-binding and other proteins. *Protein engineering*. 2002;15(10):783-98.
144. Marti-Renom MA, Stuart AC, Fiser A, Sanchez R, Melo F, Sali A. Comparative protein structure modeling of genes and genomes. *Annual review of biophysics and biomolecular structure*. 2000;29:291-325.
145. Arnold K, Bordoli L, Kopp J, Schwede T. The SWISS-MODEL workspace: a web-based environment for protein structure homology modelling. *Bioinformatics (Oxford, England)*. 2006;22(2):195-201.
146. Goujon M, McWilliam H, Li W, Valentin F, Squizzato S, Paern J, et al. A new bioinformatics analysis tools framework at EMBL-EBI. *Nucleic acids research*. 2010;38(Web Server issue):W695-9.
147. Drozdetskiy A, Cole C, Procter J, Barton GJ. JPred4: a protein secondary structure prediction server. *Nucleic acids research*. 2015;43(W1):W389-94.
148. Noda NN, Kumeta H, Nakatogawa H, Satoo K, Adachi W, Ishii J, et al. Structural basis of target recognition by Atg8/LC3 during selective autophagy. *Genes to cells : devoted to molecular & cellular mechanisms*. 2008;13(12):1211-8.

149. Itoh T, Kanno E, Uemura T, Waguri S, Fukuda M. OATL1, a novel autophagosome-resident Rab33B-GAP, regulates autophagosomal maturation. *The Journal of cell biology*. 2011;192(5):839-53.
150. Kabeya Y, Mizushima N, Ueno T, Yamamoto A, Kirisako T, Noda T, et al. LC3, a mammalian homologue of yeast Apg8p, is localized in autophagosome membranes after processing. *The EMBO journal*. 2000;19(21):5720-8.
151. Chappie JS, Acharya S, Leonard M, Schmid SL, Dyda F. G domain dimerization controls dynamin's assembly-stimulated GTPase activity. *Nature*. 2010;465(7297):435-40.
152. Paz Y, Elazar Z, Fass D. Structure of GATE-16, membrane transport modulator and mammalian ortholog of autophagocytosis factor Aut7p. *The Journal of biological chemistry*. 2000;275(33):25445-50.
153. Coyle JE, Qamar S, Rajashankar KR, Nikolov DB. Structure of GABARAP in two conformations: implications for GABA(A) receptor localization and tubulin binding. *Neuron*. 2002;33(1):63-74.
154. Stangler T, Mayr LM, Willbold D. Solution structure of human GABA(A) receptor-associated protein GABARAP: implications for biological function and its regulation. *The Journal of biological chemistry*. 2002;277(16):13363-6.
155. Pacheco V, Ma P, Thielmann Y, Hartmann R, Weiergraber OH, Mohrluder J, et al. Assessment of GABARAP self-association by its diffusion properties. *Journal of biomolecular NMR*. 2010;48(1):49-58.
156. Knight D, Harris R, McAlister MS, Phelan JP, Geddes S, Moss SJ, et al. The X-ray crystal structure and putative ligand-derived peptide binding properties of gamma-aminobutyric acid receptor type A receptor-associated protein. *The Journal of biological chemistry*. 2002;277(7):5556-61.
157. Huang L, Hofer F, Martin GS, Kim SH. Structural basis for the interaction of Ras with RalGDS. *Nature structural biology*. 1998;5(6):422-6.
158. Singh R, Kaushik S, Wang Y, Xiang Y, Novak I, Komatsu M, et al. Autophagy regulates lipid metabolism. *Nature*. 2009;458(7242):1131-5.
159. Jailwala P, Waukau J, Glisic S, Jana S, Ehlenbach S, Hessner M, et al. Apoptosis of CD4+ CD25(high) T cells in type 1 diabetes may be partially mediated by IL-2 deprivation. *PLoS One*. 2009;4(8):e6527.
160. Hunn JP, Feng CG, Sher A, Howard JC. The immunity-related GTPases in mammals: a fast-evolving cell-autonomous resistance system against intracellular pathogens. *Mammalian genome : official journal of the International Mammalian Genome Society*. 2011;22(1-2):43-54.

161. Hunn JP, Koenen-Waisman S, Papic N, Schroeder N, Pawlowski N, Lange R, et al. Regulatory interactions between IRG resistance GTPases in the cellular response to *Toxoplasma gondii*. *The EMBO journal*. 2008;27(19):2495-509.

Zusammenfassung

'GTPases of IMmunity Associated Proteins' (GIMAPs) sind eine septin-verwandte GTPase-Familie, die mit dem angeborenen Immunsystem assoziiert ist. GIMAPs spielen eine wichtige Rolle in der Entwicklung von Lymphozyten, der Segregation mitochondrialer DNA, Apoptose sowie in der Autophagie. Strukturstudien zeigten, dass einige GIMAPs GTP-abhängige Proteingerüste bilden, in dem sie über zwei Interaktionsflächen auf der Oberfläche von Membranen assemblieren. Biochemische Studien deuten darauf hin, dass andere GIMAP Mitglieder das Proteingerüst zerlegen können. Das Ziel dieser Doktorarbeit war es, die zelluläre Funktion von GIMAPs zu charakterisieren, in dem Interaktionspartner gefunden und biochemisch und strukturell analysiert werden.

Interaktionspartner von GIMAPs wurden massenspektrometrisch identifiziert und spielen Funktionen in der Apoptose, Autophagie, Proteinfaltung sowie dem Vesikeltransport. Insbesondere wurden das Autophagie-assoziierte GABARAPL2 und GIMAP6 als spezifische Interaktionspartner von GIMAP7 gefunden. Die GIMAP6-GIMAP7 Interaktion wurde biochemisch charakterisiert; es konnte gezeigt werden, dass GIMAP6 die GTPase-Funktion von GIMAP7 bei äquimolaren Verhältnissen inhibieren kann. Basierend auf Homologiemodellen und biochemischen Analysen konnte gezeigt werden, dass die GTPase-Domäne von GIMAP6 der entscheidende Faktor für die GTPase-Inhibierung ist, zu der zusätzlich C-terminale Helices beitragen. GABARAPL2 interagiert mit nanomolarer Affinität mit GIMAP6, wie durch isotherme Titrationskalorimetrie (ITC) und Bioschicht-Interferenz gezeigt werden konnte. Ein C-terminales, 10 Aminosäuren langes GIMAP6 Peptid, das in vorhergehenden Studien in der Interaktion impliziert wurde, band in ITC-Messungen nicht an GABARAPL2, was auf einen neuen Interaktionsmodus hinweist. Die Kristallstruktur von GABARAPL2 wurde bei atomarer Auflösung bestimmt. Die Struktur zeigt eine konservierte Ubiquitin-faltung und eine Kopf-zu-Schwanz Oligomerisierung im Kristall. Dies könnte darauf hindeuten, dass GABARAPL2 ein Proteingerüst auf der Oberfläche von "Autophagosomen" bilden kann. Abschließend wird in dieser Doktorarbeit ein Modell für die Funktion von GIMAP6, GIMAP7, GABARAPL2 sowie GIMAP6 vorgeschlagen. Die hier gewonnenen Erkenntnisse werden als Basis für viele weitere Mutations- sowie zellbiologische Studien dienen, die die molekulare Charakterisierung von GIMAPs zum Ziel haben.

Publication

Part of the work shown in this thesis is published in the following paper

- Structural insights into the mechanism of GTPase activation in the GIMAP family

Schwefel D, **Arasu BS**, Marino SF, Lamprecht B, Köchert K, Rosenbaum E, Eichhorst J, Wiesner B, Behlke J, Rocks O, Mathas S, Daumke O.
Structure 2013, 21 (4):550-9

The majority of the data in my thesis is not yet published and we intend to publish it in future

Acknowledgements

First and foremost, I am deeply thankful to Prof. Dr. Oliver Daumke for letting me pursue PhD in his lab. Without his constant support and guidance the research work presented here would not have taken this shape. He is an excellent scientist and also a great team leader and it was a great pleasure to work with him. I would like to also thank Dr. David Schwefel for making me familiar with the lab practice in the initial days. It is this familiarization which helped me a lot in my work in the later days. It gives me immense pleasure to thank Dr. Florian Paul from the lab of Prof. Dr. Mathias Selbach in whose lab few of the important results were obtained. A very big thanks to all of AG Selbach who helped me handle SILAC based materials and methods. Heartfelt thanks to Dr. Oliver Rocks for letting me use his sophisticated microscope. I would also like to thank Prof. Dr. Udo Heinemann for this valuable suggestion during the seminars. Many thanks to MDC and SFB958 for funding me during these years. I would like to also thank Prof. Dr. Mrinalini Puranik, my former supervisor for her guidance in my initial days of research career.

I am also thankful to all of my former and current lab mates. It was great fun to work with them. There were gossips going around that AG Daumke is the best and most friendly lab that MDC has ever seen! I would cherish the memory of working in my experimental bench (nice music played by Alexej, most of the times), cell culture hoods and microscope. A heartfelt thanks to Daniel for his thought inspiring ideas ranging from science to world politics. I would like to personally thank Alexej for being a translator of Deutsch to me during all these years. His help was indispensable. I would also personally thank Sabine for helping me in early morning colony picking and many more technical assistance she offered me. This acknowledgement would be incomplete, if I don't thank my friends in MDC. Back in India, I would like to personally thank Nirjala for teaching me protein purification from *E.coli* (AlkB is a DNA repair enzyme...blah blah blah...& Beer-Lambert law). I am also happy to thank my friends Pugal, Joe, Baskar, Sendhil (Remoji) and Vicky and Arun (arunT) for their well wishes.

I deeply indebted to my parents without whom I would not have become what I am today. Many thanks to my sister, Akila for her motivation and support. I would like to thank my ever supporting and cooperating wife, who is my life, Pallavi for being with me to realize this goal. Together with the little one, whom I and Pallavi are expecting soon, I would like to thank everyone again who have helped me to do this PhD.

Erklärung

Ich versichere, dass ich die von mir vorgelegte Dissertation selbständig angefertigt, die benutzten Quellen und Hilfsmittel vollständig angegeben und die Stellen der Arbeit - einschließlich Tabellen, Karten und Abbildungen - die anderen Werken im Wortlaut oder dem Sinn nach entnommen sind, in jedem Einzelfall als Entlehnung kenntlich gemacht habe; dass diese Dissertation noch keiner anderen Fakultät oder Universität zur Prüfung vorgelegen hat. Die Bestimmungen der Promotionsordnung sind mir bekannt. Die von mir vorgelegte Dissertation ist von Prof. Dr. O. Daumke und Prof. Dr. U. Heinemann betreut worden.

Berlin, November 2015

Arasu Balasubramaniyam Sivanandam

For reasons of data protection, the curriculum vitae is not published in the electronic version

For reasons of data protection, the curriculum vitae is not published in the electronic version